U. of Iowa 66-33

Distribution of this document is unlimited.

AD639908

THE UNIVERSITY OF IOWA
FOUNDED 1847

CLEARINGHOUSE
FOR FEDERAL SCIENTIFIC AND TECHNICAL INFORMATION

Hardcopy	Microfiche	
$ 5.00	$ 1.00	187 pp

ARCHIVE COPY

D D C
RECEIVED
SEP 20 1966
A

This work was supported in part by the office of Naval Research under Contract No. Nonr-1509(06)

Department of Physics and Astronomy
THE UNIVERSITY OF IOWA
Iowa City, Iowa

VLF RAY TRACING IN A MODEL IONOSPHERE*

by

Stanley D. Shawhan+

A dissertation submitted in partial fulfillment of the requirements for the degree of Doctor of Philosophy in the Department of Physics and Astronomy in the Graduate College of the University of Iowa

August 1966

Chairman: Assistant Professor Donald A. Gurnett

*Research supported in part by the Office of Naval Research under contract Nonr 1509(06).

+National Aeronautics and Space Administration Graduate Trainee.

ACKNOWLEDGEMENTS

I am particularly indebted to Dr. D. A. Gurnett for suggesting this thesis study and for his constructive criticism during its undertaking; to Dr. J. A. Van Allen for his encouragement and for providing the necessary research facilities; and to Mr. G. W. Pfeiffer for his contribution to the experimental aspects of this study. I am sincerely grateful to Mr. K. Chang for his endurance in running the computer programs for this study; to Mrs. D. Walker for running the Injun III data reduction equipment; to Mr. R. Anderson, Mr. T. Burns, and Mr. G. Davida for their assistance in providing and plotting the computer and experimental data; and to Mrs. E. Robison for her efficient and unerring typing of this manuscript.

This study was performed while I was a National Aeronautics and Space Administration Graduate Trainee. This research at the University of Iowa was supported by the Office of Naval Research under contracts N9onr-93803 and Nonr 1509(06).

ABSTRACT

A VLF ray tracing study in a model ionosphere including ions is presented. A review of previous VLF ray tracing methods is given. The physical meaning of rays and ray paths is discussed and it is concluded that for ray tracing in the ionosphere the wave packet and Poynting vector approaches give the same results. Two-dimensional ray tracing equations are derived for the case of a horizontally stratified ionosphere and the derivation of three dimensional equations for the curved ionosphere is sketched. These ray tracing equations are integrated for the special cases of exactly transverse and exactly longitudinal propagation but it is concluded that neither case can persist for very-low-frequency radio waves in the ionosphere. Also the conditions for reversibility of a ray path are derived. It is found that the computer program for numerical integration of the ray tracing equations can retrace a path to 0.3% in latitude and 0.02% in wave normal angle and can reproduce known results for the horizontally stratified model.

Using this ray tracing program the behavior of ray paths for variations of frequency, initial latitude, initial wave normal

angle, initial altitude and ionospheric model are shown. The most important results were with variation of the initial wave normal angle; two ray paths for the same frequency can cross and rays can turn around at low altitudes for frequencies less than the local lower hybrid resonance frequency. Spectrograms of proton, helium, and oxygen whistlers as well as negative ion whistlers are presented. It is predicted that oxygen whistlers can be observed at all altitudes below the oxygen gyrofrequency and that negative ion whistlers can be observed below 30 cps at altitudes near 300 km. Experimental data on the hook whistler, riser and check whistlers, 'transverse' whistlers, and satellite observed VLF noise bands are presented and summarized. The hook whistler is explained as a multiple path whistler at equatorial latitudes for which the earlier trace has increased dispersion at low frequencies due to large wave normal angles along the path. This increased dispersion gives the characteristic joining of the two traces at low frequencies. A calculated hook whistler spectrogram is presented. The riser and check whistlers are explained as whistlers for which the ray has propagated transverse and nearly

transverse to the magnetic field line along its path. The point of transverse propagation produces the characteristic riser dispersion of increasing time delay with increasing frequency. For the check whistler apparently both the upgoing and downgoing rays are observed at the satellite giving a normal whistler dispersion followed by a riser-like tail. It is demonstrated that previous experimental data on the 'transverse' whistler may have been misinterpreted and that the dispersion increases with decreasing frequency rather than decreases as previously reported. The transverse whistler is explained as a whistler which has acquired added dispersion at low frequencies because of propagation nearly transverse to the magnetic field along the path. Finally it is shown that waves can be trapped in the ionosphere between altitudes of decreasing transverse refractive index. It is proposed that these trapped waves can explain the satellite and ground observed ion gyrofrequency noise bands.

TABLE OF CONTENTS

Chapter		Page
I.	Introduction	1
II.	Derivation and Discussion of Ray Tracing Equations	12
III.	Special Cases of Ray Tracing Equations	29
IV.	Ray Tracing Computer Program	44
V.	Characteristics of Ray Paths	55
VI.	Ion Cyclotron Whistlers	67
VII.	Hook Whistlers	77
VIII.	Riser and Check Whistlers	84
IX.	'Transverse' Whistlers	96
X.	Wave Trapping and VLF Noise Bands	104
XI.	Conclusions	108
XII.	Appendices	113
References		137
Figure Captions		144
Figures 1-33		147-179

TABLE OF TABLES

Table No.		Page
I.	Minimum Delay Frequency of Proton Whistler vs Crossover Frequency	73
II.	'Transverse' Whistler Dispersion	96
III.	Ray Tracing Program Flow Chart	131

I. INTRODUCTION

Since the study of very-low-frequency (VLF) whistlers and related ionospheric radio noise phenomena first began in 1894 [Preece, 1894], many experimental and theoretical investigations have been undertaken to characterize and to explain the properties of these naturally occurring radio noises. Helliwell [1965] gives an excellent review of whistlers and related ionospheric phenomena: the history, the current experimental characteristics as determined by ground-based and satellite-borne receivers, and the present theoretical interpretations. Gallet [1959] has organized the types of VLF ionospheric noise phenomena into two broad groups:

(1) Whistlers, which are caused by lightning discharges and for which all frequencies are emitted at once. The whistler shape is due to dispersion of the energy as it propagates along the path in the ionosphere; and

(2) VLF emissions, which are not caused by lightning discharges but which have a source of energy contained within the ionosphere itself and may be due to plasma instabilities or to electromagnetic radiation from high energy particles.

Several species of whistlers have been reported: electron whistlers [Storey, 1953]; nose whistlers [Helliwell et al., 1956]; proton and helium whistlers [Gurnett et al., 1965, and Barrington et al., 1966], subprotonospheric whistlers [Carpenter et al., 1965, and Smith, 1964], transverse whistlers [Carpenter and Dunkel, 1965, and Kimura et al., 1965], and most recently the riser and check whistlers [Pfeiffer et al., 1966]. Shawhan [1966] has suggested that negative ion whistlers may be observable at extremely low frequencies (ELF). The group of VLF emissions is itself divided into two types:

(1) Continuous emissions in both time and frequency which tend to maintain a steady state. Hiss [Ungstrup, 1959; Gurnett, 1966; see also Helliwell, 1965, and Gallet, 1959, for more references], lower hybrid resonance bands [Barrington et al., 1963, and Brice and Smith, 1963], and noise bands near the ion gyrofrequencies [Gustafsson et al., 1963, and Gurnett, 1965] seem to fit this type.

(2) Discrete emissions often with a repetitive and even periodic character which tend to be transient.

Chorus [Allcock, 1957; see also Helliwell, 1965, for further references], periodic emissions [Helliwell, 1963], and various other transient discrete emissions such as hooks, pseudo-whistlers, and pseudo-noses [see Gallet, 1959] have been reported.

A powerful and important analytical method for studying the propagation characteristics of both whistlers and VLF emissions in the ionosphere is that of ray tracing. In an anisotropic, inhomogeneous, but non-absorbing medium, such as the ionosphere and magnetosphere, the trajectory of energy flow for an electromagnetic disturbance is the ray path for this disturbance. Therefore, with the ray path method, the trajectory of energy from a lightning discharge at the base of the ionosphere or from a plasma instability in the ionosphere itself to an observation point can be determined. This ray path method can be used to produce new explanations for the observed characteristics of whistlers and VLF emissions, to test existing explanations, or to predict new ionospheric noise phenomena.

Two approaches have been taken for the determination of ray paths [see review in Kelso, 1964], the direction of the ray being defined by the direction of the Poynting vector (energy flow) or

by the direction of the motion of a wave packet disturbance. Booker [1936, 1938, 1949] developed a wave-packet method for determining ray paths for waves obliquely incident at the base of a horizontally-stratified, doubly refracting ionosphere. He solved a quartic equation called the Booker quartic, for a quantity which completely characterizes the wave behavior in each strata. From the variation of the quantity q and the Booker quartic with electron density and incident angle, it is possible to construct the ray path for the wave packet. Improvement on this method was made by Millington [1951, 1954].

A very important Poynting-vector approach to ray tracing was developed by Poeverlein [1948, 1949, 1950]. He assumed a plane stratified and non-absorbing model ionosphere. In this case, the ray direction is perpendicular to the index of refraction surface at a point on the surface given by the direction of propagation for the waves. His graphical method consists of calculating the index of refraction surface (a plot of the index of refraction vs the angle from the magnetic field direction) using the local plasma parameters (concentration and magnetic field strength) at a given point on the ray path. At each point along the ray path, the component of the refractive index parallel to the planes of stratification has to be conserved (Snell's law), therefore

the propagation direction is determined. By constructing the normal to the index of refraction surface at the point in this propagation direction, the ray direction for that point on the ray path is determined. Stepping a small distance in the ray direction a new point on the ray path is determined and a new index of refraction surface is calculated. This graphical method is discussed further in Section II. Poeverlein used this graphical method to construct ray paths for the ordinary and extraordinary modes for oblique incidence on the base of the ionosphere. The two-dimensional graphical method of Poeverlein was extended to three dimensions by Mullaly [1955]. He also demonstrated that the Poeverlein-Mullaly approach is equivalent to the Booker-Millington approach for non-absorbing media.

Scott [1950] derived expressions for the components of the Poynting-vector. From the ratios of the real parts of these components he derived a set of differential equations describing the ray path for vertical incidence on a horizontally stratified ionosphere. When collisions are included into these equations it is found that for vertical incidence there is a westward flow of energy which is not found by the Booker-Millington wave packet method. This discrepancy was investigated by Hines [1951a, 1951b, 1951c, 1951d]. He concluded that for a dispersive

absorbing, and anisotropic medium the wave packet is better than the Poynting vector method. For the case of a non-absorbing medium, both methods give the same direction for the energy flow--the same ray path.

The first calculation of whistler ray paths in a model ionosphere was performed by Maeda and Kimura [1956]. They developed a ray theory based on Fermat's principle and used the quasi-longitudinal approximation for the refractive index as given by Storey [1953]. Two approximate solutions for the ray paths were derived: one appropriate inside of a sector along the ray path and the other appropriate for the transition between sectors. The ray path is graphically determined, sector by sector. Maeda and Kimura calculated whistler ray paths and whistler dispersions (assuming only electrons in the ionosphere) for different latitudes. The results of these calculations were compared to whistler observations at high and low latitudes with satisfactory qualitative agreement.

With the availability of high speed digital computers, Haselgrove [1955] and Haselgrove and Haselgrove [1960] derived a set of first order differential equations appropriate for numerical integration. The Poynting vector approach was used,

based on the differential equations given by Hamilton [see Hamilton, 1931] for a general anisotropic medium. These differential equations are derived in general curvilinear coordinates and then specialized to spherical polar coordinates for application to the ionosphere case. Haselgrove [1957] presented calculations of whistler ray paths using his two-dimensional cartesian ray tracing equations, the quasi-longitudinal approximation to the whistler index of refraction, and the assumption of electrons only and of horizontal stratification. The resulting ray paths were in reasonable quantitative agreement with those of Maeda and Kimura [1956].

Yabroff [1961] published the first whistler ray path calculations which used the exact expression for the refractive index and which included the curvature of the ionosphere, although he assumed an ionosphere composed of electrons only. From his calculations of ray paths for different frequencies, different latitudes, and different initial wave normal angles, he graphically summarized conclusions about the behavior of ray paths in the ionosphere. An interesting problem which he treated was that of ducting of whistler energy along the magnetic field lines. He concludes that, for the initial wave normal angle

along the field line (and only electrons), ducting by columns of enhanced ionization is not necessary for guiding nearly along the field line. For other initial wave normal angles, ducting is necessary.

When the effects of ions are included in the index of refraction and ray tracing equations, Hines [1957] has shown that for VLF it is possible to have transverse propagation and to have rays refracted back toward the earth at low altitudes. Hines, Hoffman, and Weil [1959] did ray tracing including protons for the special case of transpolar propagation. Kimura [1966] published the first ray tracing results which included effects of the three dominant ions in the upper ionosphere H^+, He^+, and O^+. He presents ray paths resulting from the inclusion of no ions, one ion, and three ions. Comparison of results from this present study to those of Kimura is made in Section III. The main purpose of his ray tracing study was to confirm the interpretation of the subprotonospheric whistler given by Smith [1965]. Kimura found that, for initial wave normal angles of 20° to the vertical and for frequencies near 1 kc/s, the ray would be refracted back toward the earth's surface at altitudes near 1000 km. A space probe at an altitude lower than 1000 km could

possibly see two different time delays for a given frequency; one time for an upgoing ray and one time for a downgoing refracted ray. The ray tracing results agreed quantitatively with the observational data on subprotonospheric whistlers. This work of Kimura represents the first attempt to completely describe an ionospheric radio noise phenomena in terms of ray tracing.

This present ray tracing study has the following three objectives:

1. To develop a physical understanding of ray tracing in a model ionosphere, to discuss the derivation of the ray tracing equations, and to consider the properties of the ray paths for the special cases of exactly transverse and of exactly longitudinal propagation, and of reversibility.

2. To present a representative set of ray paths which vary in frequency, initial latitude, initial wave normal angle, and initial altitude, and from these paths to draw conclusions about the characteristics of ray paths in the ionosphere with ions included.

3. To describe observed ionospheric radio noise phenomena, such as those listed previously under whistlers and VLF emissions, in terms of ray path behavior in a model ionosphere in the manner initiated by Kimura. In particular, the proton, helium, and oxygen whistlers, negative ion whistlers, the hook whistler, the riser and check whistlers, the 'transverse' whistler, and trapping of waves to produce noise bands are discussed in terms of ray paths.

In Section II the physical meaning of rays and the validity of ray theory in an anisotropic, inhomogeneous medium such as the ionosphere is discussed. Based on this theory, the two dimensional ray tracing equations are derived by combining the Haselgrove and Poeverlein methods. The conditions for reversibility of a ray path and the solutions of the ray tracing equations for the cases of purely transverse and purely longitudinal propagation are derived in Section III. A description of the ray tracing computer program and of its special features is given in Section IV and Appendices A and B. Computational accuracy and program performance and limitations for special cases are discussed. Comparison of results is made to those of Yabroff [1961] and Kimura [1966]. Section V presents a set of ray paths calculated for a model ionosphere including ions. The characteristics of these ray paths for different frequencies, initial latitudes, initial wave normal angles, initial altitudes, and ionospheric model are summarized. It is these general ray path characteristics which are intended to suggest solutions to specific ray tracing studies.

In Section VI, features of ion cyclotron whistlers are treated. Calculated spectrograms of proton, helium, and oxygen whistlers with altitude are presented and the behavior of the

wave normal as the wave frequency becomes nearly equal to the proton gyrofrequency is studied. The frequency for which the proton whistler delay time is a minimum is compared to the cross-over frequency as a function of proton concentration. Spectrograms of negative ion whistlers are also presented. Sample spectrograms of hook whistlers, both observed and calculated, are presented and discussed in Section VII. A treatment of propagation nearly transverse to the magnetic field is given in Section VIII and theoretical fe tures of the riser and check whistlers are compared to experimentally observed spectrograms from Injun III. A calculated riser spectrogram is also presented. In Section IX the experimental data on 'transverse' whistlers are re-interpreted and a new explanation proposed. Finally, a discussion of the propagation of VLF emissions and of wave trapping to produce VLF noise bands is given in Section X.

II. DERIVATION AND DISCUSSION OF RAY TRACING EQUATIONS

The energy associated with electromagnetic wave propagation in a plasma is divided between the electromagnetic fields of the wave and the coherent particle motions. The velocity which describes the propagation of the electromagnetic wave energy is called the group velocity and, as reviewed in the Introduction, can have two interpretations: the velocity of propagation of the energy in the electromagnetic fields (in the direction of the Poynting vector) or the velocity of propagation of the wave packet itself. Hines [1951 a, b, c, d] demonstrated that, for an inhomogeneous, anisotropic, dispersive, but non-absorbing medium, the constructive interference maxima of a wave travels in the direction of the mean Poynting vector (direction of propagation of electromagnetic field energy). For an absorbing medium however the wave packet interpretation gave the more physical results. Mullaly [1955] demonstrated the equivalence of the Poeverlein-Mullaly Poynting vector method and the Booker-Millington wave packet method for a horizontally stratified, non-absorbing ionosphere. In this present ray tracing study the ray tracing equations of Haselgrove [1955] and Haselgrove and Haselgrove [1960]

are employed. These equations are based on the assumption that the direction of the Poynting vector gives the direction of the group velocity which is a valid assumption for most regions of the ionosphere. The direction of the Poynting vector (group velocity direction) is called the ray direction. Finding the ray path through a given medium is equivalent to finding the trajectory of energy flow or of the wave packet for a non-absorbing medium.

In an anisotropic and inhomogeneous medium such as the ionosphere, the directions of the normal to the wave fronts (wave normal) $\vec{k}$ ($= \omega \vec{n}/c$, where $|\vec{n}|$ is phase index of refraction, ω is the wave frequency, and c the speed of light in a vacuum) and the direction of the normal to the surface of constructive maxima of these wave fronts (ray normal) $\hat{p}$ are different. Stix [1962] has reviewed the concept of group velocity which is defined by

$$\vec{v}_g = \frac{\partial \omega}{\partial \vec{k}} = \hat{k} \frac{\partial \omega}{\partial k} + \hat{\psi} \frac{1}{k} \frac{\partial \omega}{\partial \psi} \qquad (1)$$

where $\hat{\psi}$ is the direction normal to $\vec{k}$ and in the $\vec{v}_g$, $\vec{k}$ plane. Letting α be the angular difference between $\vec{k}$ and $\vec{v}_g$, α is defined by

$$\tan \alpha = -\frac{1}{k} \frac{\partial \omega}{\partial \psi} \Big/ \frac{\partial \omega}{\partial k} \quad . \tag{2}$$

Using the definition of the phase refractive index,

$$\vec{n} = c\vec{K}/\omega \, ,$$

(2) can be written

$$\tan \alpha = -\frac{1}{n} \frac{\partial n}{\partial \psi} \quad . \tag{3}$$

With the use of Figure 1a it is shown that the group velocity direction (ray direction) is the normal to the index of refraction surface at a point determined by the wave normal direction. In Figure 1a is shown the intersection of an index of refraction surface with the plane containing the static magnetic field vector and the propagation vector $\vec{k} = \vec{n}\omega/c$; a plot of the index of refraction as a function of angle from the static magnetic field direction in the $(\vec{n}, \vec{B}_o)$ plane. For an infinitesimal change in this angle ψ of $d\psi$, the index of refraction changes by $-dn$ along $\vec{n}$ and by $nd\psi$ perpendicular to $\vec{n}$. The angle α is then given by

equation (3). Because the unit vector $\hat{p}$ is perpendicular to the line tangent to the curve at $\vec{n}$, α also is the angle between $\hat{p}$ and $\vec{n}$. Therefore, α gives the angular difference between the wave normal ($\vec{k}$ or $\vec{n}$) and the ray normal ($\hat{p}$). For the index of refraction surface shown in Figure 1a, α can become zero for $\vec{n}$ lying along the magnetic field direction or perpendicular to the magnetic field direction. Consequently the ray direction and the wave normal direction are parallel for these two wave normal directions.

A wave normal surface can be drawn for any point of interest in the medium and is determined by the local plasma parameters (concentrations and magnetic field strength) at that point and by the wave frequency. In Figure 2 are shown index of refraction surfaces at one point in the ionosphere (1000 km, 45° magnetic latitude) but for different frequencies. The surfaces for 450 cps are appropriate for frequencies below the local proton gyrofrequency but above the crossover frequency [see Smith and Brice, 1964]. In this frequency range two modes can propagate corresponding to the two branches of the refractive index. For $\psi = 0$ these surfaces correspond to the right and left hand polarized waves. [See Stix, 1962, for discussions of allowed modes and of characteristic frequencies.] For $\psi = 90°$ only the extraordinary

wave can propagate. Between the proton gyrofrequency and the lower hybrid resonance frequency, one mode can propagate for all values of ψ as illustrated by the index of refraction surface for 2000 cps, and for 10 kc/s. The index of refraction has a finite value at $\psi = 90°$ because of the inclusion of the ion terms in the expression for the index of refraction [see Appendix A]. This possibility of transverse propagation was first pointed out by Hines [1957]. For frequencies above the lower hybrid resonance frequency (12 kc/s) one mode can propagate but only for angles less than ψ_{res} as shown by the index of refraction surface for 100 kc/s; therefore, transverse propagation cannot occur for frequencies above the lower hybrid resonance frequency.

Combining the graphical ray tracing method of Poeverlein [1948, 1949, and 1950] and the mathematical expressions of Haselgrove [1955], a set of two dimensional ray tracing equations can be derived. These cartesian equations describe a ray path in a horizontally stratified ionosphere, but, by deriving them insight into the formulation of the general three dimensional equations can be gained. From Figure 1b Poeverlein's graphical ray tracing method can be illustrated. In Figure 1b is shown an index of refraction surface and a wave normal direction to the local z axis given by Δ. Poeverlein chose the x axis to be parallel to the planes of

stratification. For entrance of a wave from below the ionosphere the component of the refractive index parallel to planes of stratification is given by sin Θ_i where Θ_i is the incident angle. By Snell's law this component must be conserved along the ray path. For each point along the ray path an index of refraction surface is drawn and the direction of $\vec{n}$ determined by the surface and by Snell's law, n sin Δ = sin Θ_i. The direction of the ray is given by the normal to the surface at $\vec{n}$. After moving an increment along p, a new index of refraction surface is computed and the process continued.

This Poeverlein procedure can be generalized and used to derive a set of ray tracing equations. In Figure 1b we let z be in the direction perpendicular to the earth's surface and allow the planes of stratification to be at an angle ϕ to the z axis. The direction between the z axis and $\vec{n}$ is given by Δ, between the magnetic field and $\vec{n}$ by ψ, and between the z axis and the ray direction $\hat{p}$ by χ. By the local stratification direction we mean the direction for which ∇ n is zero for $\vec{n}$ in a fixed direction. If $\hat{l}$ is a unit vector given by ϕ then we have

$$\nabla n \cdot \hat{l} = 0$$

$$\left(\frac{\partial n}{\partial x} \hat{x} + \frac{\partial n}{\partial z} \hat{z} \right) \cdot \left(\sin \phi \hat{x} + \cos \phi \hat{z} \right) = 0$$

$$\frac{\partial n}{\partial x} \sin \phi + \frac{\partial n}{\partial y} \cos \phi = 0 . \qquad (4)$$

For the special case of $\phi = 90°$, we have $\partial n/\partial x = 0$ which was the assumption of Poeverlein. By the chain rule of differentiation

$$\frac{dn}{ds} = \frac{\partial n}{\partial x} \frac{dx}{ds} + \frac{\partial n}{\partial y} \frac{dy}{ds} + \frac{\partial n}{\partial \Delta} \frac{d\Delta}{ds} \qquad (5)$$

since $n = n(x, z, \Delta)$. From Figure 1b it can be seen that

$$\frac{dx}{ds} = \sin \chi$$
$$\frac{dz}{ds} = \cos \chi \qquad (6)$$

where ds is an element of length along the ray path. Equation (5) can then be written

$$\frac{dn}{ds} = \frac{\partial n}{\partial x} \sin \chi + \frac{\partial n}{\partial z} \cos \chi + \frac{\partial n}{\partial \Delta} \frac{d\Delta}{ds} . \qquad (7)$$

By Snell's law the component of the refractive index along the direction of stratification must be conserved along the ray path. Therefore

$$\frac{d}{ds} (n \cos (\phi - \Delta)) = 0. \qquad (8)$$

Equation (8) is differentiated with the assumption that ϕ does not change along the path ($d\phi/ds = 0$):

$$\frac{dn}{ds} \cos (\phi - \Delta) + n \sin (\phi - \Delta) \frac{d\Delta}{ds} = 0 . \qquad (9)$$

Putting equation (7) into equation (9) and dividing through by $\cos (\phi - \Delta)$, we obtain

$$\frac{\partial n}{\partial x} \sin \chi + \frac{\partial n}{\partial z} \cos \chi + \frac{d\Delta}{ds} \left(\frac{\partial n}{\partial \Delta} + n \tan (\chi - \phi) \right) = 0 . \qquad (10)$$

Equation (10) can be written in terms of Δ and of derivatives of the index of refraction by eliminating the angles χ and ϕ. From the previous discussion we demonstrated the angle α between the wave normal ($\vec{k}$ or $\vec{n}$) and the ray normal $\vec{p}$ was given by equation (3)

$$\tan \alpha = - \frac{1}{n} \frac{\partial n}{\partial \psi} \quad . \tag{3}$$

From Figure 1b it is also seen that

$$\chi = \Delta + \alpha \, . \tag{11}$$

Also from equation (4) we have

$$\tan \phi = - \partial n/\partial z \Big/ \partial n/\partial x \, . \tag{12}$$

By noting that $\partial n/\partial \Delta = - \partial n/\partial \psi$ and by using equations (3), (11), and (12) in (10), we obtain a differential equation describing the variation of Δ along the ray path:

$$\frac{d\Delta}{ds} = \frac{\frac{\partial n}{\partial z} \sin \Delta - \frac{\partial n}{\partial x} \cos \Delta}{\left(n^2 + \left(\frac{\partial n}{\partial \psi}\right)^2\right)^{1/2}} \quad . \tag{13}$$

Differential equations for the variation of x and z along the ray path are obtained by using equations (11) and (3) in equation (6):

$$\frac{dx}{ds} = \frac{n \sin \Delta + \frac{\partial n}{\partial \psi} \cos \Delta}{\left(n^2 + \left(\frac{\partial n}{\partial \psi}\right)^2\right)^{1/2}} \tag{14}$$

$$\frac{dz}{ds} = \frac{n \cos \Delta - \frac{\partial n}{\partial \psi} \sin \Delta}{\left(n^2 + \left(\frac{\partial n}{\partial \psi}\right)^2\right)^{1/2}} \quad . \tag{15}$$

Equations (13), (14), and (15) can be given in terms of an independent parameter, the phase time, by considering the phase velocity along the ray path. The projection of the phase refractive index along the ray path is given by

$$n_r = n \cos \alpha \tag{16}$$

where n_r is called the ray refractive index. Therefore, the ray velocity is written

$$v_r = \frac{ds}{dt} = \frac{1}{n \cos \alpha} = \frac{\left(n^2 + \left(\frac{\partial n}{\partial \psi}\right)^2\right)^{1/2}}{n^2} \quad . \tag{17}$$

Multiplying both sides of equations (13), (14), and (15) by (17) we obtain a set of two dimensional equations capable of describing a ray path in a horizontally stratified ionosphere with a constant magnetic field direction:

$$\frac{dx}{dt} = \frac{1}{n^2}\left(n \sin \Delta + \frac{\partial n}{\partial \psi} \cos \Delta\right)$$

$$\frac{dz}{dt} = \frac{1}{n^2}\left(n \cos \Delta - \frac{\partial n}{\partial \psi} \sin \Delta\right)$$

$$\frac{d\Delta}{dt} = \frac{1}{n^2}\left(\frac{\partial n}{\partial z} \sin \Delta - \frac{\partial n}{\partial x} \cos \Delta\right) . \qquad (18)$$

It was these ray tracing equations with the quasi-longitudinal approximation for the refractive index that Haselgrove [1957] used to calculate sample whistler ray paths.

In order to derive the set of ray tracing equations (18) two assumptions were made which are not valid for the case of an ionosphere with a centered dipole magnetic field and with concentration gradients in altitude and latitude. First it was assumed that the direction of the planes of local stratification, given by ϕ, was constant along the ray path ($d\phi/ds = 0$). Second,

it was assumed that the direction of the magnetic field was constant ($\partial n/\partial \psi = -\partial n/\partial \Delta$).

Haselgrove [1955] and Haselgrove and Haselgrove [1960] made an important contribution to the problem of ray tracing by deriving a closed set of first order differential equations in general curvilinear coordinates. This general set of equations can be written in spherical polar coordinates and both the centered dipole magnetic field and the concentration gradients can be treated without the assumptions used in deriving equations (18). Because these differential equations are first order in an independent variable (phase time), they are readily integrated numerically in a digital computer. Fermat's principle of stationary time is the starting point for the Haselgrove derivation:

$$\delta \int_{\text{path}} n_r \, ds = 0 \qquad (19)$$

where n_r is the ray refractive index given by equations (16) and (17) and ds is an element of path length. Equation (19) states that the time of travel of the phase front of the wave along a particular ray path between two points is a maximum or a minimum for small variations of the path. General functions are then written

to describe the two surfaces: (1) the refractive index surface in terms of the three spatial coordinates and the three components of the refractive index (vector), and (2) the ray surface in terms of the three spatial coordinates and the three components of the ray velocity. It is found that these two surfaces are the reciprocal surfaces of Hamilton [see Synge, 1954]. From the properties of these reciprocal surfaces and from Fermat's principle it is found that the expressions for these two surfaces satisfy Euler's equations. By considering a special case for Finsler spaces, Haselgrove [1955] writes the equations for a ray path in terms of the Christoffel symbol of the second kind which includes the curvilinear metric. By using the metric for spherical polar coordinates, a three-dimensional set of ray tracing equations appropriate for tracing ray paths in a model ionosphere is obtained:

$$\frac{dr}{dt} = \frac{1}{n^2} \left(\rho_r - n \frac{\partial n}{\partial \rho_r} \right)$$

$$\frac{d\theta}{dt} = \frac{1}{n^2} \left(\rho_\theta - n \frac{\partial n}{\partial \rho_\theta} \right)$$

$$\frac{d\phi}{dt} = \frac{1}{r\, n^2 \sin\theta} \left(\rho_\phi - n \frac{\partial n}{\partial \rho_\phi}\right)$$

$$\frac{d\rho_r}{dt} = \frac{1}{n} \frac{\partial n}{\partial r} + \rho_\theta \frac{d\theta}{dt} + \rho_\phi \frac{d\phi}{dt} \sin\theta$$

$$\frac{d\rho_\theta}{dt} = \frac{1}{r} \left(\frac{1}{n} \frac{\partial n}{\partial \theta} - \rho_\theta \frac{dr}{dt} + r\, \rho_\phi \frac{d\phi}{dt} \cos\theta\right) \qquad (20)$$

$$\frac{d\rho_\phi}{dt} = \frac{1}{r \sin\theta} \left(\frac{1}{n} \frac{\partial n}{\partial \phi} - \rho_\phi \frac{dr}{dt} \sin\theta - r\rho_\phi \frac{d\theta}{dt} \cos\theta\right) .$$

where r, θ, ϕ are the spherical polar coordinates, n is the phase refractive index, ρ_r, ρ_θ, ρ_ϕ are the components of the index of refraction vector $n^2 = \rho_r^2 + \rho_\theta^2 + \rho_\phi^2$, and t is the phase time along the ray path.

One important feature of ray tracing with spherical polar coordinates in the ionosphere not emphasized by Haselgrove [1955] is that there is no generalized form of Snell's law. Only in the case that ∇n is a constant vector for a given $\vec{n}$, can a form of Snell's law be derived from this generalized coordinate treatment.

In cartesian coordinates equations (4) and (8) for our two-dimensional case can be recovered under this condition.

For this present ray tracing study, the equations (20) are specialized to expressions for ray tracing in a magnetic meridian. Neglect of deviations of the ray path in the ϕ direction is a good first approximation when a centered dipole approximation for the magnetic field is used, and when the magnitude of concentration gradients in the ϕ direction is considered. The expression for a dipole magnetic field has no ϕ dependence, therefore the ϕ component of ∇B is zero. Also, the longitudinal (diurnal) gradients in the electron and ion concentrations in the ionosphere are generally much smaller than the gradients with radial distance and with latitude and, too, the index of refraction is greater perpendicular to the magnetic meridian so that lightning energy tends to be refracted into the magnetic meridian. Therefore, the refractive index has a small ϕ and ρ_ϕ dependence and the ray path would not be expected to deviate appreciably in the ϕ direction. For the case that $\rho_\phi = 0$ initially and where $\partial n/\partial\phi = 0$ and $\partial n/\partial \rho_\phi = 0$, the ray must stay in the magnetic meridian. The two dimensional ray tracing equations used in this ray tracing study are

$$\frac{dr}{dt} = \frac{1}{n^2} \left(\rho_r - n \frac{\partial n}{\partial \rho_r}\right)$$

$$\frac{d\theta}{dt} = \frac{1}{rn^2} \left(\rho_\theta - n \frac{\partial n}{\partial \rho_\theta}\right)$$

$$\frac{d\rho_r}{dt} = \frac{1}{n} \frac{\partial n}{\partial r} + \rho_\theta \frac{d\theta}{dt}$$

$$\frac{d\rho_\theta}{dt} = \frac{1}{r} \left(\frac{1}{n} \frac{\partial n}{\partial \theta} - \rho_\theta \frac{dr}{dt}\right) \qquad (21)$$

where the expressions for n, $\frac{\partial n}{\partial \rho_r}$, $\frac{\partial n}{\partial \rho_\theta}$, $\frac{\partial n}{\partial r}$, and $\frac{\partial n}{\partial \theta}$ are given in Appendix A based on the formulation of Stix [1962] for a cold plasma. In addition, differential equations for the path length along the ray path and the group delay time are given by Haselgrove [1955]:

$$\frac{dS}{dt} = \frac{1}{n^2} \left(n^2 + \left(\frac{\partial n}{\partial \psi}\right)^2\right)^{1/2} \qquad (22)$$

$$\frac{dT}{dt} = \frac{1}{c} \left(1 + \frac{\omega}{n} \frac{\partial n}{\partial \omega}\right) \qquad (23)$$

where ψ is the angle between the magnetic field direction and the

index of refraction vector $\vec{n}$ (see Figure 1b), ω is the wave frequency in rad sec^{-1}, and c is the velocity of light in a vacuum.

III. SPECIAL CASES OF RAY TRACING EQUATIONS

The two dimensional ray tracing equations (21) cannot in general be integrated in closed form for the case of a curved ionosphere with a centered dipole magnetic field. There are, however, two special cases for which the ray trajectory and the direction of the index of refraction vector $\vec{n}$ along this trajectory can be completely specified analytically. From Figure 1a we saw that the angle α between the wave normal direction ($\vec{n}$) and the ray normal direction (p) became zero for propagation exactly perpendicular and exactly parallel to the magnetic field direction. Since the phase index of refraction can be finite for $\psi = 0°$ and $\psi = 90°$ (for frequencies less than the lower hybrid resonance frequency, see Hines [1957]), it must be the case, from equation (3), that

$$\frac{\partial n}{\partial \psi} = 0 . \qquad (24)$$

The fact that $\partial n/\partial \psi$ must be zero can also be seen from the explicit equations for $\partial n/\partial \psi$ (A17) and (A18) in Appendix A. Both $\partial A/\partial \psi$ and $\partial B/\partial \psi$ depend on the product $\sin \psi \cos \psi$ so that they are zero for

$\psi = 0°$, $\psi = 90°$ and consequently $\partial n/\partial\psi = 0$. Then by equation (A15) in Appendix A,

$$\frac{\partial n}{\partial \rho_r} = 0$$

$$\frac{\partial n}{\partial \rho_\theta} = 0 \,. \tag{25}$$

With the expressions (25) the two dimensional ray tracing equations become

$$\frac{dr}{dt} = \frac{\rho_r}{n^2} \,. \tag{26}$$

$$\frac{d\theta}{dt} = \frac{\rho_\theta}{r n^2} \,. \tag{27}$$

$$\frac{d\rho_r}{dt} = \frac{1}{n}\frac{\partial n}{\partial r} + \frac{\rho_\theta^2}{r n^2} \,. \tag{28}$$

$$\frac{d\rho_\theta}{dt} = \frac{1}{r}\left(\frac{1}{n}\frac{\partial n}{\partial \theta} - \frac{\rho_r \rho_\theta}{n^2}\right) . \tag{29}$$

These equations can now be integrated for the cases of exactly transverse and of exactly longitudinal propagation. This development is similar to that of Hoffman [1960].

A. Exactly Transverse Propagation

Just as propagation nearly longitudinal to the magnetic field lines was found to occur at high latitudes in the case of electron whistlers [Storey, 1953], one might expect that at the equatorial latitudes, effects due to nearly transverse propagation would occur. In the equatorial region energy from lightning sources coupled into the ionosphere nearly radially has initial wave normal angles (ψ) that are very close to 90° to the magnetic field direction. Because of the observational data from the Injun III satellite near the equatorial plane presented by Pfeiffer et al. [1966] and Pfeiffer [1966] suggest transverse propagation, we consider the case of propagation exactly transverse to the magnetic field lines.

For a centered dipole geomagnetic field we have by equation (A36) in Appendix A that

$$\tan \gamma = \frac{1}{2} \tan \theta \qquad (30)$$

where γ is the angle of the magnetic field direction at a point on the ray path with respect to the radius from the center of the earth to that point, and θ is the colatitude angle. As shown in

Figure 1b, Δ is the angle between the index of refraction vector $(\vec{n})$ and the radius so that

$$\rho_r = n \cos \Delta$$

$$\rho_\theta = n \sin \Delta \, . \qquad (31)$$

Because propagation is exactly transverse to the magnetic field lines $\Delta = \gamma - 90°$ and equations (31) can be written

$$\rho_r = n \sin \gamma$$

$$\rho_\theta = -n \cos \gamma \, . \qquad (32)$$

Using equations (32) in the specialized ray tracing equations (26) and (27) we obtain

$$\frac{dr}{dt} = \frac{1}{n} \sin \gamma$$

$$\frac{d\theta}{dt} = -\frac{1}{rn} \cos \gamma$$

and therefore

$$\frac{1}{r}\frac{dr}{dt} = -\tan\phi\ \frac{d\theta}{dt}$$

and from (30)

$$\frac{1}{r}\frac{dr}{dt} = -\frac{1}{2}\tan\theta\ \frac{d\theta}{dt}\ . \qquad (33)$$

Equation (33) is an exact differential equation in which the variables are separated and can be written

$$\frac{d}{dt}\ln r = -\frac{1}{2}\tan\theta\ \frac{d\theta}{dt}$$

for which the solution is

$$\ln r = \frac{1}{2}\ln\cos\theta + \text{const}$$

or

$$r = K_1\cos^{1/2}\theta\ . \qquad (34)$$

Equation (34) is the trajectory of the ray which propagates exactly transverse to the magnetic field lines; K_1 parameterizes a set of curves that are everywhere perpendicular to the dipole magnetic lines of force.

From equations (28) and (29) the required variation of the phase index of refraction (n) along the ray path in order that transverse propagation be maintained can be obtained. From the definition of the angle Δ in terms of ρ_r and ρ_θ

$$\Delta = \cos^{-1} \frac{\rho_\theta}{(\rho_r^2 + \rho_\theta^2)^{1/2}}$$

it is found that

$$\frac{d\Delta}{dt} = \frac{1}{n^2} \left(\rho_r \frac{d\rho_\theta}{dt} - \rho_\theta \frac{d\rho_r}{dt}\right)$$

and using equations (28) and (29) and the relations (32)

$$\frac{d\Delta}{dt} = \frac{1}{n} \left(\frac{\sin\gamma}{r} \frac{\partial n}{\partial \theta} + \cos\gamma \frac{\partial n}{\partial r} + \frac{n \cos\gamma}{r} \right) . \qquad (35)$$

Also from the relation of γ and Δ and the relation of γ and θ we have

$$\frac{d\Delta}{dt} = -\frac{d\gamma}{dt} = \frac{-2}{1 + 3\cos^2\theta} \frac{\cos\phi}{r} = \text{equation (35).} \qquad (36)$$

Equation (36) can then be expressed

$$- \tan \theta \frac{\partial}{\partial \theta} \ln n^2 - 2r \frac{\partial}{\partial r} \ln n^2 = 12 \frac{1 + \cos^2 \theta}{1 + 3 \cos^3 \theta} . \tag{37}$$

Following the usual procedure for the solution of partial differential equations we must solve two of the following equations:

$$- \frac{d\theta}{\tan \theta} = \frac{dr}{-2r} = \frac{d \ln n^2}{12 \frac{1 + \cos^2 \theta}{1 + 3 \cos^2 \theta}} . \tag{38}$$

The solution to

$$\frac{d\theta}{\tan \theta} = \frac{dr}{2r}$$

is

$$\frac{\sin \theta}{r^{1/2}} = C_1 , \tag{39}$$

and

$$- \frac{d\theta}{\tan \theta} = \frac{d \ln n^2}{12 \dfrac{1 + \cos^2 \theta}{1 + 3 \cos^2 \theta}}$$

has the solution

$$\frac{n^2 \sin^6 \theta}{1 + 3 \cos^2 \theta} = C_2 . \tag{40}$$

With the relations (39) and (40) the most general solution to the partial differential equation (37) is obtained:

$$\frac{n^2 \sin^6 \theta}{1 + 3 \cos^2 \theta} = f \left(\frac{\sin \theta}{r^{1/2}} \right)$$

or

$$n_T^2 = K_2 \frac{1 + 3 \cos^2 \theta}{\sin^6 \theta} f \left(\frac{\sin \theta}{r^{1/2}} \right) \tag{41}$$

where n_T is the transverse phase refractive index, K_2 is a const, $f \left(\frac{\sin \theta}{r^{1/2}} \right)$ is an arbitrary function of its argument, and θ is colatitude. This expression (41) for the transverse refractive index along the trajectory differs from the

expression given by Hoffman [1960] since he incorporated into his arbitrary constant (A_1) constants of the form (39).

The interpretation of equations (34) and (41) are as follows: If, for a wave propagating in the ionosphere, the wave normal angle with respect to the magnetic field direction ψ becomes $\pm$ 90°, the ray will maintain a path exactly transverse to the magnetic field lines, given by (34), if and only if the transverse index of refraction squared along this path is given by equation (41). Any deviation from (41) means that transverse propagation would not be maintained.

Hoffman [1960] concluded that the refractive index given by (41) did not appear to be appropriate to the ionosphere. In drawing this conclusion he considered two properties of his equivalent expression to equation (41). First, he equated the expression for the transverse refractive index from magnetoionic theory (equivalent to $n_T^2 = RL/S$ in Stix's formulation, see Appendix A) to equation (41) and specialized to the case of <u>free electrons only</u>. We emphasize, as Hines pointed out [1957], that when only electrons are considered, propagation transverse to the magnetic field cannot occur at any frequency. The index of refraction surface for all frequencies is like the one for 100 kc/s in Figure 2; the index of refraction is imaginary for transverse propagation.

Hoffman's case was therefore unphysical and his conclusion about possible transverse propagation in the ionosphere invalid from that consideration. Second, Hoffman argued that the angular dependence required by equation (41), $f\left(\frac{\sin\theta}{r^{1/2}}\right)$, was symmetric about the equator but not the north pole. We point out that any even function of $\sin\theta/r^{1/2}$ is symmetric about both the equator and the north pole. Again the possibility of transverse propagation in the ionosphere cannot be eliminated on the symmetry argument.

In the section on riser whistlers (Section VIII), however, we consider again this problem of transverse propagation with the effects of ions included and for frequencies less than the lower hybrid resonance frequency. In that section we find that exactly transverse propagation is not possible over appreciable path lengths near the magnetic equatorial plane.

B. Exactly Longitudinal Propagation

By a completely analogous procedure to that of part A, the ray path and the index of refraction variations along the ray path to maintain exactly longitudinal propagation are determined. For the case of exactly longitudinal propagation $\Delta = \gamma$ and we can write

$$\rho_r = n \cos \gamma$$

$$\rho_\theta = n \sin \gamma \, . \tag{42}$$

The two dimensional ray tracings equations (26), (27), (28), and (29) become

$$\frac{dr}{dt} = \frac{n \cos \gamma}{n^2} \tag{43}$$

$$\frac{d\theta}{dt} = \frac{n \sin \gamma}{r\, n^2} \tag{44}$$

$$\frac{d\rho_r}{dt} = \frac{1}{n} \frac{\partial n}{\partial r} + \frac{\sin^2 \gamma}{r} \tag{45}$$

$$\frac{d\rho_\theta}{dt} = \frac{1}{rn} \frac{\partial n}{\partial \theta} - \frac{\sin \gamma \cos \gamma}{r} \, . \tag{46}$$

Equations (43) and (44) are solved for the ray path which is given by

$$r = K_3 \sin^2 \theta \tag{47}$$

and which is just the equation of a magnetic field line as we would expect. Equations (45) and (46) are combined to give $d\Delta/dt$ and then equated to $-d\gamma/dt$. The solution of the resulting partial differential equation is made up of the functions

$$\frac{\cos\theta}{r^2} = C_3$$

$$\frac{n^2}{\frac{1 + 3\cos^2\theta}{\cos^3\theta}} = C_4$$

from which we obtain

$$n^2 = \frac{1 + 3\cos^2\theta}{\cos^3\theta} \, f\left(\frac{\cos\theta}{r^2}\right) . \qquad (48)$$

For propagation exactly along a field line (equation (47)) the longitudinal refractive index must be given by equation (48). Considering both the case of the Alfvén fast mode and the whistler mode refractive indices, it appears that neither of these modes could maintain longitudinal propagation. For the Alfvén fast mode we have [Stix, 1962]:

$$n^2 = 1 + \frac{\pi_e^2 + \pi_i^2}{\Omega_e^2} \simeq 1 + \frac{\pi_e^2}{\Omega_e^2} \qquad (49)$$

and for the whistler mode [Storey, 1953]

$$n^2 \simeq \frac{\pi_e^2}{\omega \Omega_e} . \qquad (50)$$

Since $\Omega_e \alpha (1 + 3 \cos^2 \theta)^{1/2}$ and the electron density falls off approximately as r^{-3} or r^{-4} along a field line [J. J. Angerami, private communication], it seems that a function of $\cos \theta / r^2$ does not exist to satisfy either (49) or (50) and (48). Indeed, in Section V we find that ray paths for different frequencies do not follow the magnetic field lines nor even the same path.

C. Retraceability of Ray Paths

One last special case of the general set of ray tracing equations (21) is that of the requirement for exactly retracing a ray path. From the symmetry of the index of refraction surfaces about the magnetic field direction such as those in Figure 2 and the Poeverlein construction method in Figure 1b, it can be expected that the changing of the wave normal direction by 180° would cause a ray path to be retraced exactly. This retraceability requirement can be deduced from the general ray tracing equations.

On rotating Δ and ψ by 180° we have

$$\rho_r = n \cos \Delta \rightarrow - n \cos \Delta = - \rho_r$$

$$\rho_\theta = n \sin \Delta \rightarrow - n \sin \Delta = - \rho_\theta$$

and $$\cos \psi \rightarrow - \cos \psi$$

$$\sin \psi \rightarrow - \sin \psi$$

so that $$\frac{\partial n}{\partial \rho_i} \rightarrow - \frac{\partial n}{\partial \rho_i}$$

by equations (A16) and (A15) of Appendix A. Giving a similar consideration to $\partial n/\partial x_i$ in the form given by equation (A19) it is found that $\partial n/\partial x_i$ do not change sign. Therefore for $\vec{n}$ (wave normal direction) rotated by 180° at any point on the ray path, the ray tracing equations transform as follows:

$$\frac{dr}{dt} \rightarrow - \frac{dr}{dt}$$

$$\frac{d\theta}{dt} \rightarrow - \frac{d\theta}{dt}$$

$$\frac{d\rho_r}{dt} \rightarrow \frac{d\rho_r}{dt}$$

$$\frac{d\rho_\theta}{dt} \rightarrow \frac{d\rho_\theta}{dt} \quad . \qquad (51)$$

The ray path would be retraced. This retraceability feature is important in determining the integration accuracy of the ray tracing computer program.

With Sections II and III we have met the first objective of this ray tracing study. We found that, for an anisotropic, inhomogeneous, but non-absorbing medium such as the ionosphere, the Poynting vector and wave packet methods of specifying a ray path were identical. By ray path we mean the trajectory which the energy associated with an electromagnetic wave takes through the medium. Based on a generalized form of Poeverlein's graphical ray tracing method with index of refraction surfaces, a two dimensional set of ray tracing equations appropriate for a horizontally stratified medium, was derived. In the derivation we illustrated the use of Snell's law and described the use of index of refraction surfaces for understanding ray behavior. Solutions were obtained to the ray tracing equations for the two special cases that can be solved in closed form; propagation exactly transverse and exactly parallel to the magnetic field direction. Also it was determined that a ray path would be exactly retraced if the wave normal were rotated by 180° ($\vec{n} \rightarrow -\vec{n}$).

IV. RAY TRACING COMPUTER PROGRAM

In the preceding section the two-dimensional ray tracing equations (21) were integrated for the very special cases of exactly transverse and exactly longitudinal propagation with respect to the magnetic field direction. For the general case in which the angle with respect to the magnetic field ψ is not initially 0 or 90° and can also vary along the ray path, the equations (21) can be integrated numerically on a digital computer. Haselgrove [1955] derived the equations in the particular form (21) for numerical integration.

A. Brief Description of Program

A computer program capable of integrating the ray tracing equations (21) has been written for this ray tracing study. The integration routine is started by the fourth Runge-Kutta routine and these starting points are fed into a modified Adam-Bashforth fourth order routine for the bulk of the ray path calculations [Abranowitz and Stegen, 1964]. Starting values for altitude, latitude, initial wave normal direction Δ with respect to the radius vector, and wave frequency are required. Also, the reference altitude, electron density, fractional ion density, and temperature at this reference

altitude must be specified for the particular diffusive equilibrium ionosphere desired (see equations (A27) to (A32) in Appendix A). For each point along the ray path the program computes and prints out radial altitude, latitude, wave normal angle with respect to the radius Δ, r-component of the refractive index ρ_r, θ-component of the refractive index ρ_θ, total path length to that point, total time delay to that point, the wave normal angle with respect to the magnetic field direction, and any other desired quantities for the specific ray tracing problem. In Appendix B a block diagram of the computer program is explained and the special features of the program discussed. In Appendix C the model ionospheres used for this ray tracing study are illustrated and discussed.

B. Comparison with Previous Results

Two other ray tracing studies by numerical integration of the ray tracing equations (21) have been carried out. As reviewed in the Introduction, Yabroff [1961] considered the case of electrons only. Kimura [1966] was the first worker to publish results of ray paths in the ionosphere with the effects of ions included to explain observed phenomena. Below we compare the results of this ray tracing program to those of Yabroff and Kimura.

1. Comparison with Yabroff [1961]

In order to compare the results of the present program and those of Yabroff we expressed the electron density as a function of geocentric distance in the same form used by Yabroff:

$$n_e = 1.8 \times 10^5 \exp(-4.183119 (r - 1.0471)) \qquad (52)$$

where r is in earth radii from the center of the earth. The specialization of the program to the case of electrons only was accomplished by limiting the summation of terms for the refractive index and the various derivatives given in Appendix A to the electron terms only. The program was otherwise unchanged from the program including ion terms. Ray paths were calculated starting at 45° latitude and 300 km altitude with an initial wave normal angle to the radius vector of $\Delta_o = 0°$ and for frequencies of 5 kc/s to 500 kc/s.

For frequencies above 200 kc/s the calculated ray paths were nearly coincident; within 100 km and 2°. For frequencies below 20 kc/s, however, the calculated ray paths reached higher altitudes (by 1000 km) than those presented by Yabroff. We argue that this discrepancy can be resolved by the following facts:

a. Yabroff reports that he used an Adams predictor-corrector integration method and that the corrector was applied only every five or ten points. This present program, however, uses both the predictor and corrector for every point. For frequencies below 20 kc/s the path lengths were longer than for the higher frequencies therefore in Yabroff's program appreciable integration error could accumulate for the longer paths.

b. He also reports that his integration interval was one-half an earth radii. This present program, however, used a much smaller integration interval of approximately 15 km which improves the integration accuracy. From a numerical integration argument it appears that the present computer program would have much less integration error and should calculate more exact ray path since the corrector is applied for every point and the integration interval is much smaller.

c. From a physical argument it would seem that the maximum altitude of a ray path should increase with decreasing wave frequency. From the 100 kc/s index of refraction surface in Figure 2 we see that for all wave normal angles, the ray propagates very nearly along the magnetic field line. Assume that a similar index of refraction surface is obtained when $\omega/\Omega_e \simeq C_1$, the wave frequency-electron gyrofrequency ratio is equal to a given value.

With guiding along the field line a ray would reach a maximum altitude for this frequency ratio near the equator and then tend to follow the field line down. Therefore, for a lower wave frequency Ω_e would be lower and the maximum altitude would be higher. Yabroff's ray paths exhibit, however, a constant maximum altitude for frequencies less than 20 kc/s. In the next section it is found that with ions included the lower frequency ray paths do reach a higher maximum altitude.

2. Comparison with Kimura [1966]

To compare the results of the present program including ions to those of Kimura, a diffusive equilibrium model ionosphere similar to Kimura's was used. The model had the following parameters at the reference altitude:

Reference altitude:	500 km
Temperature:	1000° K
H^+ percent:	0.156
He^+ percent:	1.96
Electron density:	38000 cm^{-3}

Comparison of the two ray paths starting at 30° magnetic latitude with an initial wave normal angle of $\Delta_0 = 0$ (radially upward) for a frequency of 1 kc/s is made in Figure 3. To a

latitude of approximately 30° S the ray paths are nearly coincident. Our ray path attains a higher altitude presumably because the electron density chosen for the model (3.8×10^4 cm^{-3} at 500 km) was not exactly the value used by Kimura. Another reason for this difference may be due to slightly different integration routines. At 30° S latitude, however, the two ray paths differ quite markedly. Kimura's ray path is refracted to higher altitudes and reflects back and forth between approximately $\pm$ 30° latitude while increasing in altitude. The maximum altitude of 3 R_E Kimura reports to be the altitude at which the lower hybrid frequency is equal to the wave frequency (1 kc/s). Our ray is not, however, refracted upward but continues downward and intercepts 300 km altitude at a latitude of approximately 55° S (much in the same manner as Yabroff's results). We present the following arguments to justify our result:

a. On the ray path of Kimura the wave normal direction was not indicated. From our ray path, however, we can obtain the behavior of the wave normal since if the wave normal angle variation along our ray path were very much different than along the path obtained by Kimura (to 30° S), the ray paths would also be significantly different.

b. At the altitude and latitude in question (approximately 5000 km and 30° S) we find that the wave normal with respect to the magnetic field ψ is at 45° and that the radial component of the index of refraction ρ_r has gone to zero giving a wave normal angle with respect to the radius of 90°. From the index of refraction surfaces in Figure 2 for 2 and 10 kc/s we see that the ray could not possible turn around for $\psi = 45°$. Transverse propagation and abrupt changes of direction can occur only when ψ goes through 90°. We suggest that, as ρ_r went through zero in Kimura's program, the sign of ρ_r did not change, therefore, the wave normal ψ changed discontinuously with respect to the magnetic field and the ray began propagating upward.

c. In order to test the consistency of our program we reversed the ray direction by 180° at the final altitude and latitude. From the reversibility condition derived in Section III we expected that the ray would retrace its path which it did to within a few tenths of a percent in ending latitude and wave normal direction.

d. In the following sections we present the explanations of several observed VLF noise phenomena based on our ray tracing program and for the case that the ray is not refracted as shown by Kimura. Since these explanations exhibit quantitative agreement with the observed phenomena we conclude that our program is correct.

Comparisons of ray paths with Kimura for larger initial wave normal angles (Δ_o) and for paths from 30° have been made. For Δ_o = 20° (with respect to the radius vector) the two programs agree within 50 km and 0.5° latitude for a ray refracted at approximately 800 km [see Kimura, 1966, Figure 8]. In this case the condition for ψ = 90° was reached before Δ = 90° ($\rho_r \rightarrow 0$) indicating that the two programs are in agreement except for the problem discussed above.

C. Self-Consistency of Computer Program

To obtain the quantitative accuracy of the computer program and its self-consistency, two tests were performed. First, the program was converted to perform ray tracing in a horizontally stratified medium for which the results are known analytically, and second, several ray paths were retraced.

1. Horizontally Stratified Ray Tracing

As demonstrated by our derivation of the two dimensional ray tracing equations for a horizontally stratified ionosphere (18) in Section II, Snell's law is applicable. For any ray path in a horizontally stratified ionosphere, the component of the refractive index along the direction of stratification must be

conserved. To test the ray tracing program but to maintain its polar coordinate system a coordinate transformation was performed: $X = r \cos \theta$, $Z = r \sin \theta$. B was chosen constant in the Z-direction (parallel to the equatorial plane) and the ion and electron densities consequently varied only in the Z-direction. The geometry for the ray tracing is depicted by the insert in Figure 4. In terms of the coordinate transformation the X component of the refractive index is given by

$$\rho_x = \rho_\theta \sin \theta - \rho_r \cos \theta \tag{53}$$

and it is this component which should be conserved.

In Figure 4 are shown three ray paths, two for 2.5 kc/s with $\Delta_o = 30°$ and 0°, and one for 100 kc/s with $\Delta_o = 0°$. The direction of stratification and of the magnetic field lines are indicated in the coordinate system of radial altitude and magnetic latitude. As indicated in the insert and on the drawing, the starting latitude was 30° N and altitude 300 km. Curve A for 100 kc/s indicates that the ray did not propagate along the field line but did continue upward with no marked refractions. Curve C for 2.5 kc/s (again $\Delta_o = 0°$), however, turned around at 665 km

since this wave frequency was less than the lower hybrid resonance frequency and transverse propagation was possible. This turning around occurred exactly at the altitude where ρ_x was equal to the phase index of refraction n as predicted. Note that the index of refraction surfaces in Figure 2 illustrate that transverse propagation and therefore refraction ($\psi \rightarrow 90°$) can occur for 2 kc/s but not for 100 kc/s. The ray given by curve B was launched exactly along the field line and continued to propagate along the field line to 4000 km where the integration was stopped. This result is predicted since the strata were exactly perpendicular to the magnetic field direction.

Quantitative evaluation of the integration accuracy can be obtained from the variation of ρ_x along the path. For the eleven cases of different frequency, and initial wave normal angle Δ_o, the maximum deviation of ρ_x along the path was 1.0% and the minimum 0.04% with the average being 0.3%. This constancy of ρ_x to 0.3%, the refraction of curve C, and the guiding of curve B along the field line indicate that the ray tracing program is consistent with ray theory in a horizontally stratified media. We therefore expect this same program to give valid results for the curved ionosphere with a centered dipole field.

2. Reversibility of Ray Paths

Since in Section 3 we showed that if the ray is reversed by 180° it must retrace the same ray path, we have the means for testing the integration accuracy of the program in the case of the model ionosphere. Starting at 30°, 300 km, and $\Delta_o = 0$, a ray path was calculated and then reversed at 300 km in the other hemisphere. After 1330 integration steps and a path length of 44,000 km, the ray returned to within 0.2° (0.6%) of its starting latitude and within 0.06° (0.03%) of its initial wave normal angle at 300 km. The one way integration error would be one half these values which is quite acceptable error for any quantitative evaluation.

V. CHARACTERISTICS OF RAY PATHS

In the preceding sections we have developed a physical understanding of ray paths and have briefly described a computer program capable of computing ray paths in a diffusive equilibrium model ionosphere with a centered dipole magnetic field. In this section we establish the basis for using ray paths as a tool for predicting new VLF noise phenomena, for explaining observed phenomena, and for testing previous explanations of observed phenomena. Yabroff [1961] graphically summarized the characteristics of ray paths in a model ionosphere which contained only electrons. He presented ray path characteristics for variations of frequency, initial latitude, and initial wave normal angle. We now summarize the characteristic behavior of ray path in a model ionosphere which includes electrons and O^+, He^+, H^+ ions in diffusive equilibrium. These characteristics are parameterized by a five parameter set: frequency, initial latitude, initial wave normal angle, initial altitude, and the diffusive equilibrium model, i.e., f, θ_o, Δ_o, R_o, and model. To exhibit the ray path characteristics, four of these parameters are held constant and the fifth parameter varied. Most of the

characteristics of the resulting ray paths are illustrated in Figures 5 through 17. In the next five parts each figure is briefly discussed and the important characteristics summarized.

A. Variation with Wave Frequency f

In Figure 5 are shown ray paths for 5, 10, 20, 50, 100, 200, and 500 kc/s for an initial latitude of $\theta_o = 30°$, an initial wave normal angle of $\Delta_o = 0°$, an initial altitude of $R_o = 300$ km and for the mid-latitude diffusive equilibrium model ionosphere (see Appendix C). In Figures 6 and 7 are plotted the final latitude, maximum altitude, total path time delay and whistler dispersion, and wave normal ψ along the path all as a function of frequency. We note that the ray tracing equations as given in Appendix A are equally valid for all frequencies for which the cold plasma approximation is also valid. We, therefore, summarize the characteristics of ray paths as a function of frequency.

1. From Figure 5 and Figure 6a it is seen that the higher the frequency, the shorter the ray traveled in latitude when it reached the starting altitude of 300 km. The 5 kc/s ray reached 53° S magnetic latitude while the 200 kc/s ray reached only 23° S latitude. Rays for frequencies in between fall on the curve of final latitude vs frequency given in Figure 6a.

Yabroff's results for electrons only [Yabroff, 1961] indicated some latitude focusing for frequencies near 30 kc/s for rays started at $\theta_o = 45°$. In Figure 6a no latitude focusing is apparent.

2. From Figure 5 and 6b it is seen that the higher the frequency, the lower the maximum altitude and the nearer to the starting latitude this maximum altitude occurs. The 5 kc/s ray reached 6000 km at 9° S latitude whereas the 200 kc/s ray reached only 1900 km and at 10° N latitude. Yabroff [1961] found that with electrons only frequencies below the 'nose' frequency (1/4 minimum electron gyrofrequency along the path) attained the same maximum altitude. Figure 6b indicates that the maximum altitude-frequency curve is flatter at 5 kc/s but this frequency is very much below the nose frequency (25 kc/s) for this path.

3. The 500 kc/s ray in Figure 5 achieves a maximum altitude of 600 km at 22° N latitude, begins to fall, and then bends up quite rapidly. From the 100 kc/s index of refraction surface in Figure 2 it is seen that for large wave normal angles ψ, the normal to the surface, which gives the ray direction, can be pointed away from the magnetic field line in a direction opposite of that of the wave normal. For a wave normal angle of approximately

$+\psi_{res}$, the ray can make an angle of $-\beta$ to the magnetic field direction causing the ray to propagate upward in altitude as seen in Figure 5.

4. In Figure 7a is shown the total path time delay and the Eckersley's whistler dispersion

$$D = t\, f^{1/2}$$

as a function of frequency. With increasing frequency the delay time decreases, but the whistler dispersion D tends to increase. For the 5 kc/s ray the dispersion is 36 $sec^{1/2}$ and for the 200 kc/s ray 43.5 $sec^{1/2}$. This dispersion characteristic for the ray paths shown in Figure 5 indicates an interesting feature about whistlers. It would be possible to place a ground VLF receiver at 47° S and to receive a whistler from 5 kc/s to 50 kc/s for which the Eckersley dispersion constant varied only 5.5% over this frequency range. Note that the ray paths for these different frequencies did not follow the same path, nor were the paths guided or ducted nearly along the 30° magnetic field line as was assumed by Storey [1953] and is assumed by others [as in 'nose' whistler analysis, see Smith, 1961]. The final wave normal angles Δ_f (see Figure 7b) were all within 5° of vertical so that the rays could penetrate the lower ionosphere.

5. Figure 7b illustrates the behavior of the wave normal angle with respect to the magnetic field direction ψ along the path. In Figure 5 the wave normal direction for the 50 kc/s ray is indicated by the arrows. A positive value is given to ψ if it is southward of B_o in the northern hemisphere. Initially ψ is -41° and increases to almost -50° for 5 kc/s and to only -44° for 200 kc/s. As the rays approach their final latitude the wave normal is refracted in such a wave that the final wave normal angle with respect to the radius vector Δ_f is very nearly 180°; for 5 kc/s Δ_f = 176.3° and for 200 kc/s, Δ_f = 175.1°.

B. Variation with Initial Latitude, θ_o

In Figure 8 are shown ray paths for θ_o = 5, 10, 15, 20, 30, 40, 45, and 50° latitude with f = 5 kc/s, Δ_o = 0°, R_o = 300 km, and for the mid-latitude model ionosphere. The maximum altitude, total path time delay and dispersion, and final latitude are plotted against the initial latitude in Figures 9a, 9b, and 9c. We conclude the following for the characteristics of ray paths with variation of initial latitude:

1. From Figure 8 and Figure 9a it is seen that the higher the initial latitude, the higher the maximum altitude for a ray.

The ray from 5° initial latitude reached 600 km whereas the ray from 45° reached 17,250 km. Note that as can be seen by comparing the 50° field line and the ray for θ_o = 50° in Figure 8, the ray does not travel along the field line.

2. With increasing latitude the path lengths of the rays become longer and consequently the total path delay becomes longer and the Eckersley dispersion D becomes greater. For the ray from 5° the dispersion was 12 $sec^{1/2}$ and from 45°, 140 $sec^{1/2}$ as shown in Figure 9b.

3. Besides the increasing maximum altitude with increasing initial latitude, Figures 8 and 9c illustrate that the range in latitude also increases. The ray from 5° reached a final latitude (at 300 km altitude) of 9° S while the ray from 45° latitude reached 68° S.

C. Variation with Initial Wave Normal Angle Δ_o.

In Figure 10 are shown ray paths for Δ_o = -10°, -5°, 0°, 5°, and 10° with f = 4 kc/s, θ_o = 30°, R_o = 300 km and for the mid-latitude model ionosphere. Figures 11a, 11b, 11c summarize the variation of maximum altitude. path time delay and dispersion, and final latitude with initial wave normal angle.

1. From Figure 10 and Figure 11a one sees that the maximum altitude is higher for $\Delta_o = 0°$ than for $\Delta_o = \pm 5°, \pm 10°$.

2. Figure 11c illustrates that the range in latitude for $\Delta_o = 10°$ is longer than the range for $\Delta_o = 5°$. Since the maximum altitude was higher for the $\Delta_o = 5°$ ray, the two ray paths must cross as shown in Figure 10 at -8.5° latitude and 1050 km. In Section VII we find that it is this effect of two distinct ray paths for one frequency leads to the explanation of the hook whistler.

3. Another characteristic of ray paths is illustrated by the path for $\Delta_o = -10°$ in Figure 10. At an altitude of 2780 km the ray was refracted to a higher latitude. The wave normal directions along this ray path are given by the arrows. At the top of the ray path $\psi = 90°$ and the ray begins to move transverse to the magnetic field lines returning to the earth at a higher latitude. This same sort of refraction was found to occur in the horizontally stratified ionosphere illustrated in Figure 4. The turning around of rays at low altitudes is an important characteristic and is discussed again in Section VIII on the riser and check whistlers. This refraction at higher latitudes is also the basis for an explanation of the subprotonospheric whistler given by Smith [1964] and Kimura [1966].

4. Because of the difference in path lengths, the time delays for the ray paths are also different as shown in Figure 11b. The sharply refracted path (Δ_o = -10°), however, has proportionately more time delay because it traveled part of its path very nearly transverse to the field line (see Section VIII).

D. Variation with Initial Altitude R_o

Figures 12 to 16 illustrate the characteristics of ray paths for a source of VLF energy located at 4 R_E (R_o = 19113 km) and at the equator θ_o = 0°. Figure 12 shows the behavior of ray paths for f = 1, 5, 10 kc/s and for Δ_o = -90°; Figure 14 and Figure 15 show the behavior of ray paths for 5 kc/s and 1 kc/s, respectively, with Δ_o = -30°, -60°, -90°, -120°, and -150°. The arrows in Figures 12, 14, and 16 give the wave normal direction along the path. From these plots we conclude the following:

1. For an initial wave normal angle of Δ_o = -90° (ψ = 180°), rays for 1, 5, and 10 kc/s traced trajectories given in Figure 12. From Figure 13a we see that the time delay was a minimum for 5 kc/s which is very close to the nose frequency (3 kc/s) for 4 R_E and therefore this result is expected.

2. Figure 13b indicates that the 10 kc/s ray would be seen at a lower latitude 55.5° N (at 300 km) than would 1 kc/s (63° N). If a source of VLF energy were at 4 R_E and emitted all frequencies at $\Delta_o = -90°$, we would expect to see the higher frequencies first with increasing latitude.

3. In Figures 14 and 15 are shown ray paths for a range of Δ_o values and for 5 kc/s and 1 kc/s respectively. Figure 16a illustrates that the time delays for the two frequencies are proportionately the same ($t_1/t_2 = f_1^{-1/2}/f_2^{-1/2}$) for all values of Δ_o except $\Delta_o = -150°$. This 5 kc/s ray propagated up in altitude with its wave normal nearly transverse to the magnetic field. Consequently the time delay was longer for this ray than derived from the Eckersley dispersion law for longitudinal propagation.

4. Figures 14 and 15 and Figure 16b show that the 1 kc/s ray paths spread out further in latitude at 300 km than do the 5 kc/s paths. The 1 kc/s paths cover from 43° to 75° latitude while the 5 kc/s paths cover from 47° to 69° latitude.

5. To obtain any quantitative correspondence between ray paths from a source at high altitudes and VLF noise phenomena

observed at low altitudes, the frequency-time and wave normal direction-time behavior of the source has to be known or assumed.

E. Variation with Model Ionosphere

For the previous calculations, the mid-latitude model ionosphere has been used. This model is discussed in Appendix C (see also Figure 31 and Figure 32). To obtain ray tracing results that can be compared quantitatively to experimental observations of VLF radio noise, one must also know the effects of the particular ionospheric model on these results. In Figure 17 the variation of maximum altitude, final latitude, and time delay and whistler dispersion with frequency are shown. These ray paths have $\theta_o = 30°$, $\Delta_o = 0°$, $R_o = 300$ km, and f = 5, 10, 50, 100, 500 kc/s. The diffusive equilibrium model ionosphere used was the equatorial model discussed in Appendix C (see also Figure 33). On comparing Figure 17 to Figures 6 and 7 for the mid-latitude model ray paths we find the following characteristics:

1. Comparison of Figure 6b and Figure 17a indicates that the maximum altitude vs frequency curves for the two models agree within 200 km.

2. On comparing Figures 6a and 17b we find that the final latitudes for all frequencies agree within 3° for the two models.

3. The significant difference between these two models is shown by comparing Figure 7a and Figure 17c. The total path time delay and therefore whistler dispersion differ by a factor of 2, with the time delay being higher for the equatorial model. This increased time delay is discussed in Section VII in connection with hook whistlers.

In this and the preceding section we have satisfied our second objective of this ray tracing study as given in the introduction. In Section IV we briefly described a computer program to numerically integrate the ray tracing equations for a model ionosphere, including ions, with a centered dipole magnetic field. In this section we exhibited the variations of ray paths with frequency, initial latitude, initial wave normal angle, initial altitude, and ionospheric model. We found that with decreasing frequency the maximum altitude of a ray was higher and the range of latitude greater while the whistler dispersion was nearly constant. With increasing latitude, the maximum altitude, range in latitude, and time delay all increased. As the initial wave normal angle was varied, it was found that two ray paths for the same frequency could cross and that turning around of the ray at low altitudes could also occur. For a source

of VLF energy at high altitudes emitting at all initial wave normal angles, the lower frequency rays were found to spread more in latitude at low altitudes than the higher frequency rays. For different frequencies at one wave normal angle, the higher frequency ray path ended at a lower latitude. With a different ionospheric model it was found that the rays were nearly the same but that the time delay for a given frequency was twice as long.

It is these characteristic features of ray paths that are needed to formulate the explanations for observed VLF radio noise phenomena. We give several examples of the capability and utility of this ray tracing method in the next five sections.

VI. ION CYCLOTRON WHISTLERS

With this and the next four sections we illustrate the capabilities and the limitations of the ray tracing method for predicting new VLF radio noise phenomena, for explaining newly observed VLF phenomena, and for testing existing explanations.

A. Proton and Helium Whistlers: Prediction of Oxygen Whistler

Smith et al. [1965] announced discovery of an ion gyrofrequency VLF phenomenon observed in Injun III and Alouette I satellites. This phenomenon was explained by Gurnett et al. [1965] and Gurnett [1965] as an ion cyclotron whistler associated with the existence of protons (H^+) in the ionosphere. This proton whistler represents the first distinct VLF phenomena due to the presence of ions in the ionosphere. Shawhan [1966a] has studied the occurrence of proton whistlers in the Injun III data. These Injun III proton whistlers have been used to obtain the fractional concentration of H^+, the H^+ number density, the electron density, the proton gyrofrequency, and the proton temperature at the satellite [Shawhan and Gurnett, 1966; Gurnett and Shawhan, 1966; Gurnett

and Brice, 1966]. Based on the explanation of the proton whistler Gurnett et al. [1965] and Gurnett [1965] predicted that a helium whistler and possibly an oxygen whistler should also occur because of the existence of He^+ and O^+ ions in the ionosphere. Following the launching of Alouette II satellite with a VLF frequency response as low as 50 cps a helium whistler was indeed discovered [Barrington et al., 1966]. As yet observation of an oxygen whistler has not been reported.

With the ray tracing method we have the capability of testing the explanation for the observed proton and helium whistlers and of obtaining information about the existence of the oxygen whistler. In Figure 18 is shown calculated ion cyclotron whistler spectrograms for the mid-latitude model ionosphere shown in Figure 31. The ray paths were started at 100 km and 45° magnetic latitude with an initial wave normal angle of $\Delta_o = 0°$. We find at all three altitudes (500 km, 835 km, and 1500 km) that not only the proton and helium whistlers occur but an oxygen whistler can also occur.

This altitude sequence of calculated proton whistlers is comparable to the altitude sequences of observed proton whistlers given by Shawhan [1966a]. The ratio of the crossover frequency

(frequency at which the proton and electron whistler traces are joined) to the proton gyrofrequency (designated Ω_1 in Figure 18) decreases with the increasing percentage of H^+ in agreement with theory and observation. The characteristic of the calculated helium whistler can be compared to the helium whistler observed by Alouette II and shown in Figure 19 [Barrington et al., 1966]. From the proton and helium whistler crossover frequencies, the percentage of all three ions was deduced in the manner given by Gurnett et al. [1965], Gurnett [1965], and Shawhan and Gurnett [1966]: H^+, 89%; He^+, 3.8%; and O^+, 7.2%. Note that the time and frequency scales are different in Figures 18 and 19.

Since Figure 18 is in quantitative agreement with observed proton and helium whistlers, we can use it to deduce characteristics of oxygen whistlers:

1. The resonance frequency for the oxygen whistler is 1/4 the helium gyrofrequency as expected from the ion mass ratios.

2. With the assumption that mode coupling [see Gurnett et al., 1965, and Gurnett, 1965] can occur below the peak in the electron density where O^+ is the dominant ion we find that no crossover frequency occurs and that the lowest frequency for the oxygen whistler is zero frequency.

3. With no crossover frequency, the oxygen whistler is predicted to be observable at all altitudes for frequencies lower than the local oxygen gyrofrequency. If mode coupling does not occur and ions heavier than O^+ exist below the satellite, then a crossover frequency must exist with the same characteristics as the H^+ and He^+ crossover frequencies.

Figure 18 represents the first ray tracing calculation of ion cyclotron whistlers and predicts the existence of an oxygen whistler.

B. Behavior of Proton Whistler Wave Normal Along Path

An example of the use of ray tracing to examine a theoretical hypothesis of wave propagation is given by this discussion of the behavior of the proton whistler wave normal near the resonance altitude. Near the resonance where the wave frequency is nearly equal to the proton gyrofrequency, the index of refraction becomes very large. In Figure 18 it can be seen that in order to conserve the component of n parallel to the planes of stratification, the wave normal must become nearly perpendicular to these planes. Also near resonance the gradient of the refractive index (A19) is dominated by the magnetic field (gyrofrequency) terms.

Very near resonance, therefore, we expect that the wave normal direction and direction of ∇B_o (approximately perpendicular to the planes of stratification) should coincide. Figure 20 shows the behavior of the angle α with altitude along the path, where α is the angle between the wave normal and the ∇B_o direction. For three different values of the initial wave normal angle, the curves illustrate that α becomes large along the path but as the resonance altitude is approached, α goes nearly to zero. The largest value of α for the last point calculated was 5.25° where the maximum deviation of all the paths was 96°. Verification of the anticipated wave normal behavior near a resonance therefore has been given using the ray tracing method.

C. Crossover Frequency of Proton Whistler

In deriving the relations between the proton whistler crossover frequency and the fractional concentration of H^+ at the satellite, Gurnett et al. [1965] and Gurnett [1965] assumed that the propagation was directly along the magnetic field line. If this assumption is valid then the frequency at which the proton and electron whistlers are joined on a spectrogram is exactly the crossover frequency as defined by Smith and Brice [1964] and

Gurnett et al. [1965]. From Figure 20, however, we see that α may become very large which implies that the wave normal angle with respect to the magnetic field ψ may also become very large. By using ray tracing we can determine the effect of large wave normal angles on the experimentally observed crossover frequency and consequently the errors that might result in deducing the fractional concentration of H^+.

In Table 1 are shown ray tracing results for different initial wave normal angles, $\Delta_o = 0, \pm 5°, \pm 15°$. In this table we compare the fractional concentration of H^+ as deduced from the actual model, from the frequency for which the theoretical crossover occurs (D = 0), and from the frequency for which the proton whistler has the minimum delay time (the observed crossover frequency). We have chosen a wave frequency of 520 cps for which the resonance altitudes are near 780 km and the concentration of H^+ is approximately 30%. For all the cases, the frequency for the theoretical crossover (D = 0) gives the fractional concentration of H^+ to 5% of the actual concentration at that altitude. The frequencies of the minimum delay time--the observed crossover frequencies--give concentrations of H^+ that differ by only 0.007 and 0.004 for $\Delta_o = 0°$ and -15° but which can differ by as much as

Table 1

Minimum Delay Frequency of Proton Whistler vs Crossover Frequency

Ω_1 = 520 cps

θ_o = 45°

R_o = 100 km

Δ_o	f (D = 0)	f (t = min)	Mid-Latitude Model Resonance Altitude	α_1 Model	α_1^* D = 0	α_1^* Measured	ψ_{max}
0°	430. cps	422.5 cps	835.6	0.343	0.326	0.350	20
-5°	440.0	400.0	798.7	0.305	0.295	0.423	76
+5°	447.5	415.0	759.2	0.260	0.269	0.383	63
-15°	445.0	440.0	791.7	0.296	0.279	0.292	80
+15°	457.5	435.0	734.9	0.235	0.234	0.341	86

$$^*\alpha_1 \simeq \frac{264}{255}\left(1 - \left(\frac{f}{\Omega_1}\right)^2\right) = n(H^+)/n_e$$

0.123 for $\Delta_o = 5°$. It appears, therefore, that, if the wave normal approaches angles near 90° to the field line, the added delay time for frequencies near the crossover frequency (D = 0) can shift the observed crossover frequency lower which consequently might result in errors in the determination of α_1 as large as +47%. Two facts, however, indicate that the observed crossover frequency is very close to the theoretical crossover frequency:

1. From ray tracing, for higher altitudes, it is often found that the rays which have large initial wave normal angles turn around before they reach the altitude for which D = 0. Therefore, only rays with initial wave normal angles near 0° become proton whistlers.

2. From experimental observations it is found that the ordinary whistler trace is observable at the crossover frequency. Gurnett [1965] has shown that if the ordinary whistler trace is observable then mode coupling must have occurred at the satellite. For mode coupling to occur at the crossover frequency, the wave normal angle must have been near 10° to the field line. Therefore, the observed and the theoretical crossover frequency must be nearly the same.

We conclude that if the ordinary whistler trace is observed at the crossover frequency then the wave normal angle ψ must be near 10° which means that the initial wave normal angle Δ_o was

near 0°. From Table 1, therefore, we see that the observed and actual H^+ concentration may differ by only 0.2%.

D. Negative Ion Cyclotron Whistlers

Positive ion whistlers have been observed and are due to the presence of positive ions in the ionosphere. Measurements of negative ions such as those of Whitten et al. [1965] have indicated significant numbers of negative ions at low altitudes (50-100 km). Shawhan [1966b] has considered the effects of negative ions on ELF waves in the ionosphere and has sketched spectrograms of these resulting negative ion whistlers. With the ray tracing method we can actually calculate negative ion whistler spectrograms and can compare these with the sketches given by Shawhan [1966b].

In Appendix C the negative ion concentration profile deduced from the measurements of Whitten et al. [1965] is discussed. This negative ion profile, with the assumption that the negative ion was O_2^-, was incorporated into the ray tracing program. Calculations for ray paths in the model ionosphere of O_2^-, e^-, O^+, and He^+ were started at 50 km and 45° magnetic latitude with $\Delta_o = 0°$. In Figure 21 is shown the calculated negative ion spectrogram for an altitude of 300 km. For a wave that was initially

left-hand polarized at 50 km we find a right-hand polarized negative ion whistler with the delay time becoming infinite at the O_2^- gyrofrequency (22 cps). Also there is a left-hand polarized O^+ whistler above 24 cps which has an increasing delay time near the O^+ gyrofrequency (44 cps). For a wave that was initially right-hand polarized, the electron whistler trace (not shown) approaches large delay times for frequencies approaching the R = 0 cutoff (3000 cps) when mode coupling and collisions are not considered. Also there is a left-hand polarized wave which stops at approximately 21 cps. This trace has a nose at 18 cps (minimum delay time). For more explanation of negative ion whistlers and the corresponding theory, Shawhan [1966b] should be consulted. On comparing Figure 21 to Figure 8 of Shawhan one finds that the calculated negative ion whistlers exhibit the predicted features for O_2^- substituted for He^- and O^+ substituted for H^+; particularly for the spectrograms given by Shawhan [1966b] at altitude B in his Figure 8.

Figure 21 can be taken as a quantitative prediction for negative ion whistlers being observable at rocket altitudes up to approximately 300 km and for frequencies less than approximately 25 cps.

VII. HOOK WHISTLERS

Another new whistler has been found in the Injun III VLF data at equatorial latitudes and it has been named the hook whistler because of its characteristic shape on a frequency-time spectrogram. Examples of hook spectrograms are shown in Figure 22. This new VLF phenomenon was announced for the first time by Gurnett, Shaw, Shawhan, and Pfeiffer [Paper 4-4-1, 1966 Spring URSI Meeting, Washington, D. C., April 18-21, 1966]. The explanation of the hook whistler that follows is the one given by Shawhan [Paper 4-4-2, 1966 Spring URSI Meeting, Washington, D. C., April 18-21, 1966] based on the ray tracing method for the explanation of observed VLF noises.

A. Summary of Experimental Data

We summarize the frequency-time characteristics and the occurrence of hook whistlers given by Pfeiffer [1966]:

1. As shown in Figure 22, hook whistlers consist of two electron whistler-like traces having the same lightning source but joined at the lower frequencies. The dispersion vs frequency of the two traces is different. For the trace occurring later in time the whistler dispersion ($D = tf^{-1/2}$) is nearly constant but increases slightly at lower frequencies; for the earlier trace, the dispersion

increases appreciably with decreasing frequency. Many hooks can be observed on a pass mixed in with ordinary electron whistlers.

2. The time delay difference between the traces Δt tends to decrease with increasing frequency above 5 kc/s and with decreasing frequency below 5 kc/s. Values of Δt that have been observed range from 7 msec to 0.22 sec at 5 kc/s.

3. Hook whistlers have been observed to occur up to 50° magnetic latitude but are generally observed below 30°. These whistlers tend to occur fairly uniformly in altitude (observed to approximately 2800 km). None were observed, however, below 1200 km and below 10° latitude.

4. Pfeiffer [1966] also shows that hook whistlers occur at all local times but do not seem to occur between 1600 and 2400 km during local afternoon nor between 300 and 1700 km during the local night. However, for latitudes less than 40°, the hook whistlers occur nearly uniformly in local time.

B. Calculated Spectrogram for Hook Whistler

In Section V we found that it was possible for two ray paths to cross and suggested that this crossing of ray paths for the same frequency leads to the explanation of the hook whistler. To obtain a full frequency-time spectrogram of a hook whistler the

ray tracing program as described in Appendix B was used. Ray paths were started at 300 km and 15° N latitude. The stopping coordinates (satellite position) were 850 km and 25° S latitude. Ray paths were calculated starting with Δ_o = -10° for a given frequency and Δ_o was stepped until a ray path came within 15 km of the satellite position. Then Δ_o was stepped again to find any other ray paths between these two points which occur for Δ_o values up to +10°. It was found that <u>two</u> ray paths reached the satellite for a frequency range of 7 kc/s to 2.5 kc/s and that the differing time delay along these paths gave two traces that were joined at low frequencies. This calculated spectrogram is shown in Figure 23 along with a spectrogram of an observed hook.

At 5 kc/s this calculated hook whistler has a time delay difference between the two traces Δt of 11 msec and the whistler dispersion is approximately 13 $sec^{1/2}$. The observed hook whistler also has a dispersion of approximately 13 $sec^{1/2}$ and a time delay difference of 12 msec and 5 kc/s. Although the observed hook whistler occurred at 2700 km and 13° latitude, the two agree in dispersion and time delay difference. For the calculated hook whistler the two traces became indistinguishable at approximately 2 kc/s whereas the traces seem to be joined at 1.5 kc/s on the

observed hook whistler. We expect that for a larger whistler dispersion the time delay difference would tend to be larger; this tendency is supported by the observational data as suggested by the spectrograms in Figure 22. In Section V we found that ray tracing in a different model produced nearly the same ray paths, but an increase in dispersion and time delay by a factor of two which would give Δt = 22 msec for the calculated hook and longer time delays for longer path lengths. These ray tracing results, therefore, are in quantitative agreement with observed hook whistlers in typical whistler dispersions and typical time delay differences between the two traces.

The calculated ray paths for the mid-latitude model and for different frequencies are shown in Figure 24. For initial wave normal angles near -5° a bundle of ray paths occurred in the frequency range of 2.5 to 8.0 kc/s. These paths (Path 1) reached a maximum altitude near 1370 km and produced the earliest trace in time. The second bundle (Path 2) attained an altitude of approximately 1890 km for initial wave normal angles near 0° and because of the longer path length produced the later trace (Trace 2). Note that the wave normal behavior along the path, given by the arrows, is different for the paths in the two bundles. For Path 1

the wave normal angles along the path give $\psi < 50°$; for Path 2 the wave normal angle approaches 80°. In Sections VIII and XI we will see that for wave normal angles near 80°, the time delay gets longer at lower frequencies and therefore Trace 1 joins Trace 2. For the frequency of 2.5 kc/s the delay times become nearly equal even though the ray paths are different. For frequencies much less than 2.5 kc/s, the ray paths in the oundle for $\Delta_o \simeq -5°$ do not reach within 15 km of the satellite but the delay times of the two traces have already become nearly equal.

Using the ray tracing method we have developed an explanation for the hook whistler based on the behavior of ray paths and the behavior of the wave normal along the path for different initial wave normal angles. Using the calculated example we find that from the point of entrance of the energy into the ionosphere from a lightning discharge, two ray paths can exist to the satellite position for frequencies from 2 kc to 8 kc. The time delay along these two paths is different so that two whistler traces appear at the satellite. For decreasing frequency, the delay time difference becomes shorter and finally only one path can reach the satellite. This decreasing in Δt is due to the

increased dispersion of the first trace at low frequency and yields the joining of the two traces at low frequencies. Fermat's principle, which was used to derive the ray tracing equations (21), does not limit the number of solutions in an anisotropic medium. Therefore the fact that two ray paths can occur between two points is not surprising. From the bottom hook whistler in Figure 22 it appears that even three paths may occur. Three ray paths have been obtained also from the ray tracing calculations.

From knowledge of the hook whistler ray paths we can understand the occurrence data on hook whistlers. From Figures 8 and 10 we see that lightning sources at latitudes between 0° and 45° produce some rays with significant path lengths in the Injun III altitude range (to 2800 km) and that these rays range to approximately 60° latitude. But almost all of the ray paths for sources below 30° latitude would fall into the Injun III altitude range, therefore we expect to see more hooks below 30° latitude and expect them to be distributed uniformly in altitude. For both traces of a hook to appear, the energy at the point of entry must have wave normal angles (Δ) up to at least 5°. During the afternoon and early morning it may be that there is less wave scattering in the D-region of the ionosphere. It appears,

however, that hook whistlers are observable at all local times. For altitudes higher than those of Injun III, these same types of hook whistlers should be observable over a larger latitude range centered near the equator. We note that Storey [1953] on the ground observed whistler 'pairs' which seemed to consist of two closely spaced whistler traces of comparable amplitude. Both whistlers came from the same lightning discharge but the dispersion ratios ranged from 1.4 to 2.0 (not echoes). We suggest that these 'unexplained' whistler pairs are just the multiple path hook whistler that has reached the ground.

VIII. RISER AND CHECK WHISTLERS

Pfeiffer et al. [1966] have announced two new types of VLF whistlers observed at equatorial latitudes with the Injun III satellite. These whistlers are called the riser and check whistlers because of their characteristic shapes on a frequency-time spectrogram. Examples of riser whistlers are shown in Figure 25a and 25b. An example of a check whistler is shown in Figure 25d. More examples of riser and check whistlers are given by Pfeiffer [1966]. In this section we present a summary of the experimentally observed spectral characteristic and occurrence of riser and check whistlers, discuss propagation nearly transverse to the field lines, and present an interpretation of the riser and check whistlers based on ray tracing results.

A. Summary of Experimental Data

A more detailed discussion of the spectral and occurrence characteristics of riser and check whistlers is given by Pfeiffer [1966]. We present the following summary:

1. Riser whistlers (risers) appear as a rising tone on a frequency-time spectrogram. This riser starts at a frequency which varies between 2.9 and 4.1 kc/s and rises

to the upper limit of the Injun III VLF receiver (approximately 7.0 kc/s) in about 0.2 seconds. This rising tone can appear to be parabolic as in Figure 25a or linear as in Figure 25b. Neither the lower frequency nor the shape seem to be correlated to altitude, latitude, or local time. Every riser seems to look like every other riser.

2. The check whistler (checks) appear in time as a descending tone like an ordinary electron whistler which joins smoothly to a rising tail having the same frequency-time slope as that of a riser (see Figure 25d). This lower frequency of the check ranges from 5.2 to 5.8 kc/s and the check occurs in approximately 0.15 seconds. No correlation has been found for this lower frequency with altitude, latitude, or local time. Only 15 examples of checks have been found which is 1/15 the occurrence of risers and they are usually found on passes where risers are occurring. All checks appear nearly identical.

3. Except for the number of examples, the risers and checks seem to have the same occurence characteristics in altitude, latitude, and local time. They have been observed for magnetic latitudes of less than 30° and have occurred nearly uniformly in altitude above 785 km. They tend to occur nearly uniformly in local time for all altitudes with the exception of 2200 and 0600 hours when they are found only above 1700 km. Occurrence of risers and checks is nearly uniform in local time for magnetic latitudes up to 30°.

B. Riser Dispersion and the Transverse Refractive Index

The riser dispersion characteristic shown in Figures 25a and 25b departs markedly from the ordinary Eckersley dispersion law ($t = Df^{-1/2}$) for ordinary whistlers. Pfeiffer [1966] has argued, however, that this riser is a whistler as defined in the Introduction on the basis that VLF emissions have not previously been observed at equatorial latitudes and that he is able to associate spherics observed in VLF ground data with several risers observed with Injun III. Assuming, therefore, that the riser and check are whistlers [Gallet, 1959] we consider the explanation of these phenomena based on theoretical considerations and on ray tracing results.

In Figure 26 is shown the group refractive index as a function of the wave frequency to helium gyrofrequency ratio for different values of the wave normal angle ψ. This figure is appropriate for the plasma parameters at 1000 km and 0° latitude based on the mid-latitude model ionosphere (see Figure 31). The curves given are for ψ = 90°, 89.9°, 89°, 80°, and 0°. For decreasing values of ψ the resonance frequency increases. The resonance frequency for ψ = 90° is called the lower hybrid

resonance frequency and for $\psi = 0°$ the electron gyrofrequency [see Stix, 1962]. Consideration is being given to the group refractive index since the delay time for a particular wave frequency is proportional to the integral of the group refractive index along the path. From Figures 25a and 25b we observe that the time delay for the riser increases with increasing frequency from approximately 3.5 kc/s to 7 kc/s--a factor of two in frequency. In Figure 26 we see that only for $\psi = 90°$ does the group refractive increase with increasing frequency for a factor of two in frequency near the lower hybrid resonance frequency (12 kc/s). We conclude therefore that, over at least a portion of the path from the lightning discharge to the satellite, the wave must have travelled exactly transverse to the magnetic field lines.

Since it appears that transverse propagation is a significant feature of the riser and check we now derive an expression for the transverse refractive index, the transverse group refractive index, and the time delay for frequencies near the lower hybrid resonance frequency. According to Stix [1962] the transverse refractive index is given by

$$n_T^2 = \frac{RL}{S} \qquad (54)$$

where R, L, and S are given by equations (A7), (A8), and (A11) in Appendix A. Making the assumptions that $\Omega_1/\omega \ll 1$ and $\omega/\Omega_e \ll 1$ we can expand R and L to obtain

$$R = 1 + \frac{\pi e^2}{\Omega e^2} + \frac{\pi e^2}{\omega \Omega_e} - \frac{\pi k^2}{\omega^2} + \frac{\pi k^2 \Omega_1}{\omega^3}$$

$$L = 1 + \frac{\pi e^2}{\Omega_e^2} - \frac{\pi e^2}{\omega \Omega_e} - \frac{\pi k^2}{\omega^2} - \frac{\pi k^2 \Omega_1}{\omega^3}$$

$$S = 1 - \frac{\pi_1^2}{\omega^2} + \frac{\pi e^2}{\Omega e^2} \quad . \tag{55}$$

On taking the product RL we find that the term $-\pi_e^4/\omega^2\Omega_e^2$ is on the order of 1836 larger than the other terms. For (54) we can therefore write

$$n_T^2 = \frac{\dfrac{-\pi_e^4}{\omega^2 \Omega_e^2}}{\left[1 - \dfrac{\pi_k^2}{\Omega_e^2} + \dfrac{\pi_e^2}{\Omega_e^2} \right]} \tag{56}$$

or for all ions

$$n_T = \frac{\pi_e}{\Omega_e} \frac{\left[\sum_k \dfrac{\alpha_k}{M_k} \right]^{-1/2}}{\left[1 - \omega^2/\Omega_{LHR} \right]^{1/2}} \tag{57}$$

where α_k is the fractional ion concentration, M_k the ion-electron mass ratio and Ω_{LHR} the lower hybrid resonance frequency given by Smith and Brice [1964] and Gurnett [1965].

$$\Omega_{LHR}^2 = \Omega_1 \Omega_e \frac{(\alpha_1 + \alpha_2/4 + \alpha_3/16)}{[1 + (\Omega_e/\pi_e)^2]} . \qquad (58)$$

Equation (57) is the same expression as given by Kimura, Smith, and Brice [1965]. We can expand equation (57) for frequencies much less than the lower hybrid resonance frequency $(\omega/\Omega_{LHR})^2 \ll 1$ and obtain

$$n_T^2 \simeq \frac{\pi_e^2}{\Omega_e^2} \left(\sum_k \frac{\alpha_k}{M_k} \right)^{-1/2} \left(1 + \frac{\omega^2}{2\Omega_{LHR}^2}\right) . \qquad (59)$$

We compare equation (59) to the expression we derived for the transverse refractive index for persistent transverse propagation, equation (41).

$$n_T^2 = K_2 \frac{1 + 3\cos^2\theta}{\sin^6\theta} f\left(\frac{\sin\theta}{r^{1/2}}\right) = \text{eq. (59)}$$

Assuming that $\alpha_1 = 1$, that $\Omega_e/\pi_e \simeq 1$ and that $\Omega_{1,e} \alpha r^{-3}$, equation (59) has the following radial and angular dependence:

$$n_T^2 \alpha \frac{1}{\Omega_{LHR}^2} \alpha \frac{1}{\Omega^2} \alpha \frac{1}{1 + 3 \cos^2 \theta} . \qquad (60)$$

It appears impossible to find a function of $\sin \theta / r^{1/2}$ which could give the angular and radial dependence required by (60). We conclude with Hoffman [1960] therefore that exactly transverse propagation is not possible even over limited path lengths. Near the equatorial plane, however, the angular dependence in equation (41) can be neglected since $\sin \theta \simeq 1$ and $\cos \theta \simeq 0$. Therefore n_T^2 would have to go only as r^6 for transverse propagation according to equation (60) and to go as $f(r^{-1/2})$ to satisfy the general equation (57). Consequently, very near the magnetic equatorial plane, exactly transverse propagation may be possibly over path lengths long enough to give the riser dispersion characteristic.

If we assume that the frequency-time characteristic of the riser is determined predominantly by exactly transverse propagation along an appreciable portion of the path, we can derive an expression for the time delay for frequencies close to the lower hybrid resonance frequency.

By definition

$$t\ (\omega) \;=\; \frac{1}{c} \int_{path} N_T \, ds \qquad (61)$$

where the transverse group refractive index N_T is derived from equation (57)

$$N_T \;=\; n_T \;+\; \omega \frac{\partial n_T}{\partial \omega}$$

$$N_T \;=\; \frac{\pi_e}{\Omega_e} \left(\sum_k \frac{\alpha_K}{M_K} \right)^{-1/2} \left[\left(1 - \omega^2/\Omega^2_{LHR}\right)^{-1/2} \right.$$

$$\left. + \; \frac{\omega^2}{\Omega^2_{LHR}} \left(1 - \omega^2/\Omega^2_{LHR}\right)^{-3/2} \right] . \qquad (62)$$

By assuming that N_T is very large for exactly transverse propagation and that $\Delta\omega^2 = \Omega^2_{LHR} - \omega^2 \to 0$, it can be shown that

$$t\ (\omega) \;\simeq\; \frac{\pi_e}{c\ \Omega_e\ \Omega'_{LHR}} \quad \frac{\omega^2}{(\Delta\omega^2)^{1/2}}$$

where $\Omega'_{LHR} = \partial\Omega_{LHR}/\partial s$ evaluated along the exactly transverse portion of the path. For $\Delta\omega^2$ 'large' $t\ (\omega)$ goes as ω^2 giving a parabolic time-frequency shape. For frequencies very close

to Ω_{LHR}, t (ω) goes as $(\Delta\omega^2)^{-1/2}$ giving infinite time delay at $\omega = \Omega_{LHR}$. This time delay characteristic qualitatively agrees with the risers in Figure 25a and 25b.

C. An Interpretation of Riser and Check Whistlers

From the likeness of the transverse group refractive index plot against frequency for $\psi = 90°$ to the riser whistler spectrogram, we conclude that the riser ray must have propagated exactly transverse to the field line at some point along the ray path since it could not have propagated exactly transverse along the entire ray path. We note from Figure 26 that N_T is an order of magnitude or more greater for $\psi = 90°$ than for $\psi = 89°$ for frequencies within a factor of 2 of the lower hybrid resonance frequency. Therefore the delay time characteristic of the riser for frequencies between 3.5 and 7 kc/s could be almost entirely determined at the region along the ray path where $\psi \rightarrow 90°$ and for frequencies near Ω_{LHR} as given by (64). For the altitude range of 800 km to 2800 km the lower hybrid resonance frequency is greater than the upper frequency of the Injun III VLF receiver (6.5 kc/s) and ranges only between 7 and 10.2 kc/s for the equatorial model ionosphere (Figure 33). If, therefore, a ray

path can reach 2800 km and then turn around for $\psi \rightarrow 90°$, the time delay characteristic would be determined primarily by the local plasma parameters at that turning point. Since the plasma parameters (particularly Ω_{LHR}) are nearly constant from 800-2800 km we would expect the risers to appear nearly identical.

A riser spectrogram has been computed and is shown in Figure 25c. In Figure 27 we show three of the ray paths which produced this riser spectrogram. The ray paths were started at large wave normal angles, $\Delta_o = 32°$ to 23°, which are within 6° of the magnetic field line for $\theta_o = 33°$, $R_o = 300$ km, and the equatorial model ionosphere. The ray path reaches nearly 2500 km for 7 kc/s and then is turned around as $\psi \rightarrow 90°$ reaching the satellite at 1780 km and 16.7°. For this refracted 7 kc/s ray the time delay was 0.361 seconds; at least three times the time delay of a direct ray to the satellite position. Rays of 6 kc/s and 5 kc/s are refracted at lower altitudes and the time delay obtained from the transverse and nearly transverse propagation is <u>less than</u> the time delay for 7 kc/s. For 3 kc/s, the ray turns around below the satellite altitude so that that frequency would not be observed at the satellite. This lowest frequency of the riser is the frequency for which

the ray refracts just at the satellite (4.5 kc/s). It is not yet determined, however, why this lowest frequency is nearly constant for all the altitudes, latitudes, and local times that these risers have been observed. The check whistler appears to consist of the riser-like ray and the direct upgoing ray which would give the nearly Eckersley appearance earliest in time followed by the riser-like tail. This lowest frequency would be the frequency for the ray that refracted at the satellite position.

We summarize our interpretation of the riser and check whistlers as follows: The riser is caused by rays which initially propagate along the field lines at equatorial latitudes but which become refracted transverse to the field lines at altitudes between 800 km and 3000 km (ψ - 90°). Since the rays propagate transverse and nearly transverse along the paths, the time delays become large and exhibit the dispersion characteristic for transverse propagation giving the rising tone (see Figure 26 and equation (63)). The lowest frequency is the frequency for the ray that became transverse at the satellite position. For the check whistler, both the upgoing ray and downgoing nearly transverse ray are observed by the satellite with the lowest frequency being the frequency of the ray that becomes transverse at the satellite.

Because two rays for the same frequency are being observed it is expected that the check would occur less frequently. The equatorial occurrence of both of these VLF pehnomena is understandable since only at equatorial latitudes can the rays travel a significant portion of their path transverse and nearly transverse to the field line.

IX. 'TRANSVERSE' WHISTLERS

In the previous two sections we have used ray tracing to explain new VLF whistler phenomena. In this section we use ray tracing to re-evaluate the interpretation of the experimental data on 'transverse' whistlers given by Carpenter and Dunckel [1965] and to test the explanation of this phenomena given by Kimura, Smith, and Brice [1965]. We show that they have apparently mis-interpreted the experimental data and that the theoretical explanation is therefore implausible. Based on ray tracing we submit a new explanation for the transverse whistler which agrees quantitatively with the experimental data.

A. Previous Experimental Data and Explanation of Transverse Whistlers

Carpenter and Dunckel [1965] have reported a dispersion anomaly in whistlers received on the Alouette 1 satellite. An example of this anomalous whistler is given in Figure 1a of their paper. By comparing this observed whistler to curves with constant Eckersley dispersion ($D = tf^{1/2}$) of $D = 17$ and $D = 20$ $sec^{1/2}$ they conclude that the frequency-time curve of this whistler can be represented by the relation

$$t = D_o f^{-1/2} + \tau(l) \qquad (64)$$

where $D_o \simeq 17$ sec$^{1/2}$, independent of latitude and τ is a number that varies linearly with dipole latitude at the satellite, l, rising from zero at about 30° to about 0.22 sec at 44°. From the alignment of ground station records received at Stanford and the Alouette 1 spectrograms they determined the 'causative' atmospheric from which the dispersion of the whistler as a function of frequency can be determined. We have scaled the whistler given in Figure 1a of their paper and we list these dispersion values in Table 2A under the column titled 'Reported Dispersion'. From this table we find that the ratio of the dispersion for 4 kc/s to that for 1 kc/s is 1.19 which agrees quite well with the ratio of 1.2 reported by Carpenter and Dunckel [1965]. These dispersion values given in Table 2 increase with increasing frequency in agreement with equation (64) if we consider an effective frequency dependent dispersion constant

$$D_{eff}(f) = D_o + \tau(l) f^{1/2} . \qquad (65)$$

Table 2

'Transverse' Whistler Dispersion

A. Observed 'Transverse' Whistler
[Carpenter and Dunckel, 1965]

Frequency, kc/s	Reported Dispersion, $sec^{1/2}$	New Dispersion, $sec^{1/2}$
6.5	28.6	14.23
5.0	27.0	14.85
4.0	26.5	15.8
3.0	24.5	17.2
2.0	23.2	17.5
1.0	21.5	19.4

B. Calculated 'Transverse' Whistler

Frequency, kc/s	Reported Dispersion, $sec^{1/2}$	New Dispersion, $sec^{1/2}$
7.0	13.05	13.8
6.0	13.0	13.75
4.0	13.0	13.75
3.0	13.13	13.75
2.5	13.52	13.9
1.0	14.30	14.30

Kimura, Smith, and Brice [1965] have offered an explanation for this whistler which they have called a 'transverse' whistler (based on their explanation): It is suggested that this whistler is initially a normal ducted whistler propagating quasi-longitudinally. The whistler is then reflected from the base of the ionosphere or an irregularity, such as a sporadic-E layer causing a transition from quasi-longitudinal (QL) to quasi-transverse (QT) propagation. For frequencies much less than the lower hybrid resonance frequency, the time delay is approximately constant with frequency. Therefore, the portion of the path which is QT gives the added constant delay τ (1) in equation (64). The energy then leaks away from the QT trajectory which then propagates in the QL mode to the satellite. We now show that the experimental data may have been mis-interpreted by Carpenter and Dunckel [1965] and that the explanation of Kimura, Smith, and Brice [1965] must be re-examined in terms of ray tracing results.

B. Ray Tracing Explanation of Transverse Whistlers

Storey [1953] introduced a method of finding the dispersion of a whistler and the time of the causative atmospheric by plotting the time delay from an arbitrary time origin for a given frequency

against the inverse square root of the frequency. The slope of the straight line drawn through these points gives the dispersion constant D and the time delay at infinite frequency ($f^{-1/2} = 0$) gives the time of the initiating atmospheric t_o. To obtain the whistler dispersion as a function of frequency the slope for two points can be determined by using

$$D = \frac{t_1 - t_2}{f_1^{-1/2} - f_2^{-1/2}} \quad . \tag{66}$$

We used equation (66) to determine the dispersion as a function of frequency for the whistler given by Carpenter and Dunckel [1965] and the results are listed in Table 2A under the column entitled 'New Dispersion'. We find that the dispersion decreases with increasing frequency rather than increases as found by Carpenter and Dunckel [1965]. We find also that the average dispersion is 16 $sec^{1/2}$ not 25 $sec^{1/2}$. If Carpenter and Dunckel had found the time of the causative atmospheric correctly, the two methods should give the same dispersion characteristic with frequency. By plotting t against $f^{-1/2}$ we find that the causative atmospheric had to occur near 0.15 sec on the time scale given by Carpenter and Dunckel [1965, Figure 1a] not at 0.0 sec.

If they had chosen to compare the delay time of their whistler to that of a $D = 14 \sec^{1/2}$ curve, they would have found increasing time delay for all frequencies as implied by the new dispersion measurements. We submit, therefore, that Carpenter and Dunckel mis-interpreted the experimental data and that the dispersion for these whistlers actually increases with decreasing frequency.

The significance of this increasing dispersion with decreasing frequency is emphasized when we look at the results of ray tracing. For examples of two whistlers that were calculated with the ray tracing program we take the two components of the hook whistler shown in Figure 23 and discussed in Section VII. Ray tracing was started at 300 km, 15° latitude and ended at 850 km, -25° latitude. The dispersion values vs frequency are listed in Table 2B for the earlier and later traces (Trace 1 and Trace 2). For both traces the dispersion increases with decreasing frequency. There can be no question of knowing the time origin since the ray tracing is started at t = 0. Dispersion ratios for 4 kc/s to 1 kc/s are 1.10 and 1.04 respectively for the two hook whistler traces. The ratio for the new dispersion measurements of the Carpenter Dunckel whistler is 1.22 (at higher latitudes). Some whistlers scaled from the Injun III data also exhibited increasing dispersion with decreasing frequency.

Since we can produce 'transverse' whistlers with the ray tracing program, we have the information needed to explain this phenomena. We use Figure 26 and Figure 24 to explain the increased dispersion at lower frequencies. In Figure 26 the curve for $\psi = 0°$ gives the group refractive index for purely longitudinal propagation from which the Eckersley dispersion law is derived. For wave n mal angles near 80°, however, the group refractive index increases by a factor of 2 for frequencies less than 40 times the helium gyrofrequency or approximately 2.5 kc/s. Above 2.5 kc/s the curve for $\psi = 80°$ follows the Eckersley curve closely. From Figure 24 we see that the wave normal for Path 2 stayed nearly along the field line over the entire path ($\psi < 50°$); for Path 1 however the wave normal angles approached 80°. We therefore expect that the Trace 2 would have only a slight increase in dispersion at the lower frequencies and that Trace 1 would have a much larger increase in dispersion which is the case as given in Table 2B. This increased dispersion in Trace 1 is the feature which causes the joining of the two traces to form the hook whistler as discussed in Section VII.

The suggestion of Kimura, Smith, and Brice [1965] that transverse propagation is involved in the explanation of the

'transverse' whistler is substantially correct but the model which they gave is seen to be implausible and not appropriate. Rather than an abrupt transition between $\mathcal{L}$L and $\mathcal{L}$T propagation caused by reflection or scattering, we have demonstrated with ray tracing that the wave normal, at equatorial latitudes, is initially at large angles to the magnetic field and approaches angles near 90° along the path. For propagation not exactly but nearly transverse to the magnetic field lines (we showed in Sections III and VIII that exactly transverse propagation could not persist), the time delay and therefore the dispersion increases with decreasing frequency for some single whistler traces in agreement with data from Alouette I and Injun III. We would not expect to see these 'transverse' whistlers at high latitudes since the rays tend to have small wave normal angles with respect to the magnetic field and consequently would appear to follow the Eckersley dispersion law.

X. WAVE TRAPPING AND VLF NOISE BANDS

Smith et al. [1966] suggested the possibility of wave trapping in regions of the ionosphere for wave frequencies near the local lower hybrid resonance frequency. Gurnett, Shawhan, and Burns [1966] propose that waves can also be trapped in regions of the ionosphere for frequencies near the ion gyrofrequencies. We feel that this wave trapping is the key to the explanation of the VLF noise bands which occur at frequencies near the ion gyrofrequencies. In Figure 28 we show two examples of noise bands apparently associated with the presence of ions in the ionosphere. Both examples are from Injun III VLF data; the pertinent parameters are given on the figure. The proton and helium gyrofrequencies are indicated by Ω_1 and Ω_2 respectively. It appears that possibly three noise bands are occurring, the third just above the oxygen gyrofrequency ($1/4\ \Omega_2$). Preliminary ray tracing results indicate that trapped waves could produce such noise bands.

In Figure 29 we show plots of the transverse refractive index

$$n_T = \frac{RL}{S}$$

against altitude for wave frequencies of 635, 650, and 700 cps, using the mid-latitude ionospheric model and Ω_1 = 700 cps at 400 km. For all three frequencies n_T decreases with altitude to a minimum and then becomes infinite at the ion-ion hybrid resonance (S = 0, see Stix [1962]). At the altitude where L = 0 [see Stix, 1962] n_T is zero but increases to a maximum and then falls off with increasing altitude to a minimum and then begins to increase again (not shown in Figure 29). Between S = 0 and L = 0 an evanescent region exists and transverse waves cannot propagate. We note that with increasing frequency, this evanescent region becomes narrower and decreases in altitude.

It is the range of altitudes above and below the maximum of n_T in which waves can be trapped because of the decreasing index of refraction above and below which can cause reflections. Figure 30 shows the ray tracing results for waves of 635, 650, and 700 cps which were started at 600 km with an initial wave normal angle of $\psi = 90°$. For convenience in identifying the altitudes for which S = 0, L = 0, D = 0, and L = ∞ [see Stix, 1962, and Gurnett, 1965] we have removed the latitude dependence of the magnetic field. The 635 cps ray was started very near the altitude where the maximum in n_T occurred; therefore, this

ray was trapped between 596 and 600 km. The 650 cps ray was trapped between 600 km and the altitude with the same index of refraction value below the maximum, 541 km. This ray propagated down below the altitude for which L = ∞, the proton gyrofrequency. For 700 cps the ray is trapped between 600 km and 391 km as could be predicted from the corresponding index of refraction plot in Figure 29. With the latitude dependence included we find that the trapping altitude range decreases with decreasing latitude. For initial wave normal angles other than $\psi = 90°$, the ray propagates up in altitude until $\psi = 90°$ at which point it reflects and moves down in altitude until $\psi = 90°$ again due to the decreasing index of refraction near the L = 0 altitude.

These preliminary ray tracing results can be interpreted to predict that waves can be trapped in the ionosphere in an altitude range determined by the wave frequency and the wave normal angle on entering the trapping region. For a given point in the ionosphere frequencies can be trapped that range from the L = 0 frequency at that altitude to a frequency above the ion gyrofrequency which produces the minimum in n_T (above the evanescent region) at that altitude. In Figure 28 we see noise bursts which range in frequency above and below the proton gyro-

frequency but which seem to have a cutoff before the next lower ion gyrofrequency as would be expected from the existence of the evanescent region. We suggest therefore that these ion gyrofrequency bands observed in satellites are due to wave trapping of the type we have produced with ray tracing. Also, we suggest that the 800 cps noise bands seen by Gustafsson [1963] on the ground may be due to wave trapping. We noted that as the wave frequency increased the evanescent region became narrower and moved to lower altitudes. It is hypothesized that for high enough wave frequencies, like 800 cps, trapped waves can 'tunnel' through this very narrow evanescent region at altitudes where the collision frequency is large and can be seen on the ground.

With the last five sections we have met our third objective as stated in the introduction. We have shown how this ray tracing method can quantitatively reproduce spectrograms of proton and helium whistlers, can predict the oxygen whistler and negative ion whistlers, can explain the hook and transverse whistlers, can provide the explanation of the riser and check whistlers, and can demonstrate the trapping of waves in the ionosphere to produce VLF noise bands.

XI. CONCLUSIONS

In the Introduction (Section I) we listed the prominent types of VLF radio noise phenomena which fall into the broad groups of whistlers and VLF emissions. Also a review of ray tracing techniques developed to explain these VLF phenomena was given. In Section II we discussed the physical meaning of ray paths and concluded that, in a non-absorbing medium such as the ionosphere, the wave packet approach and the Poynting vector approach both gave the direction of energy propagation--the ray direction. A two dimensional set of ray tracing equations were derived for the case of a horizontally stratified ionosphere and the method of derivation of three-dimensional equations appropriate to the ionosphere was sketched. In Section III we considered three special cases of these general ray tracing equations integrating the equations for exactly transverse and exactly longitudinal propagation and giving the reversibility conditions for these ray tracing equations. A computer program capable of integrating the ray tracing equations and its special features were discussed in Section IV and Appendices A, B, and C. In Section V we used this ray tracing program to obtain the general behavior of ray

paths in the ionosphere with variation of frequency, initial wave normal angle, initial latitude, initial altitude, and the ionospheric model. Based on these ray paths characteristics we were able to explain, make predictions, or test the previous explanations of the following VLF phenomena: ion cyclotron whistlers (Section VI), hook whistlers (Section VII), riser and check whistlers (Section VIII), transverse whistlers (Section IX), and VLF noise bands (Section X). The conclusions reached in Section V to Section X are summarized:

1. With decreasing frequency the maximum altitude of a ray was higher and the range of latitude greater while the whistler dispersion was nearly constant. With increasing latitude, the maximum altitude, range in latitude and time delay all increased. As the initial wave normal angle was varied, it was found that two ray paths for the same frequency could cross and that the ray could also turn around at low altitudes. For a source of VLF energy at high altitudes emitting at all initial wave normal angles, the lower frequencies were found to spread more in latitude at low altitudes. For different frequencies at one wave normal angle, the higher frequency ray path ended at a lower latitude. With a different ionospheric model it was found that the ray paths were nearly the same but that the time delay for a given frequency was twice as long.

2. From ray tracings at frequencies below the proton gyrofrequency, spectrograms of proton, helium, and oxygen whistlers with altitude were produced. The properties of the proton and helium whistlers agreed quantitatively with observed proton and helium whistlers. With mode coupling below 300 km, the oxygen whistler is predicted to exist for all altitudes below the oxygen gyrofrequency. With the inclusion of O_2^- ions into the ionospheric model, spectrograms of negative ion whistlers were produced and these agreed with the previous predictions. It was found that the proton whistler wave normal became nearly parallel to the ∇B_o direction at the altitude where the wave frequency was equal to the proton gyrofrequency. Also, for the case of large wave normal angles along the path, the observed proton whistler crossover frequency may give values of $\alpha_1 = n(H^+)/n_e$ in error by 45%, but with mode coupling this case cannot occur.

3. For the hook whistler we found that two ray paths could exist between the lightning source and the satellite and that the whistler arriving earliest in time suffered increased dispersion at the low frequencies due to large wave normals along the path. This increased dispersion causes the two hook traces to appear joined at low frequencies. A hook whistler spectrogram was produced which agreed quantitatively in dispersion and time delay difference with an observed hook whistler.

4. From consideration of the group refractive index as a function of angle we concluded that the wave normal of the riser and check whistlers must pass through 90° at some point along the path. A riser time delay relation was derived for frequencies close to the local lower hybrid resonance frequency. A riser spectrogram was computed which shows that the riser is made up of rays which have turned around above the satellite and are observed as down-going waves at the satellite. The riser dispersion comes from the propagation transverse and nearly transverse along the path. The lowest frequency observed corresponds to the ray that just turns around at the satellite altitude. We concluded that the check is just a special case of the riser in which both the upgoing and downgoing rays are observed at the satellite.

5. We concluded from new dispersion measurements of a 'transverse' whistler that the data had been previously misinterpreted and that the proposed theory was inappropriate. These new dispersion measurements illustrated that the dispersion of the 'transverse' whistler increased with decreasing frequency rather than decreased. Also, ray tracing whistlers showed this same increase in dispersion. It was proposed, therefore, that the transverse whistler is caused by propagation at large wave normal angles along the path which gives added time delay at the lower frequencies as is observed.

6. Consideration of the transverse refractive index as a function of altitude for frequencies near the ion gyrofrequencies, has shown that a wave trapping region may exist. Spectrograms from Injun III show distinct noise bands associated with the ion gyrofrequencies at the satellite. With ray tracing we have trapped waves in the ionosphere. At a given altitude, the frequencies trapped can range from each L = 0 frequency to frequencies above the ion gyrofrequency. It is concluded that these trapped waves may cause the observed ion gyrofrequency noise bands observed in satellites and on the ground.

With this ray tracing study we have shown that the ray tracing method provides an important and powerful tool for understanding radio noise phenomena in the ionosphere.

XII. APPENDICES

A. Expressions for Ray Tracing Equations

In deriving the explicit forms for the quantities in the two dimensional set of ray tracing equations (21), Yabroff [1961] and Kimura [1966] used the Appleton-Hartree formulation for the index of refraction. In the appendix we present the expressions for n, $\frac{\partial n}{\partial \rho_r}$, $\frac{\partial n}{\partial \rho_\theta}$, $\frac{\partial n}{\partial r}$, $\frac{\partial n}{\partial \theta}$, and $\frac{\partial n}{\partial \omega}$ in the cold plasma formulation of Stix [1962].

1. Phase Index of Refraction n

According to Stix n^2 is the solution to the quadratic equation

$$An^4 - Bn^2 + C = 0 \tag{A1}$$

in the form

$$n^2 = \frac{B \pm F}{2A} \tag{A2}$$

where

$$A = S \sin^2 \psi + P \cos^2 \psi \tag{A3}$$

$$B = RL \sin^2 \psi + PS (1 + \cos^2 \psi) \tag{A4}$$

$$C = PRL \tag{A5}$$

$$F^2 = (RL - PS)^2 \sin^4 \psi + 4P^2D^2 \cos^2 \psi \tag{A6}$$

and

$$R = 1 - \sum_k \frac{\pi_k^2}{\omega} \frac{1}{(\omega + \epsilon_k \Omega_k)} \tag{A7}$$

$$L = 1 - \sum_k \frac{\pi_k^2}{\omega} \frac{1}{(\omega - \epsilon_k \Omega_k)} \tag{A8}$$

$$P = 1 - \sum_k \frac{\pi_k^2}{\omega^2} \tag{A9}$$

$$D = \frac{1}{2}(R - L) \tag{A10}$$

$$S = \frac{1}{2}(R + L) \; . \tag{A11}$$

In the expressions (A7) to (A9) we have used

$$\pi_k^2 = \frac{4\pi n_k e^2}{m_k} \qquad \text{plasma frequency squared} \tag{A12}$$

$$\Omega_k = \left| \frac{e B}{m_k c} \right| \qquad \text{gyrofrequency} \tag{A13}$$

$$\epsilon_k = e/|e| \qquad \text{sign of electronic charge} \tag{A14}$$

and the summation index k represents all ions and the electrons. Therefore m_k is the mass and n_k the number density for the k^{th}

constituent. The sign to be used in equation (A2) for the phase refractive index is determined by the particular region of the CMA diagram and by the desired mode [see Stix, 1962]. For the electron whistler mode [$\omega > \Omega_1$] the minus sign gives the correct branch.

2. Derivatives of the form $\partial n/\partial \rho_i$

Derivatives of this form can be derived from the expression

$$\frac{\partial n}{\partial \rho_i} = \frac{\partial n}{\partial \psi} \frac{\partial \psi}{\partial \rho_i} \quad . \tag{A15}$$

(a) $\dfrac{\partial \psi}{\partial \rho_i}$

Noting again that ρ_r and ρ_θ are the components of the index of refraction in the r, θ directions respectively, $\partial n/\partial \rho_i$ is derived from the definition of the angle ψ:

$$\cos \psi = \frac{\rho_r B_r + \rho_\theta B_\theta}{\rho B}$$

which yields

$$\frac{\partial \psi}{\partial \rho_i} = \frac{B \cos \psi \, \rho_i - \rho B_i}{\rho^2 B \sin \psi} \quad . \tag{A16}$$

(b) $\frac{\partial n}{\partial \psi}$

An expression for $\partial n/\partial \psi$ is obtained by differentiating equation (A1) with respect to ψ:

$$\frac{\partial n}{\partial \psi} = - \frac{n^4 \frac{\partial A}{\partial \psi} - n^2 \frac{\partial B}{\partial \psi} + \frac{\partial C}{\partial \psi}}{4An^3 - 2Bn} \quad . \tag{A17}$$

From differentiation of (A3), (A4), and (A5) with respect to ψ we have

$$\frac{\partial A}{\partial \psi} = 2 (S - P) \sin \psi \cos \psi$$

$$\frac{\partial B}{\partial \psi} = 2 (RL - PS) \sin \psi \cos \psi$$

$$\frac{\partial C}{\partial \psi} = 0 \quad . \tag{A18}$$

The expressions (A18) are used in (A17) and the product of (A17) with (A16) gives $\partial n/\partial \rho_i$.

3. Derivatives of the form $\partial n/\partial x_i$ where $x_i = (r, \Theta)$

The general expression for $\partial n/\partial x_i$ is given by

$$\frac{\partial n}{\partial x_i} = \sum_k \frac{\partial n}{\partial \pi_k^2} \frac{\partial \pi_k^2}{\partial x_i} + \sum_k \frac{\partial n}{\partial \Omega_k} \frac{\partial \Omega_k}{\partial x_i} + \frac{\partial n}{\partial \psi} \frac{\partial \psi}{\partial x_i} \quad . \tag{A19}$$

Each term of (A19) must now be evaluated.

(a) $\dfrac{\partial n}{\partial \pi_k^2}$

In the same manner as for (A17) we obtain

$$\frac{\partial n}{\partial \pi_k^2} = - \frac{n^4 \frac{\partial A}{\partial \pi_k^2} - n^2 \frac{\partial B}{\partial \pi_k^2} + \frac{\partial C}{\partial \pi_k^2}}{4An^3 - 2Bn} \tag{A20}$$

where (A3), (A4), and (A5) are used to obtain the derivatives:

$$\frac{\partial A}{\partial \pi_k^2} = \frac{1}{2} \left(\frac{\partial R}{\partial \pi_k^2} + \frac{\partial L}{\partial \pi_k^2} \right) \sin^2 \psi + \frac{\partial P}{\partial \pi_k^2} \cos^2 \psi$$

$$\frac{\partial B}{\partial \pi_k^2} = \left(R \frac{\partial L}{\partial \pi_k^2} + L \frac{\partial R}{\partial \pi_k^2} \right) \sin^2 \psi + \left(\frac{1}{2} P \left(\frac{\partial R}{\partial \pi_k^2} + \frac{\partial L}{\partial \pi_k^2} \right) + S \frac{\partial P}{\partial \pi_k^2} \right)$$

times $(1 + \cos^2 \psi)$

$$\frac{\partial C}{\partial \pi_k^2} = P \left(R \frac{\partial L}{\partial \pi_k^2} + L \frac{\partial R}{\partial \pi_k^2} \right) + RL \frac{\partial P}{\partial \pi_k^2} \qquad \text{(A21)}$$

where the derivatives of R, L, and P are obtained from (A7), (A8), and (A9):

$$\frac{\partial R}{\partial \pi_k^2} = - \frac{1}{\omega(\omega + \epsilon_k \Omega_k)}$$

$$\frac{\partial L}{\partial \pi_k^2} = - \frac{1}{\omega(\omega - \epsilon_k \Omega_k)}$$

$$\frac{\partial P}{\partial \pi_k^2} = - 1/\omega^2 . \qquad \text{(A22)}$$

Equations (A22) are used in equations (A21) to give the expression (A20).

(b) $\dfrac{\partial n}{\partial \Omega_k}$

As for (A17) and (A20)

$$\frac{\partial n}{\partial \Omega_k} = - \frac{n^4 \frac{A}{\partial \Omega_k} - n^2 \frac{\partial B}{\partial \Omega_k} + \frac{\partial C}{\partial \Omega_k}}{4An^3 - 2Bn^2} \qquad \text{(A23)}$$

and

$$\frac{\partial A}{\partial \Omega_k} = \frac{1}{2}\left(\frac{\partial R}{\partial \Omega_k} + \frac{\partial L}{\partial \Omega_k}\right) \sin^2 \psi$$

$$\frac{\partial B}{\partial \Omega_k} = \left(R \frac{\partial L}{\partial \Omega_k} + L \frac{\partial R}{\partial \Omega_k}\right) \sin^2 \psi + \frac{1}{2} P \left(\frac{\partial R}{\partial \Omega_k} + \frac{\partial L}{\partial \Omega_k}\right) (1 + \cos^2 \psi)$$

$$\frac{\partial C}{\partial \Omega_k} = P \left(L \frac{\partial R}{\partial \Omega_k} + R \frac{\partial L}{\partial \Omega_k}\right) \qquad \text{(A24)}$$

and for (A24)

$$\frac{\partial R}{\partial \Omega_k} = \frac{\pi_k^2 \epsilon_k}{\omega \left(\omega + \epsilon_k \Omega_k\right)^2}$$

$$\frac{\partial L}{\partial \Omega_k} = \frac{-\pi_k^2 \epsilon_k}{\omega \left(\omega - \epsilon_k \Omega_k\right)^2}$$

$$\frac{\partial P}{\partial \Omega_k} = 0 . \qquad \text{(A25)}$$

The equations (A25) are used in (A24) to obtain $\partial n/\partial \Omega_k$ by (A23).

(c) $\dfrac{\partial \pi_k^2}{\partial x_i}$

It is assumed, though not necessarily so, that $\dfrac{\partial \pi_k^2}{\partial \theta} = 0$. With more experimental measurements it may be found that the gradients of concentration with latitude are significant. For this present ray tracing study, they are assumed to be zero. From (A12) we have that

$$\frac{\partial \pi_k^2}{\partial r} = \frac{4\pi_e^2}{m_k} \frac{\partial n_k}{\partial r} \quad . \tag{A26}$$

Modifying the work of Angerami and Thomas [1964] for a diffusive equilibrium model of the ionosphere, we have

$$\frac{n_e(z)}{n_{eo}} = \left[\sum_{k=1}^{3} \alpha_{ko} \, e^{-z/H_k} \right]^{1/2} = Q^{1/2} \tag{A27}$$

where z is the geopotential height

$$z = r_o \, (r - r_o)/r \tag{A28}$$

for r_o being a reference altitude at which the fractional concentrations of the ions with respect to the electrons is given:

$$\alpha_{ko} = \frac{n_{ko}}{n_{eo}} \quad . \tag{A29}$$

H_k is the scale height for the k^{th} ion

$$H_k = kT/m_k\, g_o \tag{A30}$$

and g_o is the acceleration of gravity at r_o.

From these relations we obtain

$$n_e = n_{eo}\, \varrho^{1/2}$$

$$n_k = n_{eo}\, \alpha_{ko}\, e^{-z/H_k}\, \varrho^{-1/2} \quad . \tag{A31}$$

Finally

$$\frac{\partial \pi_e^2}{\partial r} = \left(\frac{r_o}{r}\right)^2 \frac{1}{2} \frac{1}{\varrho} \frac{\partial \varrho}{\partial z}\, \pi_e^2$$

$$\frac{\partial \pi_k^2}{\partial r} = -\left(\frac{r_o}{r}\right)^2 \left(\frac{1}{H_k} + \frac{1}{2} \frac{1}{\varrho} \frac{\partial Q}{\partial z}\right) \pi_k^2 \tag{A32}$$

where

$$\frac{\partial \alpha}{\partial z} = - \sum_{k=1}^{3} \frac{\alpha_{ko}}{H_k} e^{-z/H_k} .$$

(d) $\dfrac{\partial \Omega_k}{\partial x_i}$

The magnitude of the centered dipole magnetic field is given by

$$B = 0.312 \left(\frac{r_E}{r} \right)^3 (1 + 3 \cos^2 \theta)^{1/2} \qquad \text{(A33)}$$

where $r_E = 6371$ km, so that

$$\frac{\partial \Omega_k}{\partial r} = - \frac{3}{r} \Omega_k$$

$$\frac{\partial \Omega_k}{\partial \theta} = - \frac{3 \cos \theta \sin \theta}{(1 + 3 \cos^2 \theta)} \Omega_k . \qquad \text{(A34)}$$

(e) $\dfrac{\partial \psi}{\partial x_i}$

From the expression

$$\frac{\partial \psi}{\partial x_i} = \frac{\partial \psi}{\partial \gamma} \frac{\partial \gamma}{\partial x_i} \qquad \text{(A35)}$$

$\partial\psi/\partial x_i$ is obtained, where γ is the angle between the magnetic field direction and the radius vector r and is defined by

$$\tan \gamma = \frac{1}{2} \tan \theta . \tag{A36}$$

From (A36), therefore, for a centered dipole field

$$\frac{\partial \gamma}{\partial \theta} = \frac{1}{2 \cos^2 \theta + \frac{1}{2} \sin^2 \theta}$$

$$\frac{\partial \gamma}{\partial r} = 0 \quad . \tag{A37}$$

Since $B_r = B \cos \gamma$

$$B_\theta = B \sin \gamma \tag{A38}$$

the definition of ψ is used to obtain

$$\frac{\partial \psi}{\partial \gamma} = \frac{\rho_r B_\theta - \rho_\theta B_r}{\rho B \sin \psi} \quad . \tag{A39}$$

Equations (A35), (A34), (A32), (A26), (A23), (A20), and (A17) are used to evaluate (A19).

4. Derivative dS/dt

The expressions for n^2 and $\partial n/\partial \psi$ to be used in equation (22) of the text are given by (A2) and (A17).

5. Derivative dT/dt

For equation (23) of the text we have

$$\frac{\partial n}{\partial \omega} = - \frac{n^4 \frac{\partial A}{\partial \omega} - n^2 \frac{\partial B}{\partial \omega} + \frac{\partial C}{\partial \omega}}{4An^3 - 2Bn^2} \qquad (A40)$$

and

$$\frac{\partial A}{\partial \omega} = \frac{1}{2} \left(\frac{\partial R}{\partial \omega} + \frac{\partial L}{\partial \omega} \right) \sin^2 \psi + \frac{\partial P}{\partial \omega} \cos^2 \psi$$

$$\frac{\partial B}{\partial \omega} = \left(R \frac{\partial L}{\partial \omega} + L \frac{\partial R}{\partial \omega} \right) \sin^2 \psi + \left(\frac{1}{2} P \left(\frac{\partial R}{\partial \omega} + \frac{\partial L}{\partial \omega} \right) + S \frac{\partial P}{\partial \omega} \right) (1 + \cos^2 \psi)$$

$$\frac{\partial C}{\partial \omega} = P \left(R \frac{\partial L}{\partial \omega} + L \frac{\partial R}{\partial \omega} \right) + RL \frac{\partial P}{\partial \omega} \qquad (A41)$$

for which

$$\frac{\partial R}{\partial \omega} = \sum_k \frac{\pi_k^2}{\omega^2} \frac{2\omega + \epsilon_k \Omega_k}{(\omega + \epsilon_k \Omega_k)^2}$$

$$\frac{\partial L}{\partial \omega} = \sum_k \frac{\pi_k^2}{\omega^2} \frac{2\omega + \epsilon_k \Omega_k}{(\omega - \epsilon_k \Omega_k)^2}$$

$$\frac{\partial P}{\partial \omega} = 2 \sum_k \frac{\pi_k^2}{\omega^3} . \qquad \text{(A42)}$$

The equations listed in this Appendix A are the expressions necessary to calculate the ray path (r, θ), the r and θ components of the index of refraction vector $n = (\rho_r^2 + \rho_\theta^2)^{1/2}$, the total path length S, and the total time delay along the path T, for a given frequency and a given initial wave normal angle (ρ_r/ρ and ρ_θ/ρ specified). Jt should be noted that these expressions are equally valid for all frequencies. For HF, however, the equations can be simplified and computation time shortened. For ELF care must be taken in the computer program to avoid addition and subtraction of very large quantities.

B. Ray Tracing Program Logic

In Table 3 a general flow diagram of the ray tracing program is presented. The program is written in Fortran IV and is run on an IBM 7044 computer. With the present program (June, 1966) and the 7044 computer approximately 9.5 points of the ray path are calculated per second. We now describe the major parts of the ray tracing program and point out the special routines which are included. Discussion of the detailed program including notation used is given by Shawhan [1966c].

1. Read in Data

This part of the ray tracing (see Table I) is comprised of reading in the card input data for the program and of writing this data on the output listing along with the proper column headings.

a. The polar coordinates r, θ are read in for the starting point of the ray path. One or more wave frequencies are also read in and the program can calculate a ray path for each frequency in sequence.

b. Values for the reference altitude and for the electron density, fractional concentration of H^+ and He^+ and temperature at the reference altitude are read in for use in equations (A27) to (A32) in Appendix A.

c. When the program is used to calculate ray paths for different Δ values from the specified starting point to a specified stopping point, values for the stopping altitude and latitude, for the starting and ending value of Δ (wave normal angle to radius vector) and the increment size of Δ must be read in.

2. Runge-Kutta Routine

Once all of the starting parameters have been specified the fourth order Runge-Kutta integration routine is used to obtain the next three points along the ray path and the values of the ray tracing differential equations (21) at each point. It is these first four derivatives and values r, θ (polar coordinates), ρ_r, ρ_θ (r-, θ-component of index of refraction), S (path length), T (group time delay) that are needed to start the fourth order Adams-Bashforth integration routine. Values of the derivatives for the current values of r, θ, ρ_r, ρ_θ, S, and T are obtained by transferring to Part 5, Ray Tracing Expressions. For the Runge-Kutta routine three predictors and one corrector for the next point must be evaluated [Abranowitz and Stegen, 1964]. For the Adams-Bashforth routine, however, only one predictor and one corrector is calculated so that this latter routine is faster and therefore used for the bulk of the integration.

3. Adams-Bashforth Routine

Equations for the Adams-Bashforth integration routine are given by Abranowitz and Stegen [1964]. This routine can be used once the first four starting points have been obtained with the Runge-Kutta routine.

a. To insure that quantities in Part 5 are not changing too fast between integration steps, the predictor is compared to the corrector. If the percentage difference is greater than 0.1%, then the integration interval is halved and a new predictor and corrector calculated and checked until they agree to 10^{-3} for all quantities being calculated. Kimura [1966] tested only one predictor-corrector pair.

b. In Part 5 the values of ρ_r and ρ_θ are corrected in the manner suggested by Yabroff [1961] in order that $\rho_r^2 + \rho_\theta^2 \equiv n^2$. In Part 3 the values of the predictor and corrector are also corrected for ρ_r and ρ_θ so that no integration error can accumulate. This correction routine has been added to the standard Adams-Bashforth method and has yielded improvement in the integration accuracy.

c. When the wave normal angle with respect to the magnetic field ψ becomes close to 90°, the index of refraction increases markedly for frequencies near the lower hybrid resonance frequency. To keep the integration accurate, the integration step interval is reduced by 1/4 for $85 < |\psi| < 90°$.

Values of r, θ, ρ_r, ρ_θ, S, T, Δ, and ψ calculated for each point are read out after each integration.

4. Point-to-Point Routine

A unique feature of this ray tracing program is its capability of finding one or more ray paths between two specified points. This point-to-point routine can produce frequency-time spectrograms at a specified point (r_s, θ_s) for a source (lightning or VLF emission) at another specified point. For a given frequency, the parameter which is incremented is the initial wave normal direction to the radius vector Δ_o.

a. For each point on the ray path started with an initial wave normal of Δ_1, the distance between the satellite position (r_s, θ_s) and that point is calculated, x_1.

b. The magnitude of x_1 is tested for each new point and the ray path is stopped when x_1 is a minimum $XMIN_1$ and is positive if radially above the satellite and negative if below.

c. For the next ray path Δ_1 is incremented by $\Delta\Delta$ and $XMIN_2$ calculated.

d. The signs of $XMIN_1$ and $XMIN_2$ are tested; if the same, then both paths are either above or below the satellite. Then $\Delta_2 \rightarrow \Delta_1$, $XMIN_2 \rightarrow XMIN_1$ and Δ_1 is again incremented by $\Delta\Delta$ until the signs are different. This condition implies that the two ray paths bracket the satellite.

e. For this condition a new Δ is obtained by a linear approximation from $XMIN_1$ and $XMIN_2$:

$$\Delta_3 = \Delta_2 + XMIN_2\ (\Delta_1 - \Delta_2)/(XMIN_1 - XMIN_2).$$

f. When $XMIN_3$ is less than 15 km from the satellite the ray path from the starting point to the satellite point has been determined for that frequency. Values of Δ_3, $XMIN_3$, the frequency and the time delay are then printed out.

5. Ray Tracing Expressions

It is this Part 5 in which the expressions for the gyrofrequencies, plasma frequencies, index of refraction, and all of the necessary derivatives given in Appendix A are calculated. From the current values of r, θ, ρ_r, ρ_θ, S, T, the derivatives given by the ray tracing equations (21) are evaluated for use in obtaining the next point. Step d is the correction of ρ_r and ρ_θ with respect to the calculated value of the index of refraction as suggested by Haselgrove [1955] and Yabroff [1961].

After finding all the ray paths for a given range of Δ and for a given wave frequency, the entire program can be repeated for a new frequency. A plot of the time delay T vs frequency then yields the calculated frequency-time spectrogram.

TABLE 3

RAY TRACING PROGRAM FLOW CHART

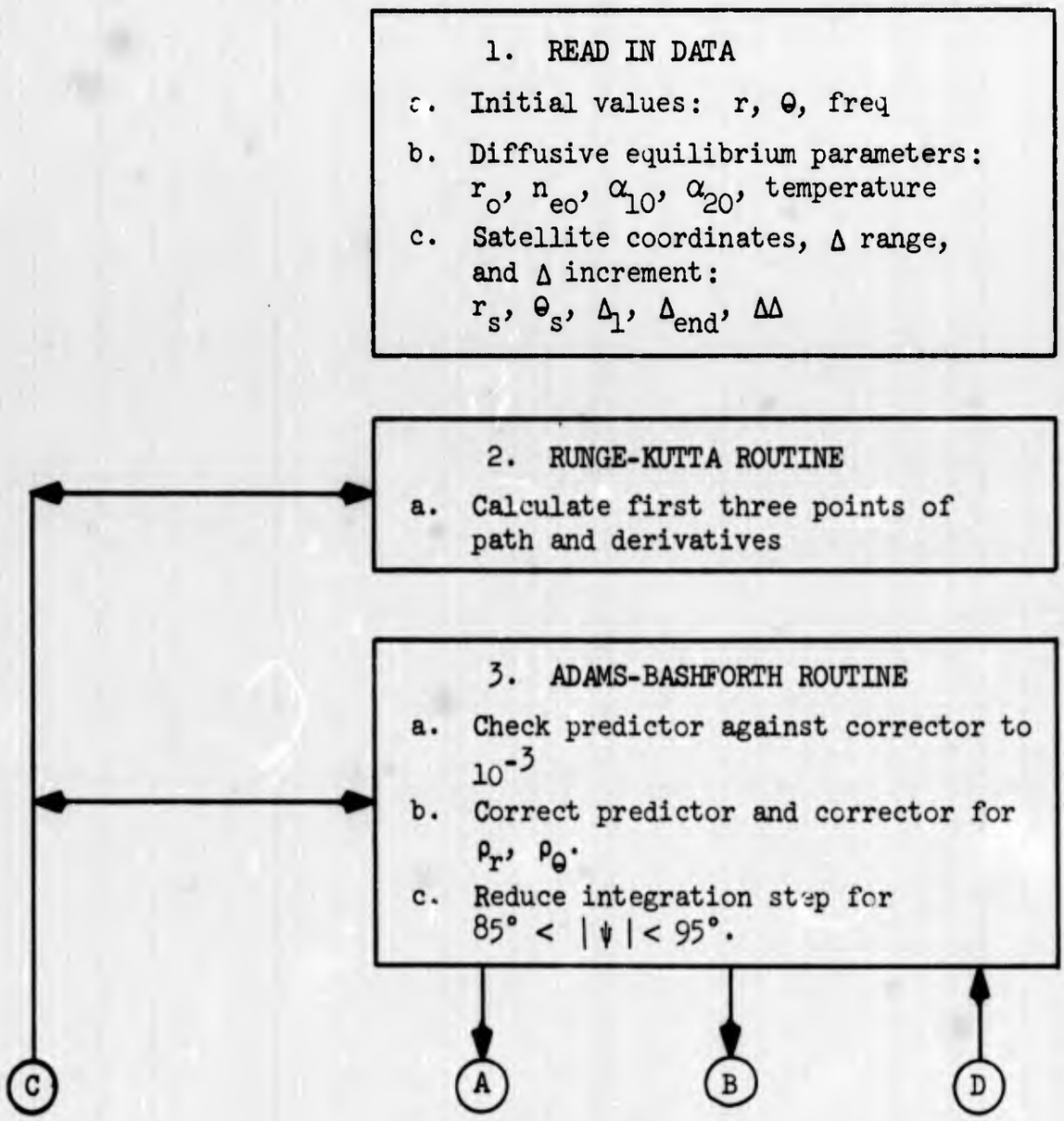

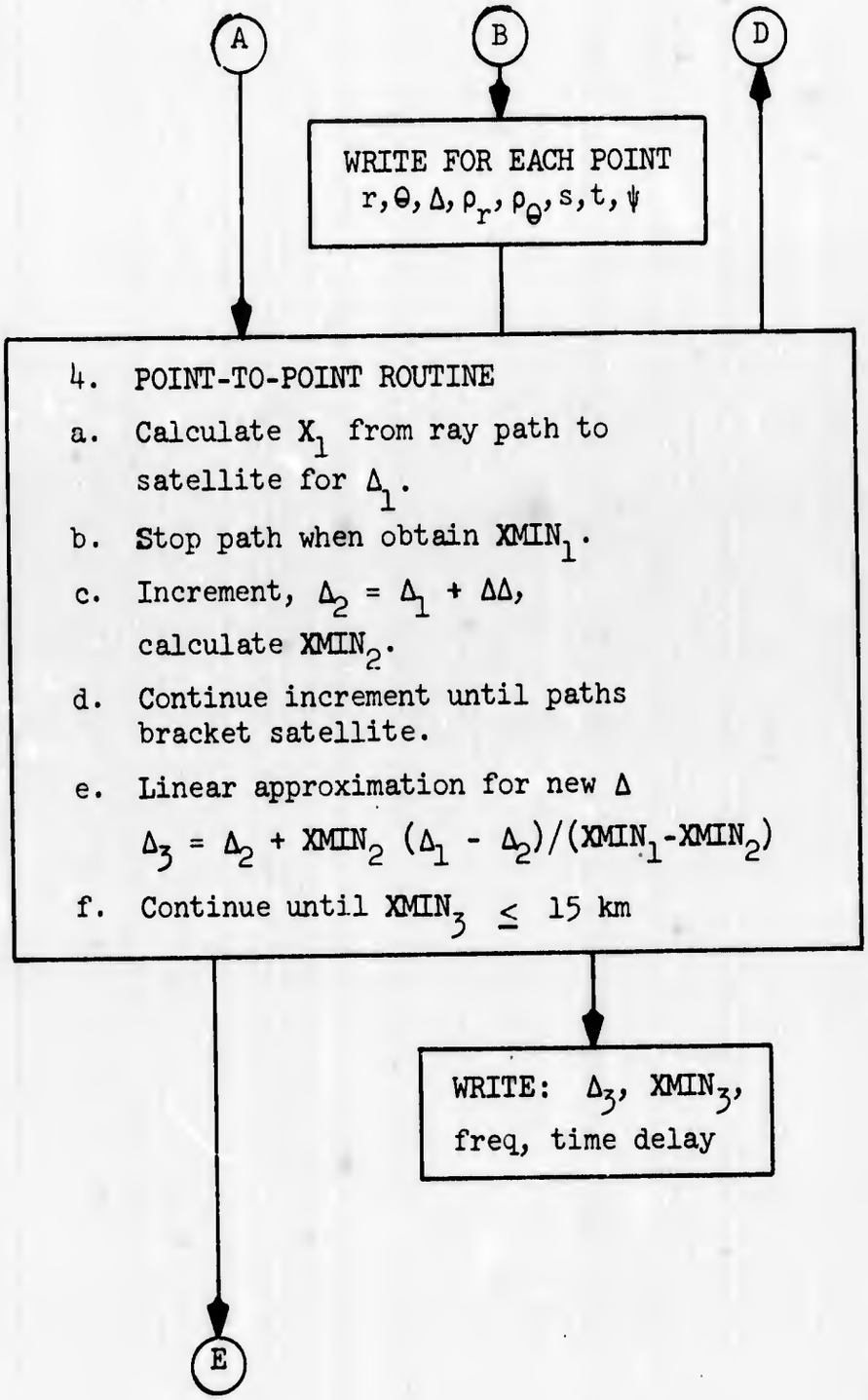
A
B
D
WRITE FOR EACH POINT
r, Θ, Δ, ρ_r, ρ_Θ, s, t, ψ
4. POINT-TO-POINT ROUTINE
a. Calculate X_1 from ray path to satellite for Δ_1.
b. Stop path when obtain XMIN_1.
c. Increment, Δ_2 = Δ_1 + ΔΔ, calculate XMIN_2.
d. Continue increment until paths bracket satellite.
e. Linear approximation for new Δ
Δ_3 = Δ_2 + XMIN_2 (Δ_1 - Δ_2)/(XMIN_1-XMIN_2)
f. Continue until XMIN_3 ≤ 15 km
WRITE: Δ_3, XMIN_3, freq, time delay
E

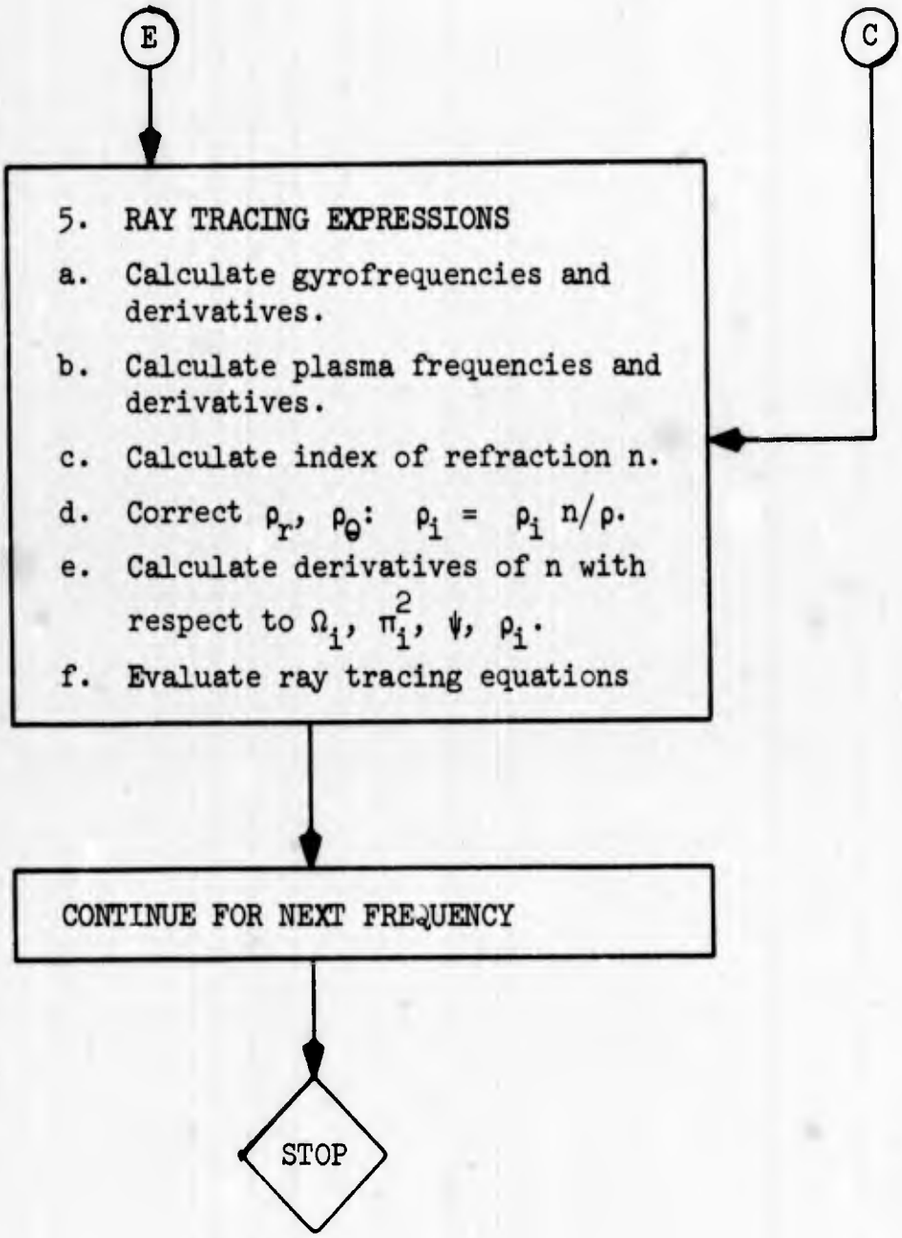
E
C
5. RAY TRACING EXPRESSIONS
a. Calculate gyrofrequencies and derivatives.
b. Calculate plasma frequencies and derivatives.
c. Calculate index of refraction n.
d. Correct ρ_r, ρ_θ: $\rho_i = \rho_i\, n/\rho$.
e. Calculate derivatives of n with respect to Ω_i, π_i^2, ψ, ρ_i.
f. Evaluate ray tracing equations
CONTINUE FOR NEXT FREQUENCY
STOP

C. Model Ionospheres

In this appendix we briefly discuss the mid-latitude and equatorial concentration models used in the ray tracing studies and compare these two models with experimental observations.

1. Mid-Latitude Model

In the lower portion of Figure 31 is shown the electron density, H^+ density and He^+ density profiles for a diffusive equilibrium model ionosphere (see Appendix A, equations (A27) to (A32)). The reference altitude, percent H^+, percent He^+, electron density, and temperature at this reference altitude are given on the figure. Below the reference altitude the electron density peak is given by the expression

$$n_e = 4 \times 10^5 \exp (- (R - 6696)^2/8100) \qquad (C1)$$

which gives the peak at 325 km altitude and an extremely small concentration at 90 km. Below 90 km the profile for O_2^- is indicated based on the measurements of Whitten et al. [1965]. In Figure 32 the fractional concentration of H^+ for this model is compared to the observed H^+ concentration from Injun III proton whistler analysis for daytime and nighttime [see Shawhan, 1966a; Shawhan and Gurnett, 1966; Gurnett and Shawhan,

1966]. The chosen temperature is also appropriate for mid-latitudes as deduced from proton whistlers [Gurnett and Brice, 1966]. This model agrees quite well with observed H^+ concentrations and therefore is appropriate for mid-latitudes in studying Injun III VLF data. For this model the lower hybrid resonance frequency is also shown [Gurnett, 1965]:

$$\Omega_{LHR} = \frac{\pi_{eff}\,\Omega_e}{[\pi_e^2 + \Omega_e^2]^{1/2}} \qquad (C)$$

where

$$\pi_{eff}^2 = \frac{4\pi n_e e^2}{m_{prot}} \left[\alpha_1 + \frac{\alpha_2}{4} + \frac{\alpha_3}{16}\right] \qquad (C2)$$

and α_i are the fractional concentrations of H^+, He^+, O^+, respectively.

In Figure 33 is shown the equatorial model ionosphere. This diffusive equilibrium model was obtained from the measured equatorial electron and ion density profiles and ion temperature by Farley [D. T. Farley, 1966] at the Jicamarca Radar Observatory. These

profiles and temperature were measured on 17 August 1965 at approximately 1700 local time. August, 1966, represents approximately the same time span after solar minimum as the 1962-1963 period of Injun III VLF data acquisition was before. Therefore this profile should be appropriate for analysis of Injun III data. The reference parameters for the diffusive equilibrium model are indicated on Figure 33. To obtain the peak in the electron density profile at 325 km, the diffusive equilibrium electron density was multiplied by another exponential function:

$$n_e = n_e \text{ (diff. equilib.) } (1 - \exp (- (R - 6461)^2/325^2)). \qquad (C3)$$

The lower hybrid resonance frequency vs altitude plot in Figure 35 was determined by equation (C2).

REFERENCES

Abranowitz, Miltin, and Irene A. Stegen, editors, Handbook of Mathematical Functions, National Bureau of Standards Applied Mathematics Series 55, 1964.

Allcock, G. M., A study of the audio-frequency radio phenomenon known as "dawn chorus", Australian J. Phys., 10 (2), 286-298, 1957.

Angerami, J. J., and J. O. Thomas, The distribution of ions and electrons in the earth's exosphere, J. Geophys. Res., 69, 4537-4560, 1964.

Barrington, R. E., A helium whistler observed in the Canadian satellite Alouette II, Nature, 210, 80-81, 1966.

Barrington, R. E., J. S. Belrose, and D. A. Keeley, VLF noise bands observed by the Alouette I satellite, J. Geophys. Res., 68, 6539-6541, 1963.

Booker, H. G., Oblique propagation of electromagnetic waves in a slowly-varying non-isotropic medium, Proc. Roy. Soc., 155A (885), 235-257, 1936.

Booker, H. G., Propagation of wave-packets incident obliquely upon a stratified doubly refracting ionosphere, Phil. Trans. Roy. Soc., 237A (781), 411-451, 1938.

Booker, H. G., Application of magneto-ionic theory to radio waves incident obliquely upon a horizontally-stratified ionosphere, J. Geophys. Res., 54, 243-274, 1949.

Brice, N. M., and R. L. Smith, Recordings from satellite Alouette 1; a VLF plasma resonance, Nature, 203, 926-927, 1964.

Carpenter, D. L., and N. Dunckel, A dispersion anomaly in whistlers received on Alouette 1, J. Geophys. Res., 70, 3781-3786, 1965.

Carpenter, D. L., N. Dunckel, and J. F Walkup, A new phenomenon: Whistlers trapped below the protonosphere, J. Geophys. Res., 69, 5009-5017, 1964.

Farley, D. T., Temperature and composition measurements at the magnetic equator, submitted to Annals de Geophysique, 1966.

Gallet, R., The very-low-frequency emissions generated in the earth's exosphere, Proc. IRE, 47, 211-231, 1959.

Gurnett, D. A., Ion cyclotron whistlers, Ph.D. Dissertation, University of Iowa, Iowa City, Research Report 65-7, June, 1965.

Gurnett, D. A., A satellite study of VLF hiss, submitted for publication, J. Geophys. Res., 1966.

Gurnett, D. A., and N. M. Brice, Cyclotron damping of ion cyclotron whistlers: A method for the determination of ion temperature, J. Geophys. Res. (submitted for publication), 1966.

Gurnett, D. A., and S. D. Shawhan, Determination of H^+ concentration, electron density, and proton gyrofrequency from the dispersion of proton whistlers, J. Geophys. Res., 71, 741-754, 1966.

Gurnett, D. A., S. D. Shawhan, N. M. Brice, and R. L. Smith, Ion cyclotron whistlers, J. Geophys. Res., 70, 1665-1688, 1965.

Gurnett, D. A., S. D. Shawhan, and T. B. Burns, Reflection and trapping of ELF waves in the ionosphere, to be published, 1966.

Gustafsson, G., A. Egeland, W. Barron, and J. Aarons, Band emissions at gyrofrequencies of ionospheric ions and hiss frequencies, AGARDOGRAPH 74, New York: Pergamon, 175-189, 1963.

Hamilton, W. R., Mathematical Papers, Vol. I, Geometrical Optics, Cambridge; University Press, 1931.

Haselgrove, C. B., and J. Haselgrove, Twisted ray paths in the ionosphere, Proc. Roy. Soc. London, 75, 357-363, 1960.

Haselgrove, J., Ray theory and a new method for ray tracing, London Physical Society, Report of Conference on the Physics of the Ionosphere, 355-364, 1955.

Haselgrove, J., Oblique ray paths in the ionosphere, Proc. Roy. Soc. London, A, 70 (7), 653-662, 1957.

Helliwell, R. A., Whistler-triggered periodic VLF emissions, J. Geophys. Res., 68, 5387-5395, 1963.

Helliwell, R. A., Whistlers and Related Ionospheric Phenomena, Stanford University Press: Stanford, 1965.

Helliwell, R. A., J. H. Crary, J. H. Pope, and R. L. Smith, The "nose" whistler--a new high latitude phenomenon, J. Geophys. Res., 61, 139-142, 1956.

Hines, C. O., Wave packets, the Poynting vector, and energy flow: Part I--Non-dissipative (anisotropic) homogeneous media, J. Geophys. Res., 56, 63-72, 1951a.

Hines, C. O., Wave packets, the Poynting vector, and energy flow: Part II--Group propagation through dissipative isotropic media, J. Geophys. Res., 56, 197-206, 1951b.

Hines, C. O., Wave packets, the Poynting vector, and energy flow, Part III--Packet propagation through dissipative anisotropic media, J. Geophys. Res., 56, 207-220, 1951c.

Hines, C. O., Wave packets, the Poynting vector, and energy flow, Part IV--Poynting and McDonald velocities in dissipative anisotropic media (conclusion), J. Geophys. Res., 56, 535-544, 1951d.

Hines, C. O., Heavy ion effects in audio-frequency radio propagation, J. Atmospheric Terrest. Phys., 11 (2), 36-42, 1957.

Hines, C. O., W. C. Hoffman, and H. Weil, Transverse whistler propagation, Final Report No. 2894-1-F, Res. Inst., Univ. of Michigan, Ann Arbor, Mich., 1959.

Hoffman, W. C., Conditions for the persistence of purely longitudinal or purely transverse propagation, J. Atmospheric Terrest. Phys., 18, 1-7, 1960.

Kelso, John M., Radio ray propagation in the ionosphere, New York; McGraw-Hill Book Co., 1964.

Kimura, I., Effects of ions on whistler-mode ray tracing, Radio Science, 1 (3) (New Series), 269-283, 1966.

Kimura, I., R. L. Smith, and N. M. Brice, An interpretation of transverse whistlers, J. Geophys. Res., 70, 5961-5966 1965.

Maeda, K., and I. Kimura, A theoretical investigation on the propagation path of the whistling atmospherics, Report Ionosphere Space Res. Japan, 10, 105-123, 1956.

Millington, G., The effect of the earth's magnetic field on short wave communication by the ionosphere, Proc. Inst. Elec. Engrs., 98 (1), Part IV, 1-14, 1951.

Millington, G., Ray path characteristics in the ionosphere, Proc. Inst. Elec. Engrs., 101 (7), Part IV, 235-248, 1954.

Mullaly, R. F., Graphical construction for ray-tracing in the ionosphere, London Physical Society, Report of Conference on the Physics of the Ionosphere, 384-393, 1955.

Pfeiffer, G. W., Non-Eckersley's law whistlers observed with satellite Injun III, Master's Thesis, Department of Physics and Astronomy, University of Iowa, Iowa City, August, 1966.

Pfeiffer, G. W., D. A. Gurnett, S. D. Shawhan, and R. R. Shaw, Non-Eckersley's law whistlers observed at equatorial latitudes with satellite Injun 3, Nature, 210, 21 May 1966.

Poeverlein, H., Strahlwege von Radiowellen in der Ionosphare I, S. B. bayer Akad. Wiss., 175-201, 1948.

Poeverlein, H., Strahlwege von Radiowellen in der Ionosphare II, Z. angew. Phys., 1 (11), 517-525, 1949.

Poeverlein, H., Strahlwege von Radiowellen in der Ionosphare III, Z. angew. Phys., 2 (4), 152-160, 1950.

Preece, W. H., Earth currents, Nature, 49 (1276), 554, 1894.

Scott, J. C. W., The Poynting vector in the ionosphere, Proc. I.R.E., 38 (9), 1057-1068, 1950.

Shawhan, S. D., Experimental observations of proton whistlers from the Injun III VLF data, J. Geophys. Res., 71 (1), 29-45, 1966a.

Shawhan, S. D., Negative ion detection in the ionosphere from effects on ELF waves (submitted for publication), J. Geophys. Res., 1966, and University of Iowa, Department of Physics and Astronomy Research Report 66-11, March, 1966b.

Shawhan, S. D., A computer program for VLF ray tracing in a model ionosphere (to be published), University of Iowa, Department of Physics and Astronomy Research Report, 1966c.

Shawhan, S. D., and D. A. Gurnett, Fractional concentration of hydrogen ions in the ionosphere from VLF proton whistler measurements, J. Geophys. Res., 71, 47-59, 1966.

Smith, R. L., Properties of the outer ionosphere deduced from nose whistlers, J. Geophys. Res., 66, 3709-3716, 1961.

Smith, R. L., An explanation of subprotonospheric whistlers, J. Geophys. Res., 69, 5019-5021, 1964.

Smith, R. L., and N. M. Brice, Propagation in multicomponent plasmas, J. Geophys. Res., 69, 5029-5039, 1964.

Smith, R. L., I. Kimura, J. Vigneron, and J. Katsufrakis, Lower hybrid resonance noise and a new ionospheric duct, J. Geophys. Res., 71, 1925-1927, 1966.

Stix, T. H., Theory of Plasma Waves, New York: McGraw-Hill, 1962.

Storey, L. R. O., An investigation of whistling atmospherics, Phil. Trans. Roy. Soc. (London), A (246), 113-141, 1953.

Synge, J. L., Geometrical Mechanics and deBroglie Waves, Cambridge: University Press, 1954.

Ungstrup, E., Observations of whistlers and VLF phenomena at Godhavn, Greenland, Nature, 184, 806, 1959.

Whitten, R. C., I. G. Poppoff, R. S. Edmonds, and W. N. Berning, Effective recombination coefficients in the lower ionosphere, J. Geophys. Res., 70, 1737-1742, 1965.

Yabroff, I., Computation of whistler ray paths, J. Res. NBS, 65D (Radio Prop.), No. 5, 485-505, 1961.

FIGURE CAPTIONS

Figure 1. a. Direction of Ray from Index of Refraction Surface.
b. Ray Tracing Equations from Index of Refraction Surface.

Figure 2. Index of Refraction Surfaces, n (ψ).

Figure 3. Comparison to Kimura [1966].

Figure 4. Ray Paths for Horizontally Stratified Medium.

Figure 5. Ray Paths from 30° for $\Delta_o = 0°$.

Figure 6. a. Final Latitude vs Frequency.
b. Maximum Altitude vs Frequency.

Figure 7. a. Total Path Delay and Dispersion vs Frequency.
b. Wave Normal--Field Line Angle Along Path.

Figure 8. Ray Paths for 5 kc/s vs Latitude.

Figure 9. a. Maximum Altitude vs Initial Latitude.
b. Total Path Delay and Dispersion vs Initial Latitude.
c. Final Latitude vs Initial Latitude.

Figure 10. Ray Paths from 30° for 4 kc/s.

Figure 11. a. Maximum Altitude vs Initial Wave Normal Angle.
b. Total Path Delay and Dispersion vs Initial Wave Normal Angle.
c. Final Latitude vs Initial Wave Normal Angle.

Figure 12. Ray Paths from 4 R_E for $\Delta_o = -90°$.

Figure 13. a. Total Path Delay and Dispersion vs Frequency.
b. Final Latitude vs Frequency.

Figure 14. Ray Paths from 4 R_E for 5 kc/s.

Figure 15. Ray Paths from 4 R_E for 1 kc/s.

Figure 16. a. Total Path Delay and Dispersion vs Initial Wave Normal Angle.
b. Final Latitude vs Initial Wave Normal Angle.

Figure 17. a. Maximum Altitude vs Frequency for Equatorial Model.
b. Final Latitude vs Frequency.
c. Total Path Delay and Dispersion vs Frequency.

Figure 18. Ion Cyclotron Whistlers.

Figure 19. Observed Proton and Helium Whistler from Alouette II.

Figure 20. Proton Whistler Wave Normal Along Path.

Figure 21. Negative Ion Cyclotron Whistlers.

Figure 22. Spectrograms of Observed Hook Whistlers.

Figure 23. Calculated Hook Whistler.

Figure 24. Hook Whistler Ray Paths.

Figure 25. Riser and Check Whistlers.

Figure 26. Group Refractive Index as Function of ψ.

Figure 27. Riser Ray Paths.

Figure 28. Spectrograms of Gyrofrequency Noise Bands.

Figure 29. Transverse Refractive Index vs Altitude.

Figure 30. Trapped VLF Waves.

Figure 31. Mid-Latitude Model Ionosphere and Lower Hybrid Resonance Frequency.

Figure 32. Model H^+ Concentration Compared to Proton Whistler Values.

Figure 33. Equatorial Model Ionosphere and Lower Hybrid Resonance Frequency.

G 66-402

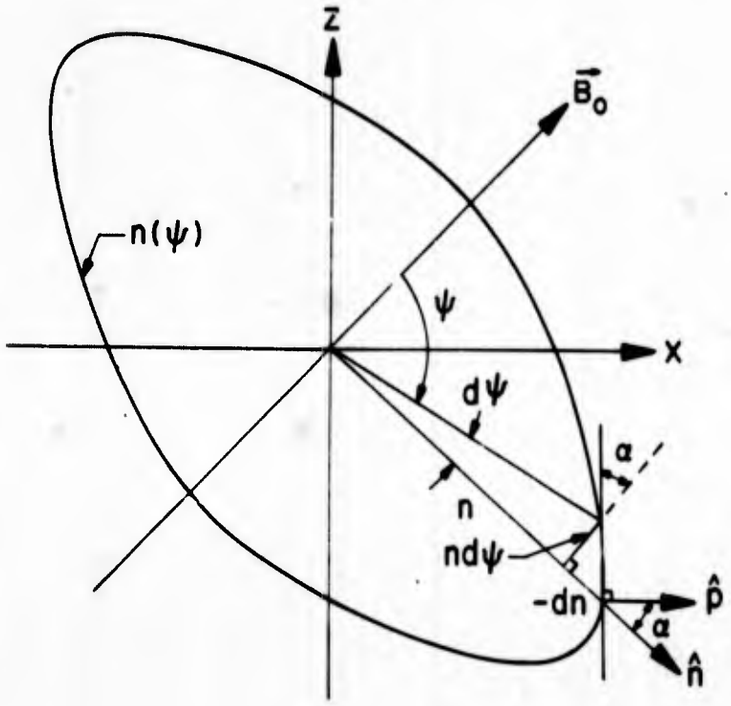

FIGURE 1a
DIRECTION OF RAY
FROM INDEX OF
REFRACTION
SURFACE

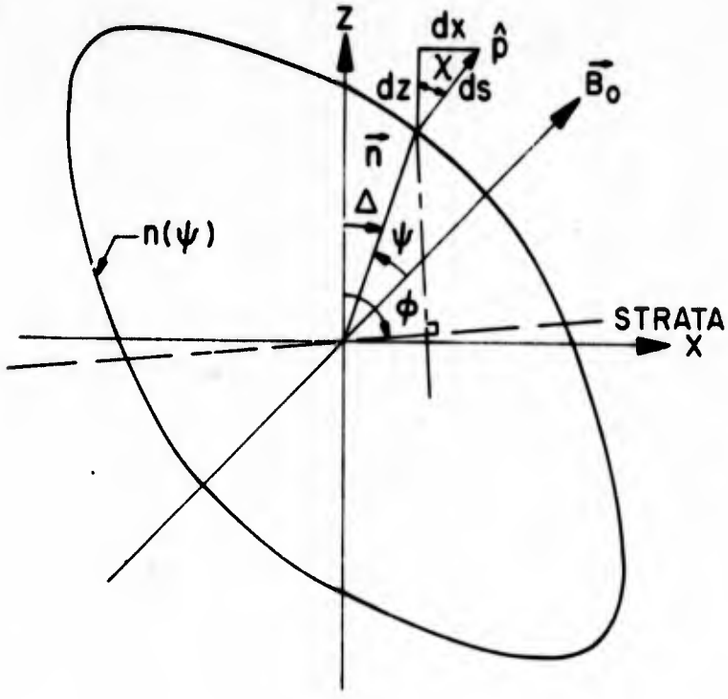

FIGURE 1b
RAY TRACING
EQUATIONS FROM
INDEX OF
REFRACTION SURFACE

Figure 1

G66-403

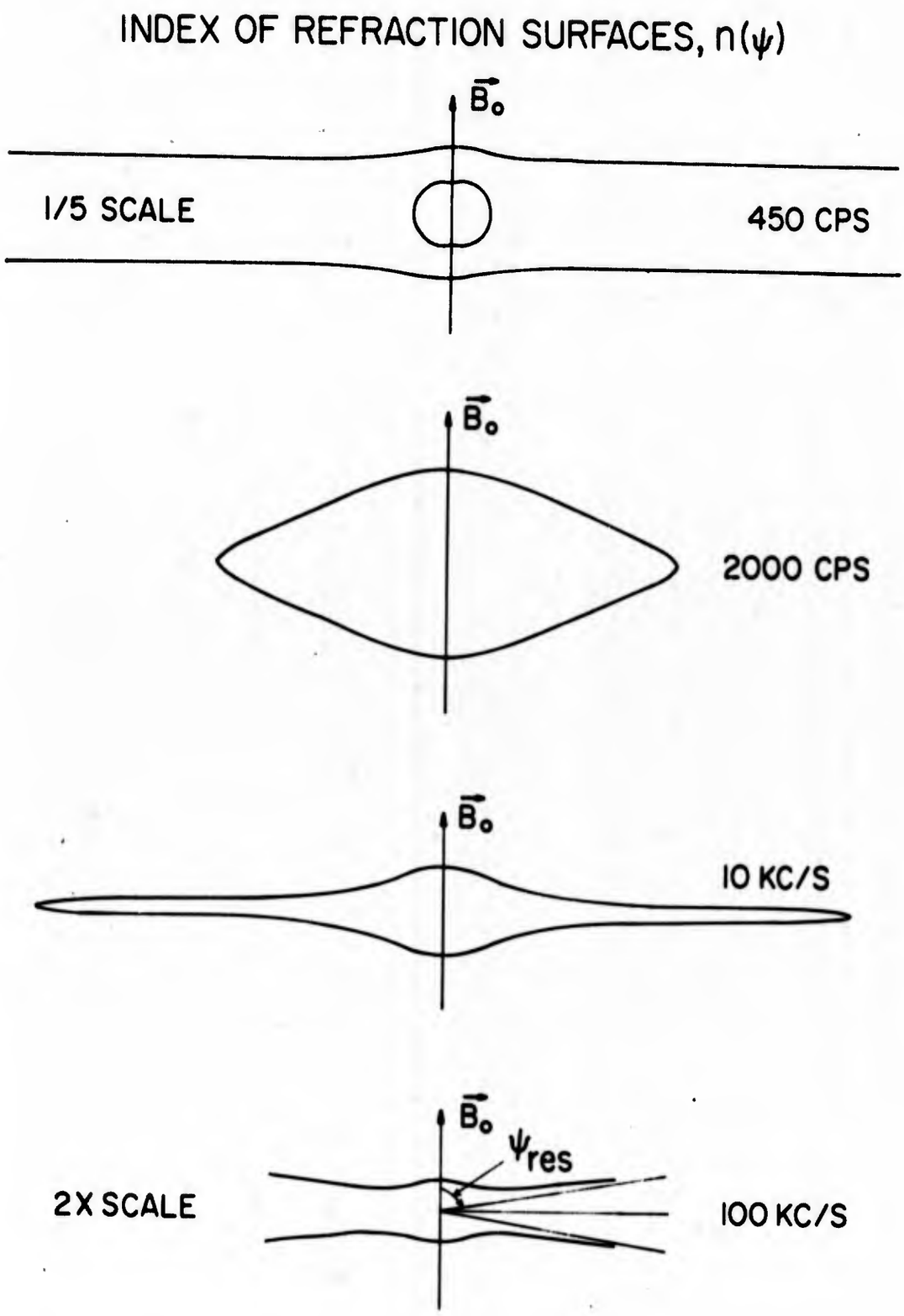

Figure 2

G66-425

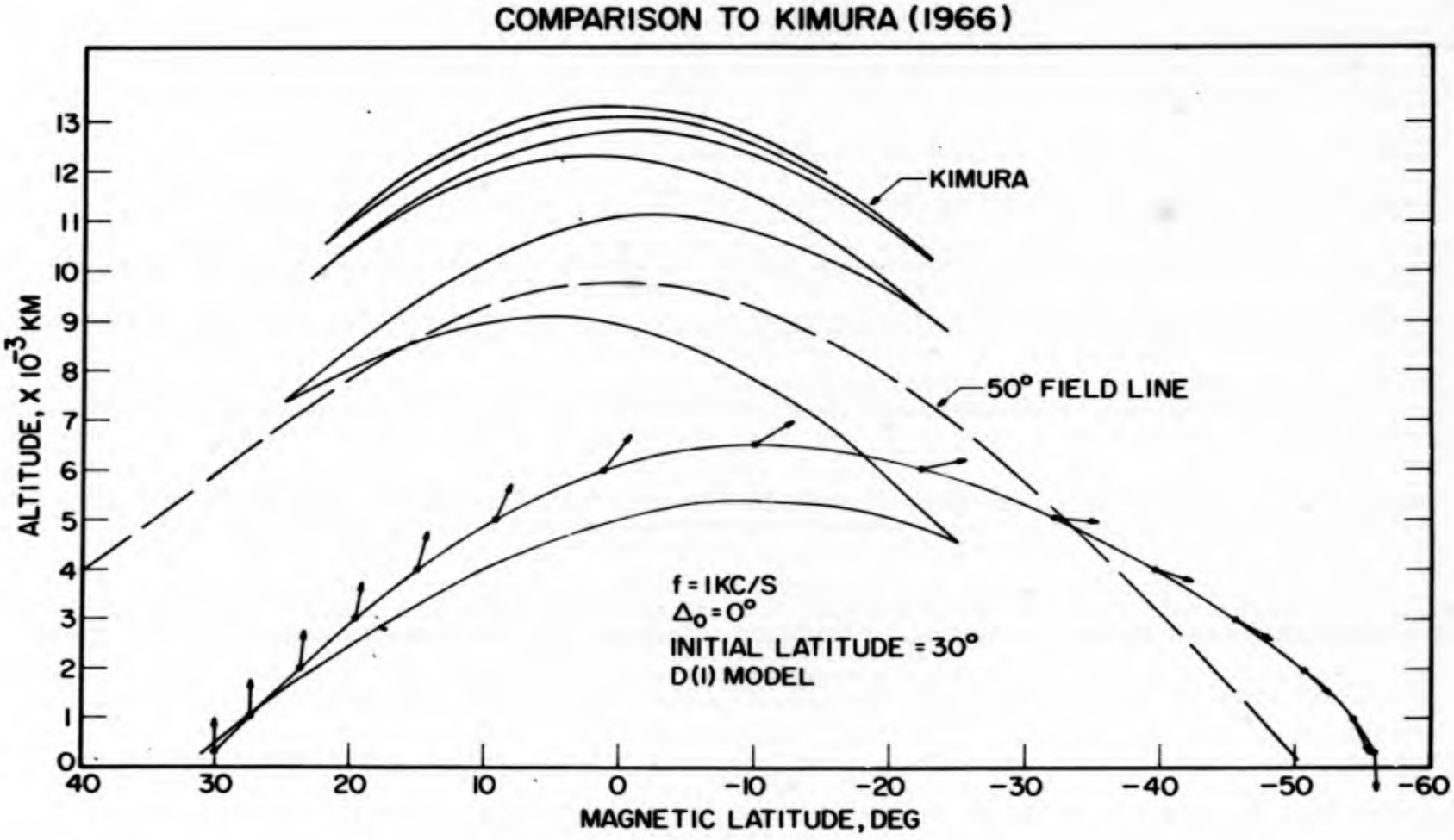

Figure 3

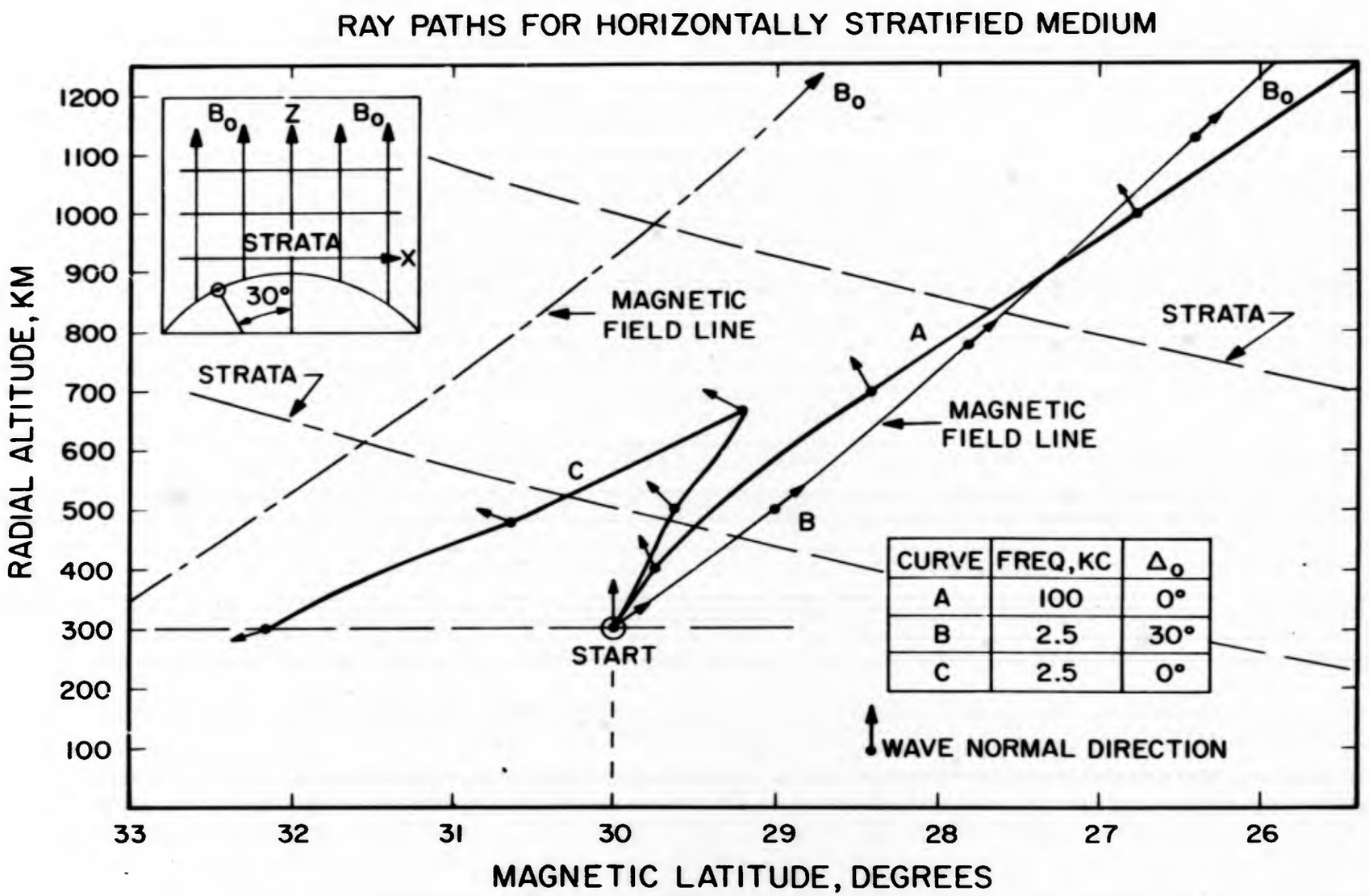
RAY PATHS FOR HORIZONTALLY STRATIFIED MEDIUM
RADIAL ALTITUDE, KM
1200
1100
1000
900
800
700
600
500
400
300
200
100
33
32
31
30
29
28
27
26
MAGNETIC LATITUDE, DEGREES
B_o
Z
B_o
STRATA
X
30°
B_o
B_o
MAGNETIC FIELD LINE
STRATA
STRATA
A
MAGNETIC FIELD LINE
C
B
START
CURVE | FREQ, KC | Δ_o
A | 100 | 0°
B | 2.5 | 30°
C | 2.5 | 0°
WAVE NORMAL DIRECTION

Figure 4

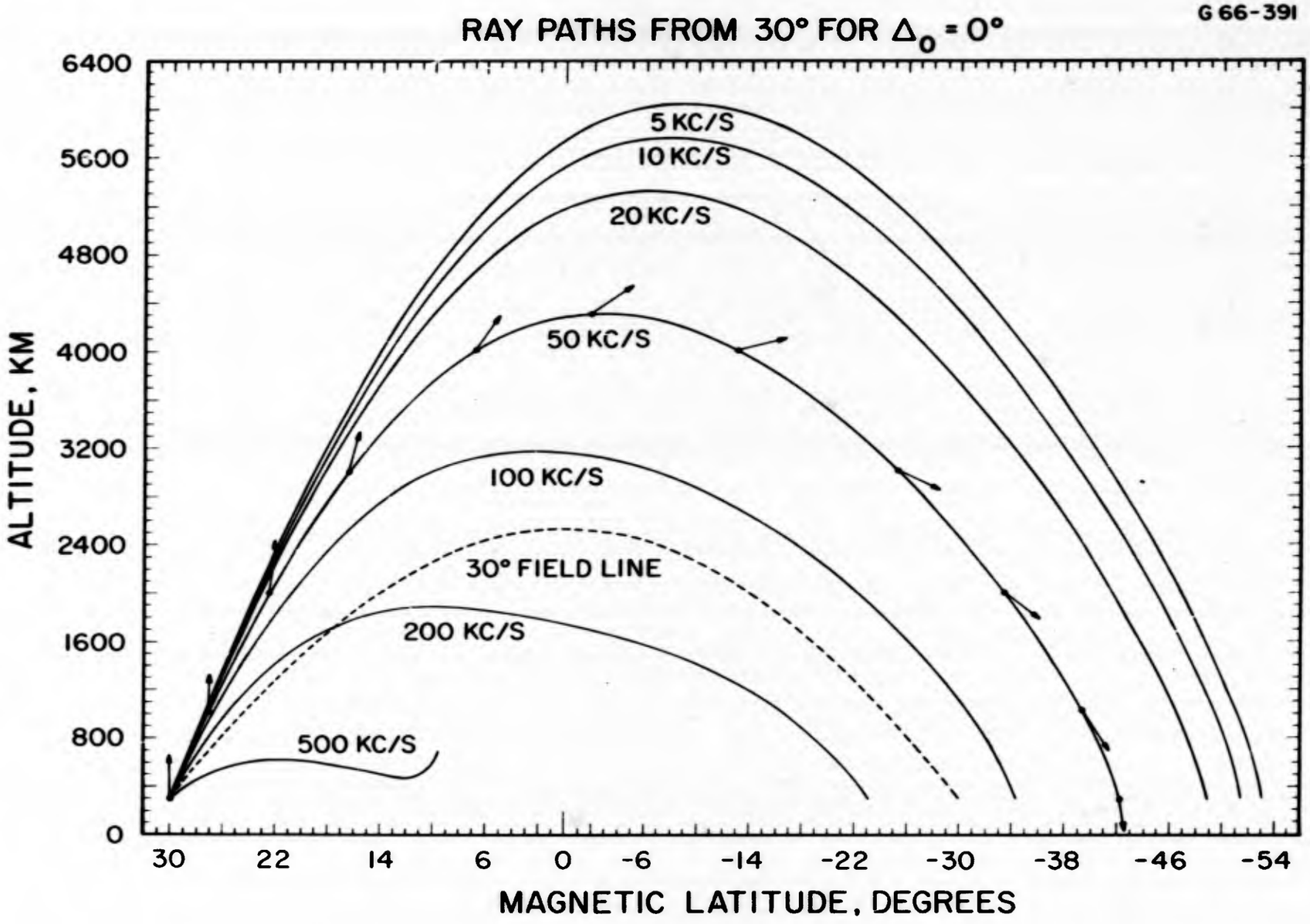
RAY PATHS FROM 30° FOR $\Delta_0 = 0°$
G 66-391
ALTITUDE, KM
6400
5600
4800
4000
3200
2400
1600
800
0
5 KC/S
10 KC/S
20 KC/S
50 KC/S
100 KC/S
30° FIELD LINE
200 KC/S
500 KC/S
30
22
14
6
0
-6
-14
-22
-30
-38
-46
-54
MAGNETIC LATITUDE, DEGREES

Figure 5

G66-389

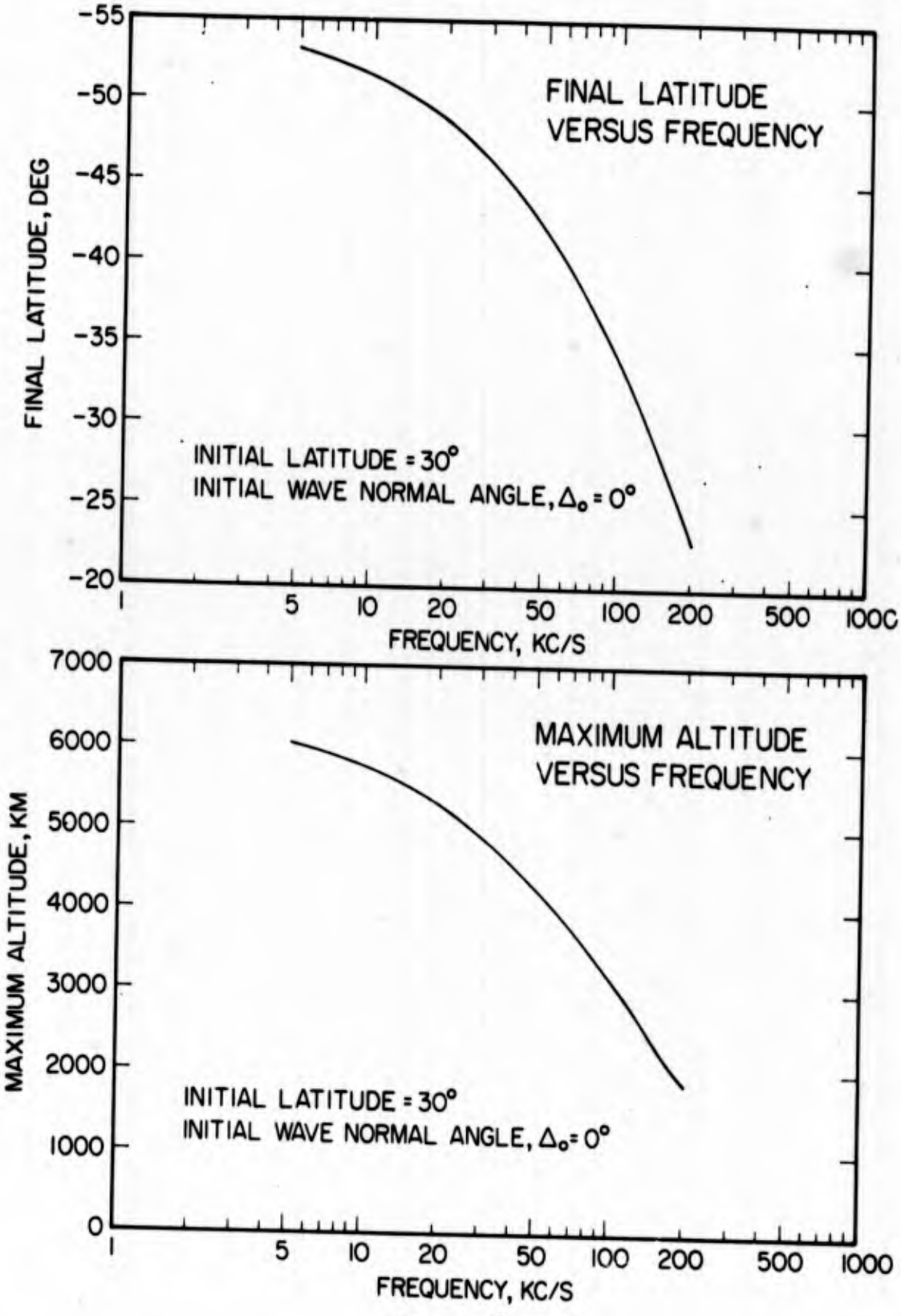

Figure 6

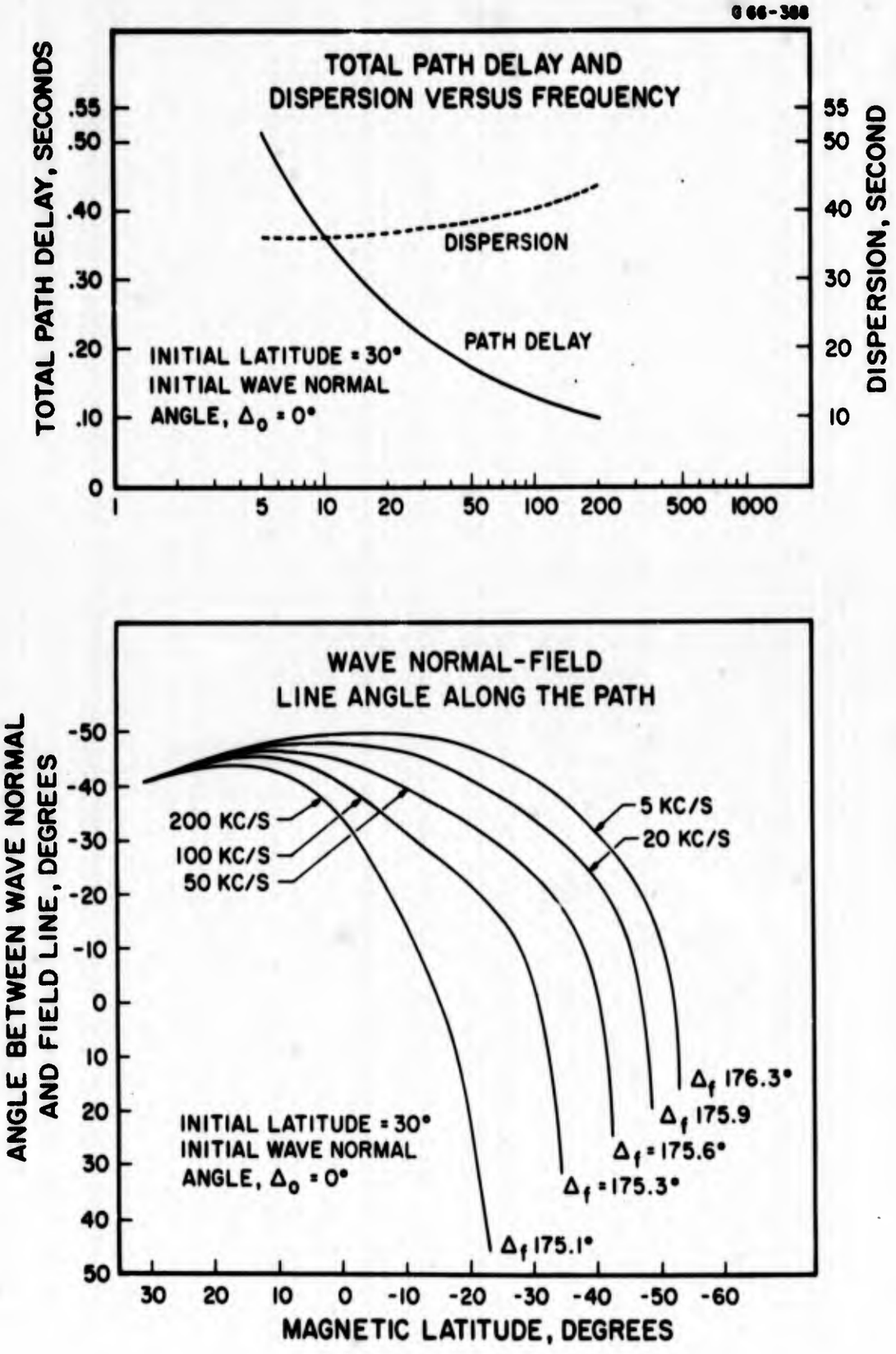
666-388
TOTAL PATH DELAY AND
DISPERSION VERSUS FREQUENCY
TOTAL PATH DELAY, SECONDS
DISPERSION, SECOND
.55
.50
.40
.30
.20
.10
0
55
50
40
30
20
10
DISPERSION
PATH DELAY
INITIAL LATITUDE = 30°
INITIAL WAVE NORMAL
ANGLE, Δ0 = 0°
1
5
10
20
50
100
200
500
1000
WAVE NORMAL-FIELD
LINE ANGLE ALONG THE PATH
ANGLE BETWEEN WAVE NORMAL
AND FIELD LINE, DEGREES
-50
-40
-30
-20
-10
0
10
20
30
40
50
200 KC/S
100 KC/S
50 KC/S
5 KC/S
20 KC/S
Δf 176.3°
Δf 175.9
Δf = 175.6°
Δf = 175.3°
Δf 175.1°
INITIAL LATITUDE = 30°
INITIAL WAVE NORMAL
ANGLE, Δ0 = 0°
30
20
10
0
-10
-20
-30
-40
-50
-60
MAGNETIC LATITUDE, DEGREES

Figure 7

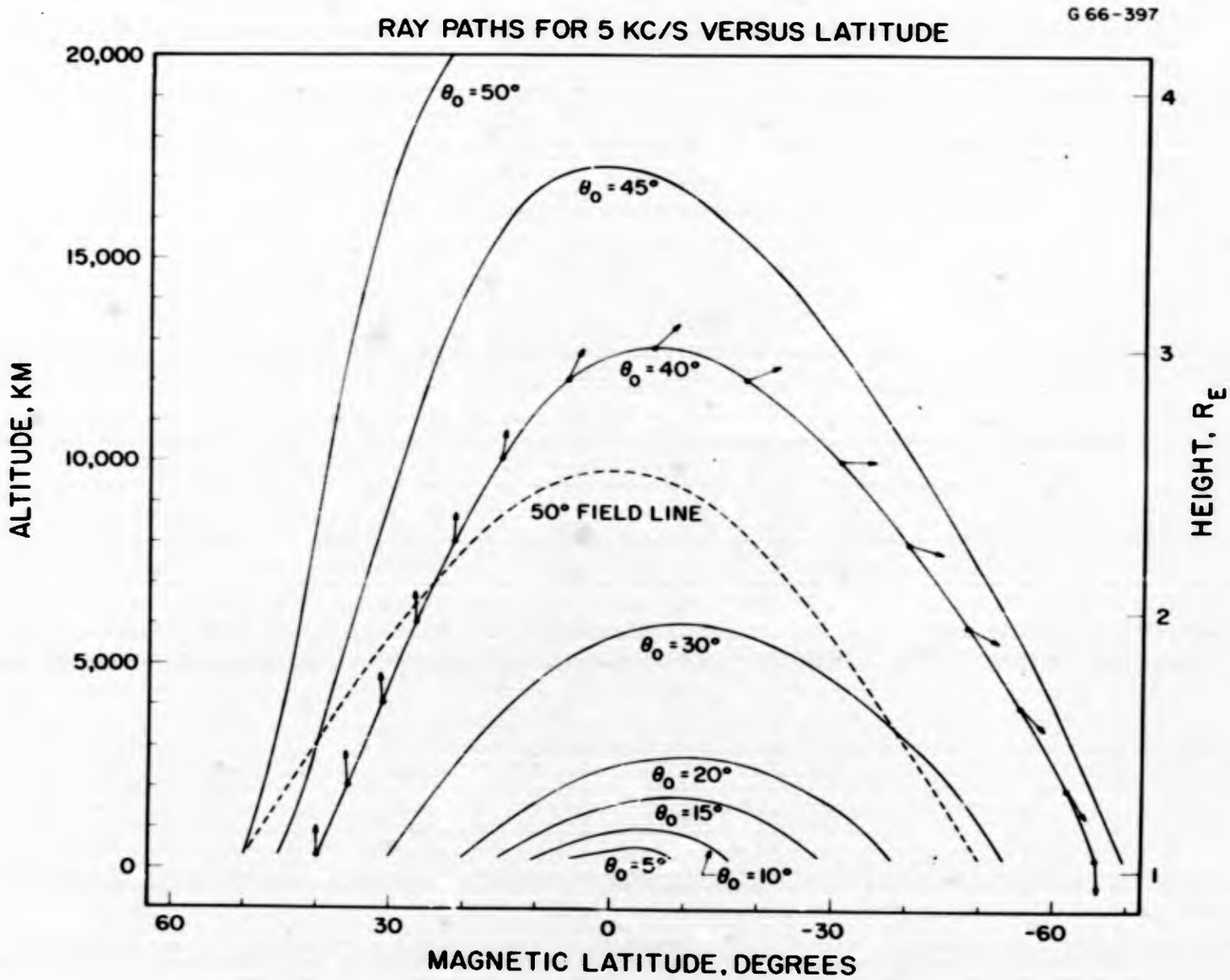
RAY PATHS FOR 5 KC/S VERSUS LATITUDE
G 66-397
20,000
15,000
10,000
5,000
0
ALTITUDE, KM
4
3
2
1
HEIGHT, R_E
$\theta_0 = 50°$
$\theta_0 = 45°$
$\theta_0 = 40°$
50° FIELD LINE
$\theta_0 = 30°$
$\theta_0 = 20°$
$\theta_0 = 15°$
$\theta_0 = 5°$
$\theta_0 = 10°$
60
30
0
-30
-60
MAGNETIC LATITUDE, DEGREES

Figure 8

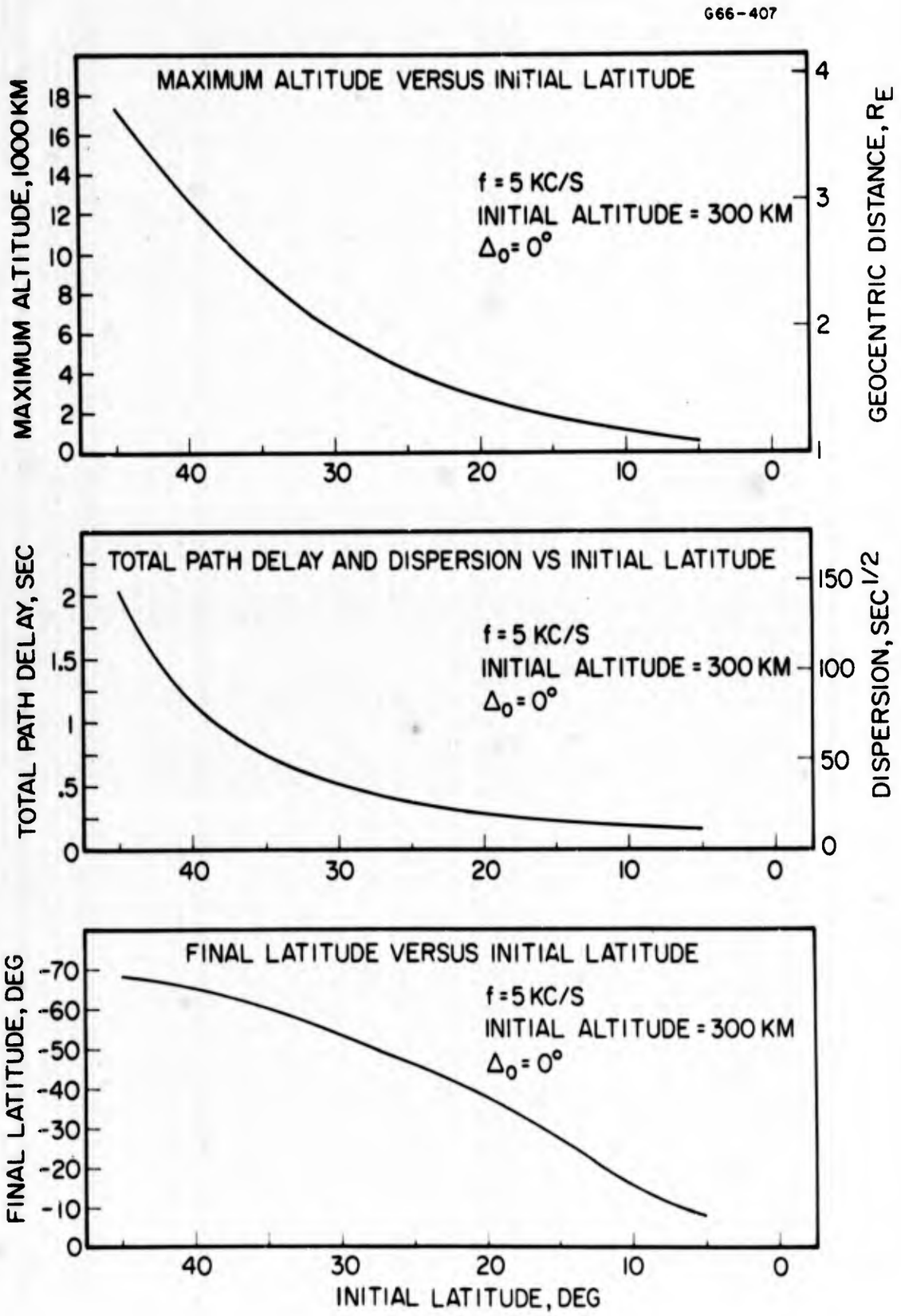
G66-407
MAXIMUM ALTITUDE VERSUS INITIAL LATITUDE
f = 5 KC/S
INITIAL ALTITUDE = 300 KM
Δ0 = 0°
MAXIMUM ALTITUDE, 1000 KM
GEOCENTRIC DISTANCE, RE
TOTAL PATH DELAY AND DISPERSION VS INITIAL LATITUDE
TOTAL PATH DELAY, SEC
DISPERSION, SEC 1/2
FINAL LATITUDE VERSUS INITIAL LATITUDE
FINAL LATITUDE, DEG
INITIAL LATITUDE, DEG

Figure 9

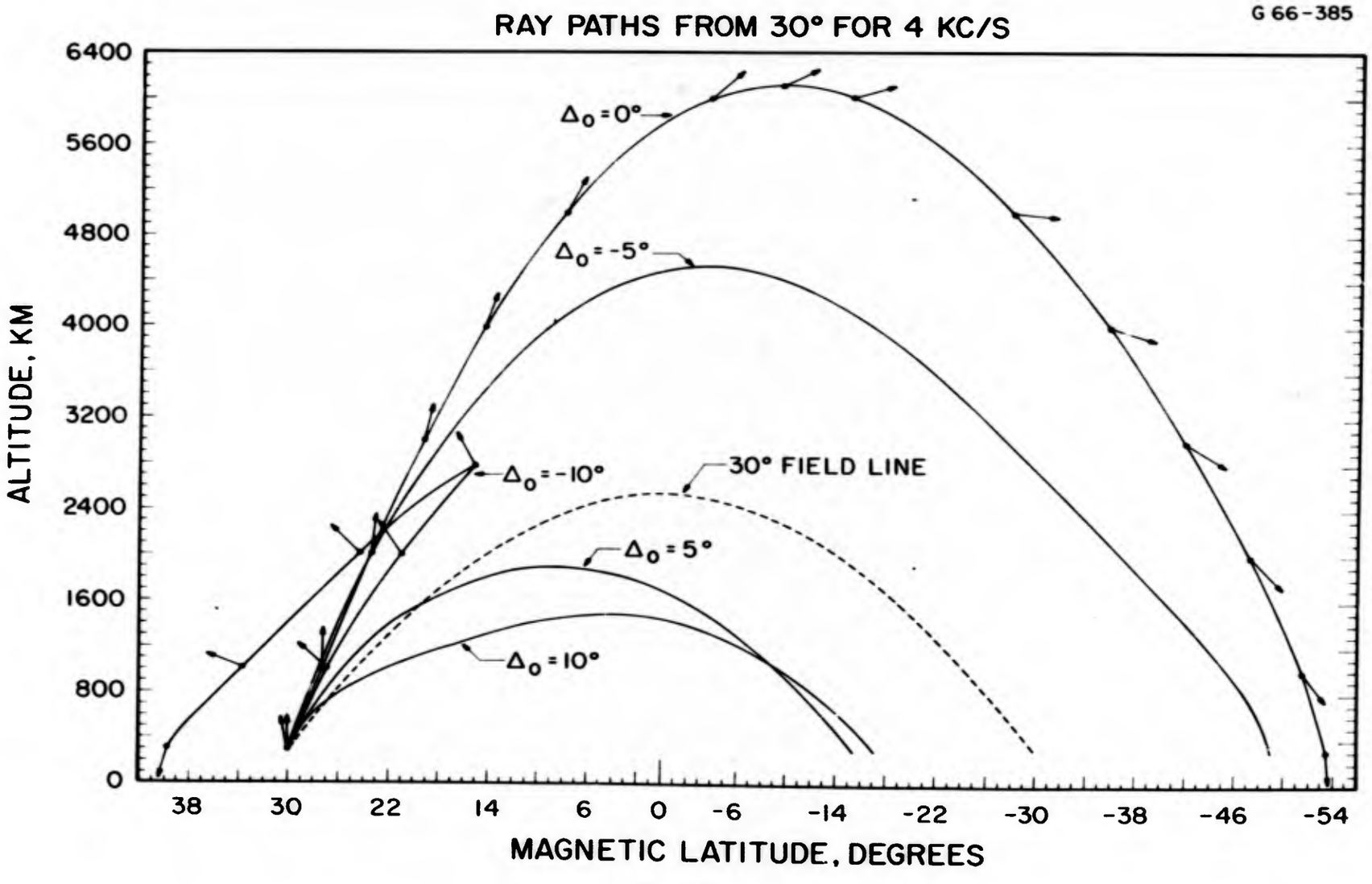
RAY PATHS FROM 30° FOR 4 KC/S
G 66-385
ALTITUDE, KM
6400
5600
4800
4000
3200
2400
1600
800
0
$\Delta_0 = 0°$
$\Delta_0 = -5°$
$\Delta_0 = -10°$
30° FIELD LINE
$\Delta_0 = 5°$
$\Delta_0 = 10°$
38
30
22
14
6
0
-6
-14
-22
-30
-38
-46
-54
MAGNETIC LATITUDE, DEGREES

Figure 10

G66-392

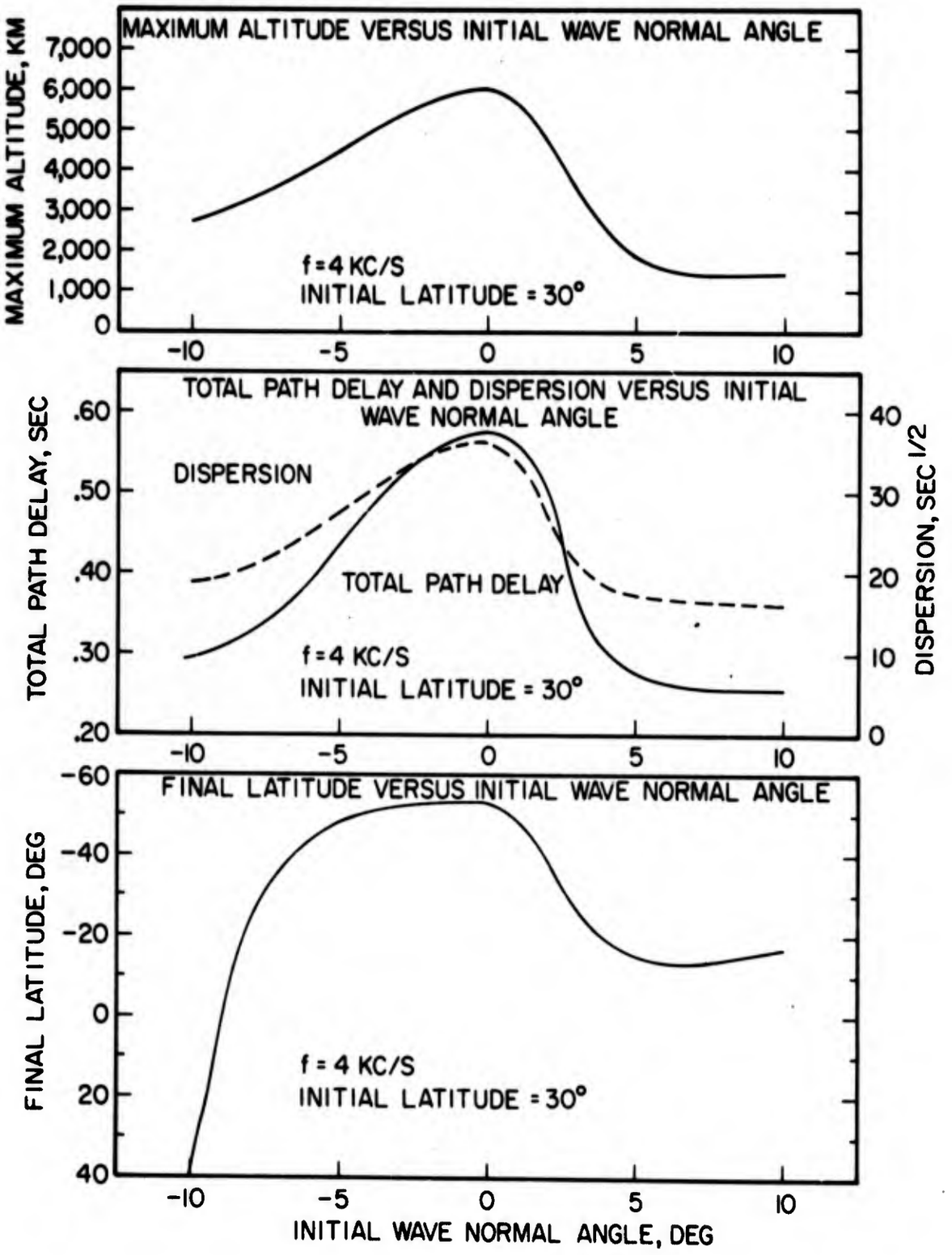

Figure 11

G66-398

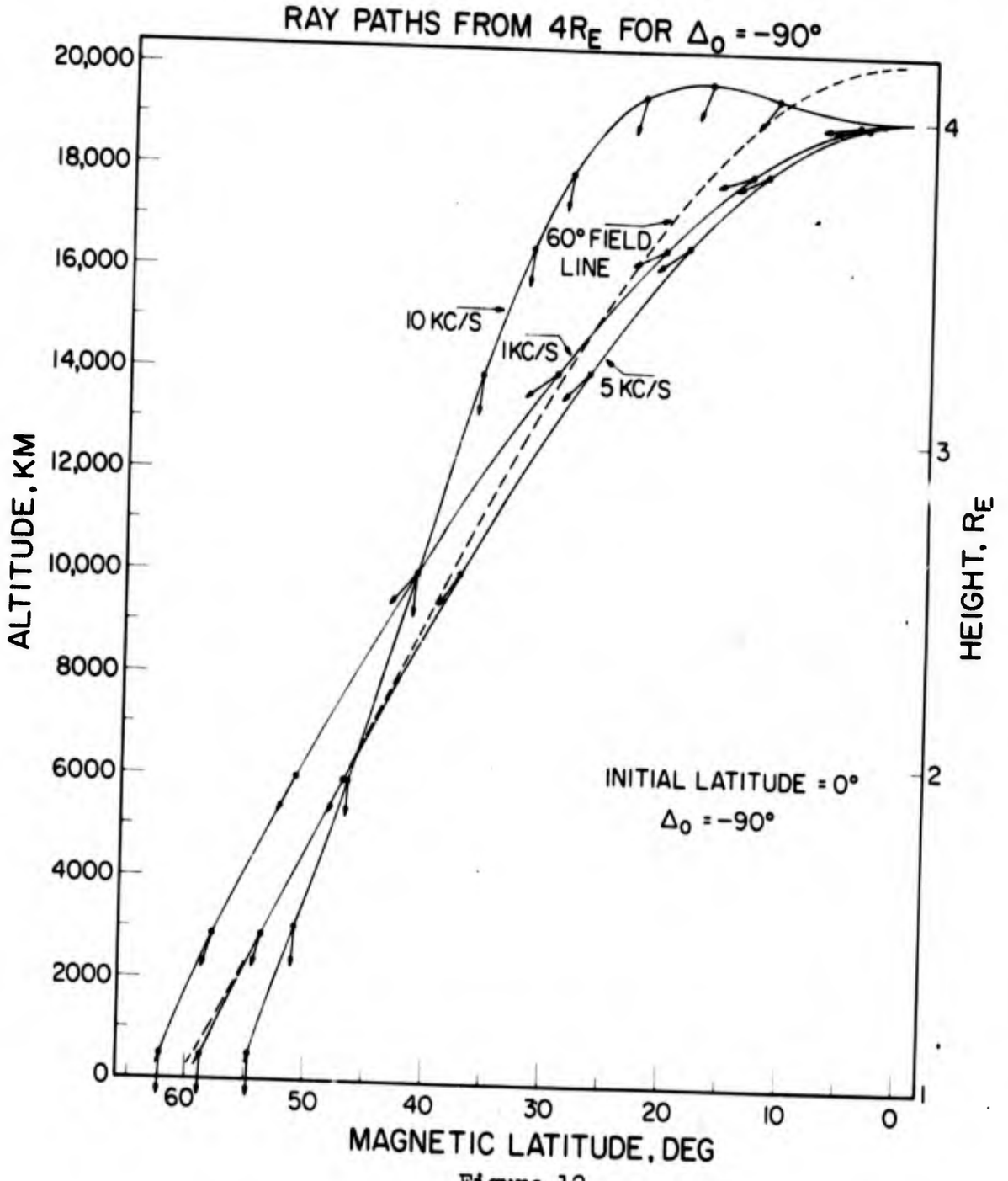

Figure 12

G66-405

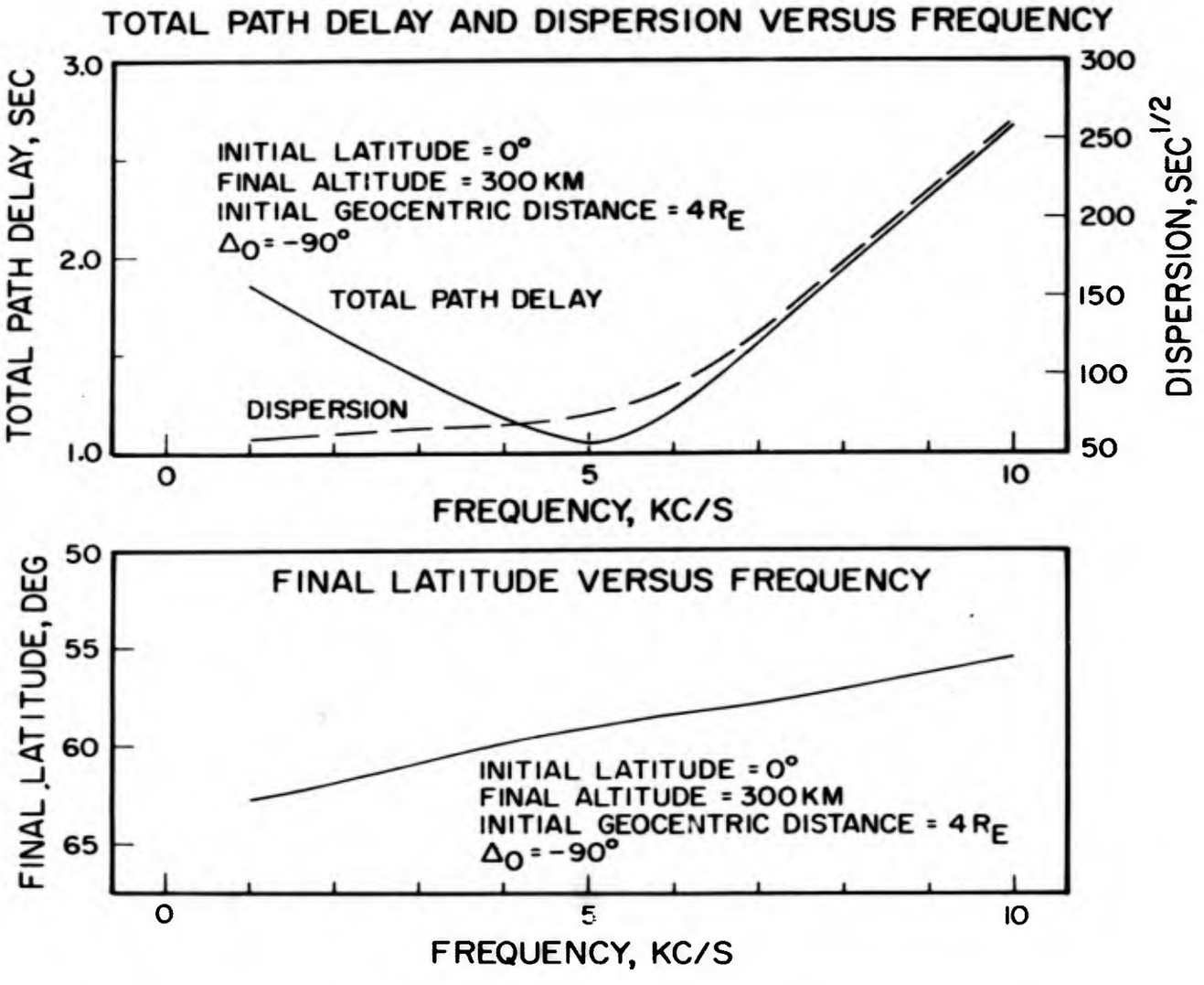

Figure 13

G66-390

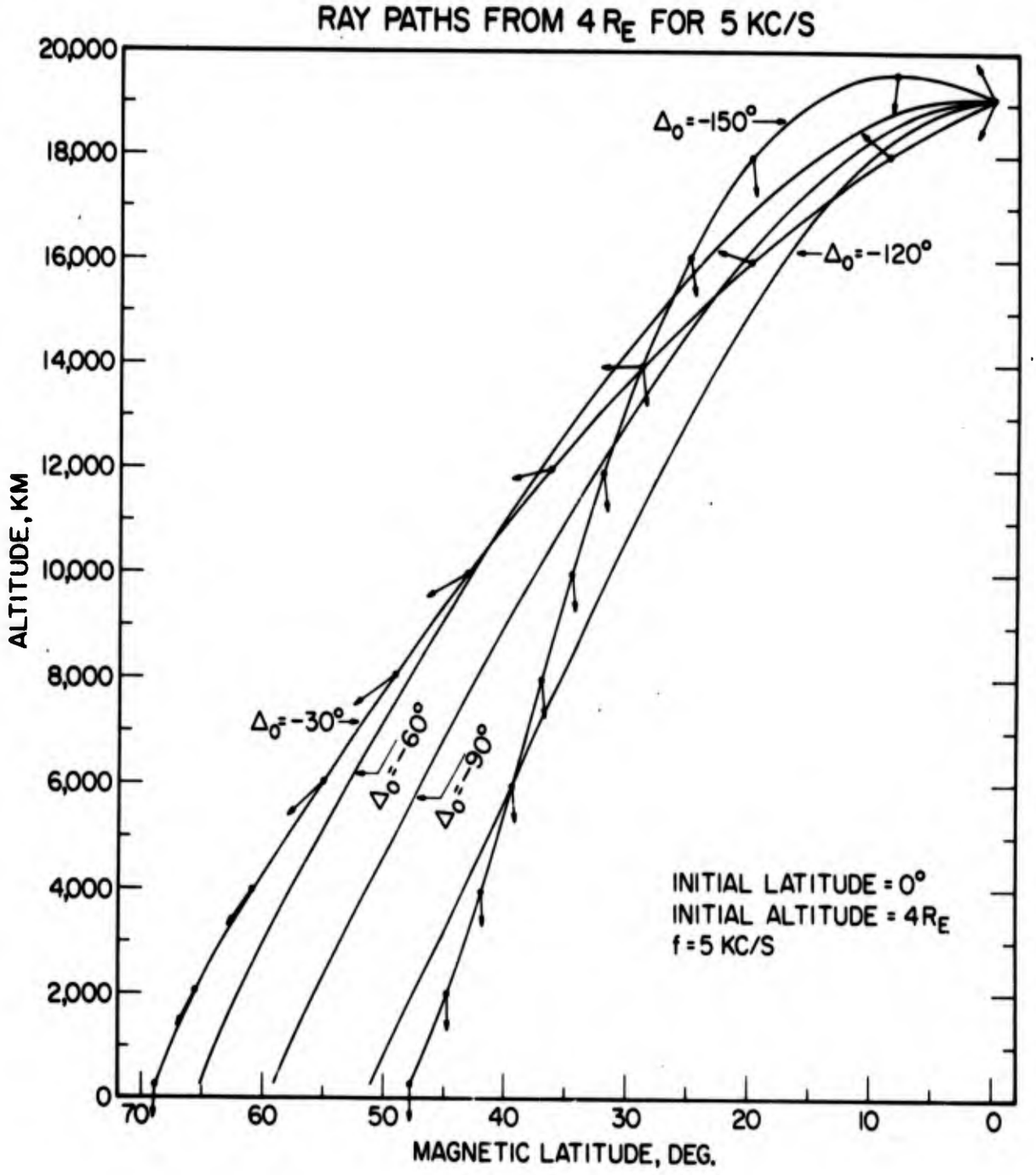

Figure 14

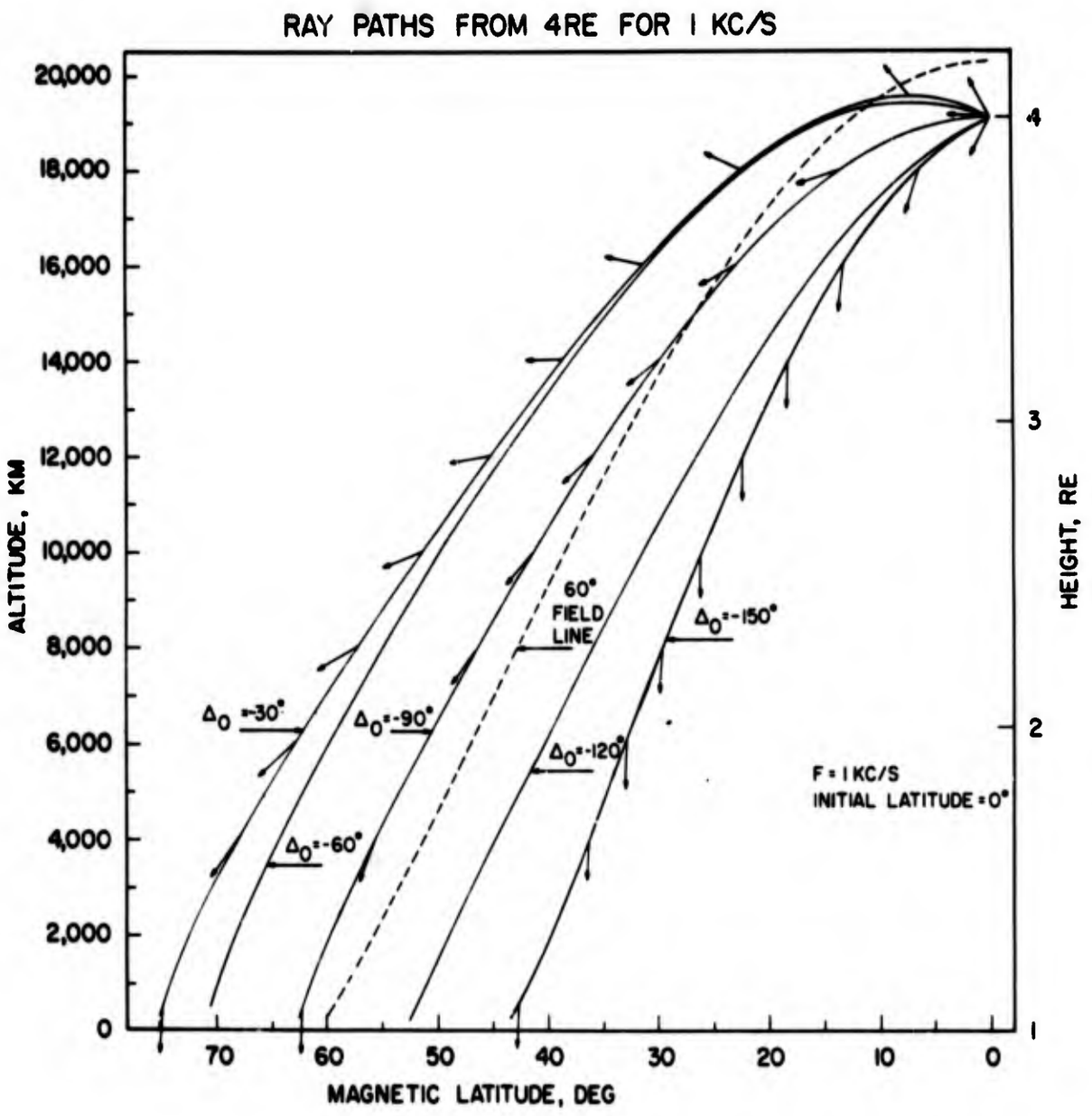
RAY PATHS FROM 4RE FOR 1 KC/S
ALTITUDE, KM
HEIGHT, RE
MAGNETIC LATITUDE, DEG
20,000
18,000
16,000
14,000
12,000
10,000
8,000
6,000
4,000
2,000
0
4
3
2
1
70
60
50
40
30
20
10
0
Δ0 =-30°
Δ0=-60°
Δ0=-90°
Δ0=-120°
Δ0=-150°
60° FIELD LINE
F = 1 KC/S
INITIAL LATITUDE = 0°

Figure 15

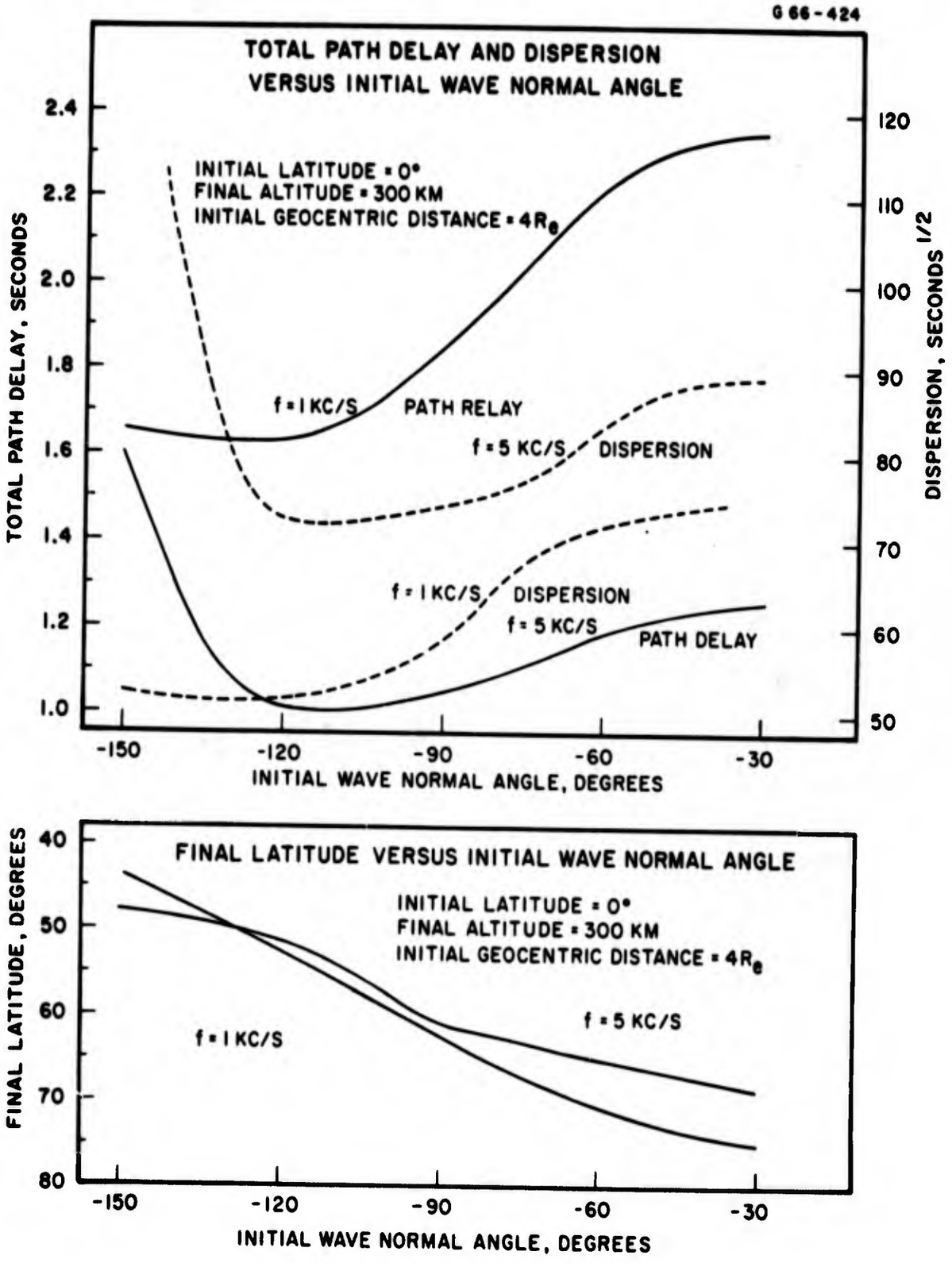
G 66-424
TOTAL PATH DELAY AND DISPERSION
VERSUS INITIAL WAVE NORMAL ANGLE
INITIAL LATITUDE = 0°
FINAL ALTITUDE = 300 KM
INITIAL GEOCENTRIC DISTANCE = 4Re
f = 1 KC/S PATH RELAY
f = 5 KC/S DISPERSION
f = 1 KC/S DISPERSION
f = 5 KC/S PATH DELAY
TOTAL PATH DELAY, SECONDS
DISPERSION, SECONDS 1/2
INITIAL WAVE NORMAL ANGLE, DEGREES
FINAL LATITUDE VERSUS INITIAL WAVE NORMAL ANGLE
INITIAL LATITUDE = 0°
FINAL ALTITUDE = 300 KM
INITIAL GEOCENTRIC DISTANCE = 4Re
f = 5 KC/S
f = 1 KC/S
FINAL LATITUDE, DEGREES
INITIAL WAVE NORMAL ANGLE, DEGREES

Figure 16

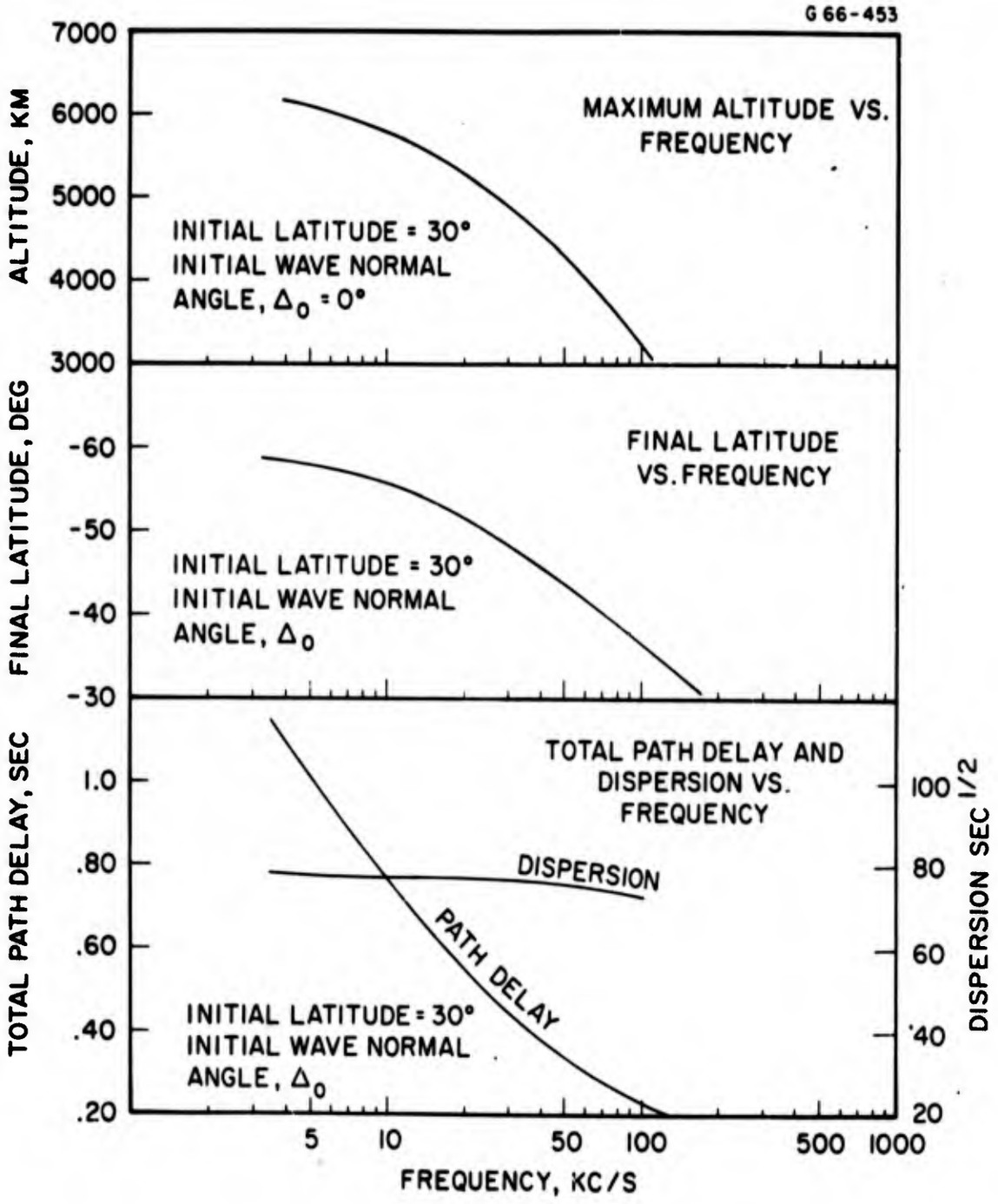
G 66-453
MAXIMUM ALTITUDE VS. FREQUENCY
INITIAL LATITUDE = 30°
INITIAL WAVE NORMAL ANGLE, Δ_0 = 0°
ALTITUDE, KM
7000
6000
5000
4000
3000
FINAL LATITUDE VS. FREQUENCY
INITIAL LATITUDE = 30°
INITIAL WAVE NORMAL ANGLE, Δ_0
FINAL LATITUDE, DEG
-60
-50
-40
-30
TOTAL PATH DELAY AND DISPERSION VS. FREQUENCY
DISPERSION
PATH DELAY
INITIAL LATITUDE = 30°
INITIAL WAVE NORMAL ANGLE, Δ_0
TOTAL PATH DELAY, SEC
1.0
.80
.60
.40
.20
DISPERSION SEC$^{1/2}$
100
80
60
40
20
5
10
50
100
500
1000
FREQUENCY, KC/S

Figure 17

G66-406

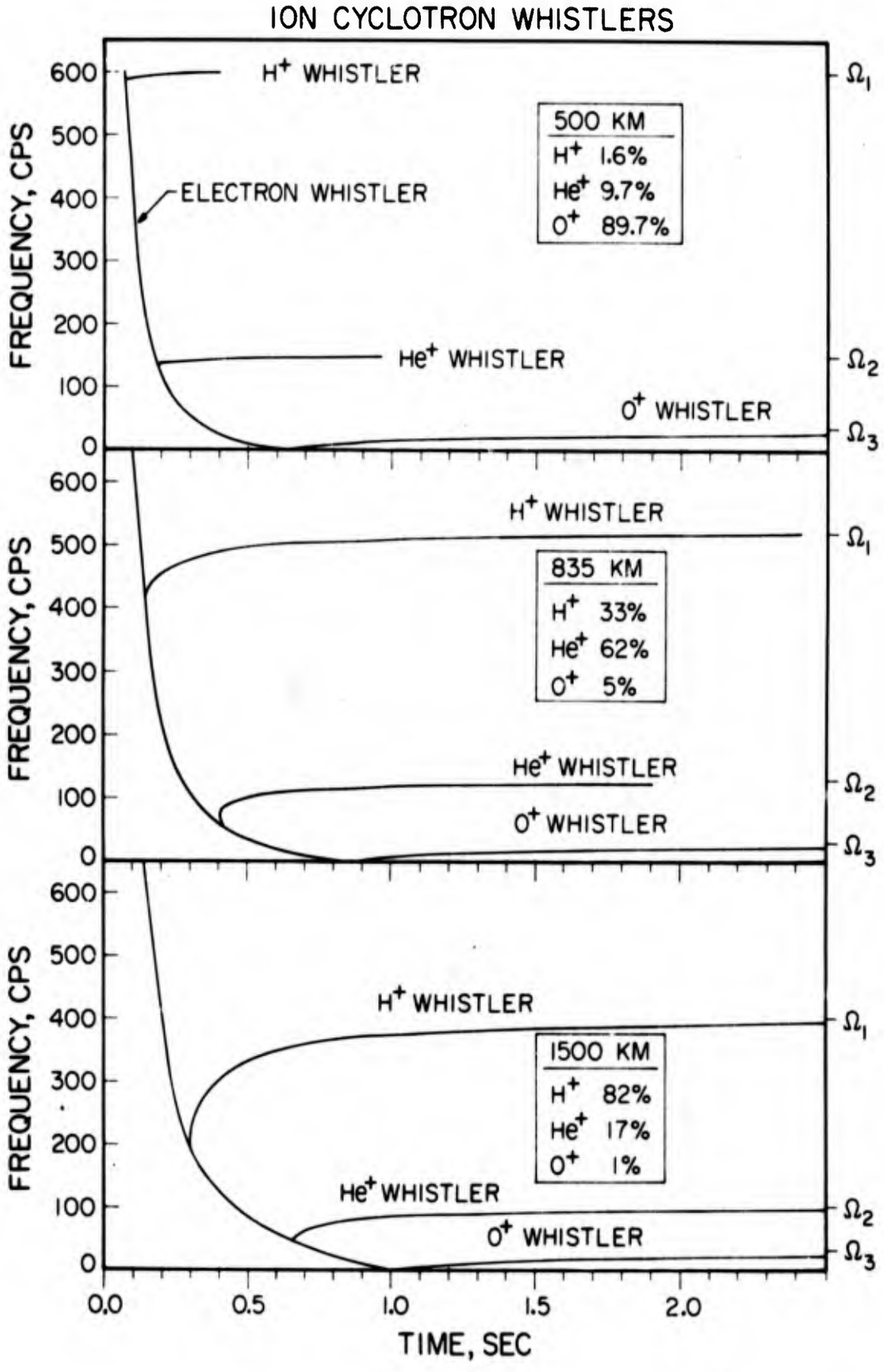

Figure 18

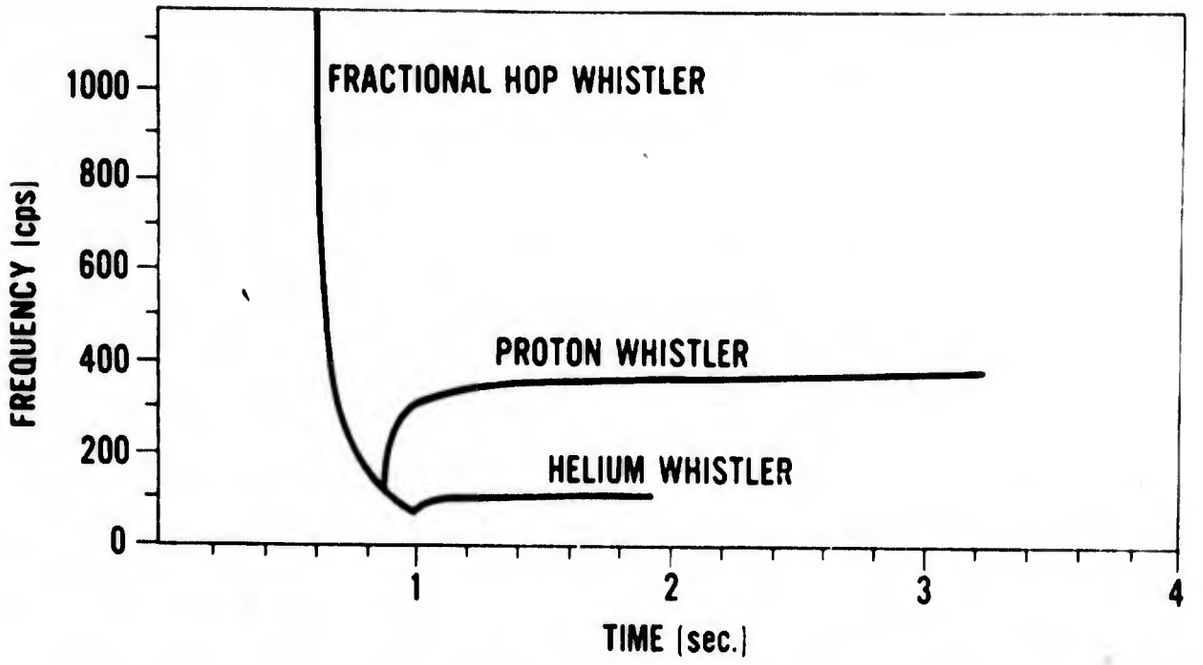

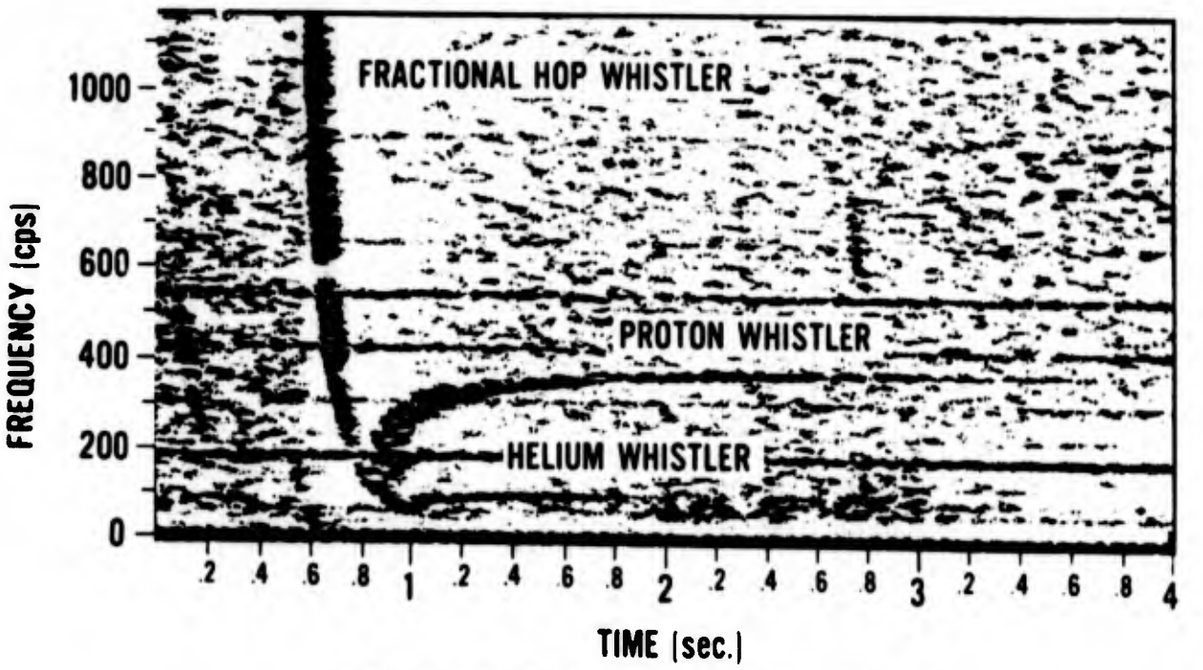

ORORAL AUSTRALIA DEC. 3 1965 1221:15 U.T.
132° E LONG. 32° S LAT. 2007 KM HEIGHT

Figure 19

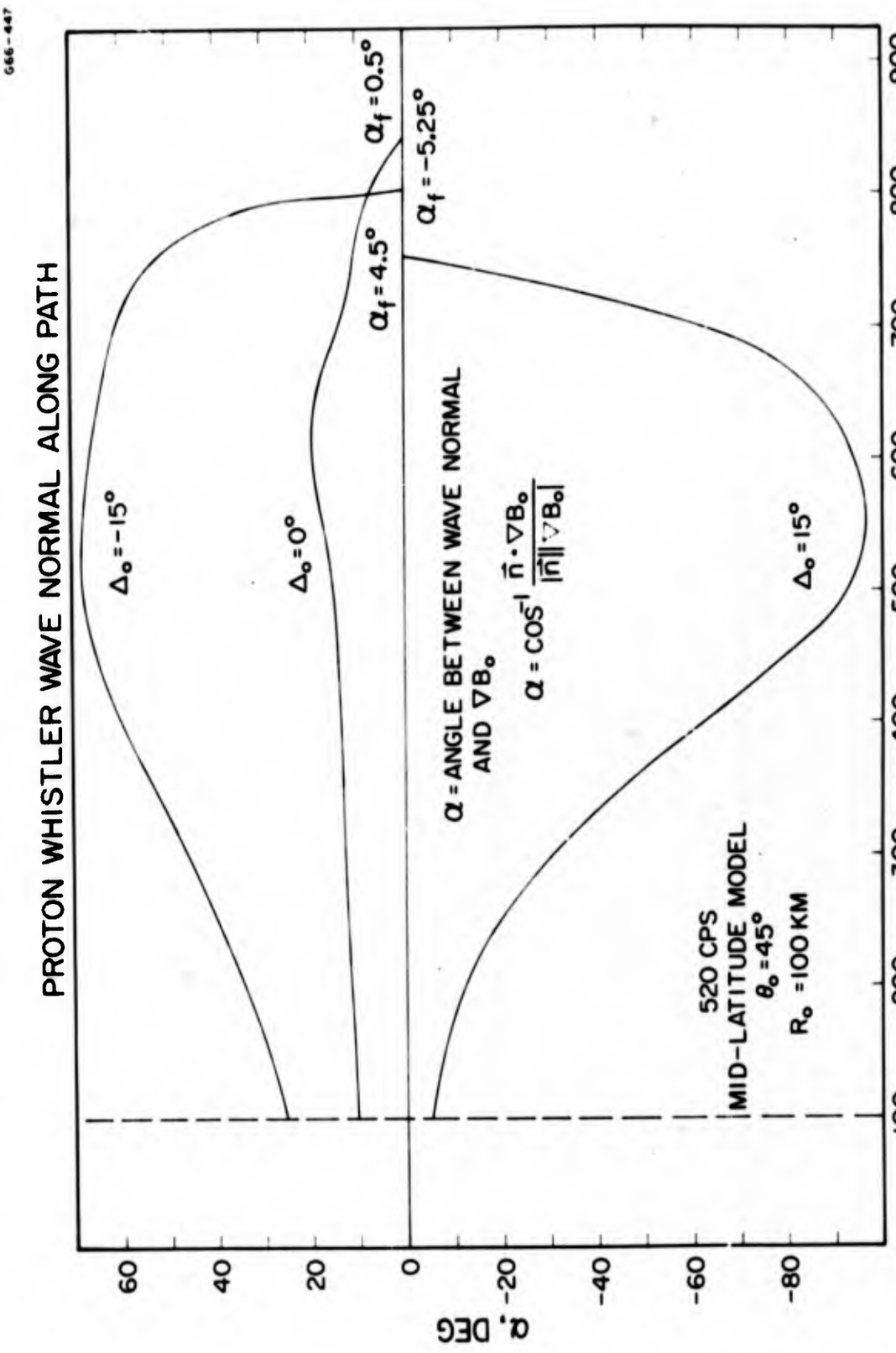
PROTON WHISTLER WAVE NORMAL ALONG PATH
$\Delta_o = -15°$
$\Delta_o = 0°$
$\Delta_o = 15°$
$\alpha_f = 0.5°$
$\alpha_f = -5.25°$
$\alpha_f = 4.5°$
α = ANGLE BETWEEN WAVE NORMAL AND ∇B_o
$\alpha = \cos^{-1} \frac{\hat{n} \cdot \nabla B_o}{|\hat{n}||\nabla B_o|}$
520 CPS
MID-LATITUDE MODEL
$\theta_o = 45°$
$R_o = 100$ KM
α, DEG
ALTITUDE, KM
60
40
20
0
-20
-40
-60
-80
100
200
300
400
500
600
700
800
900

Figure 20

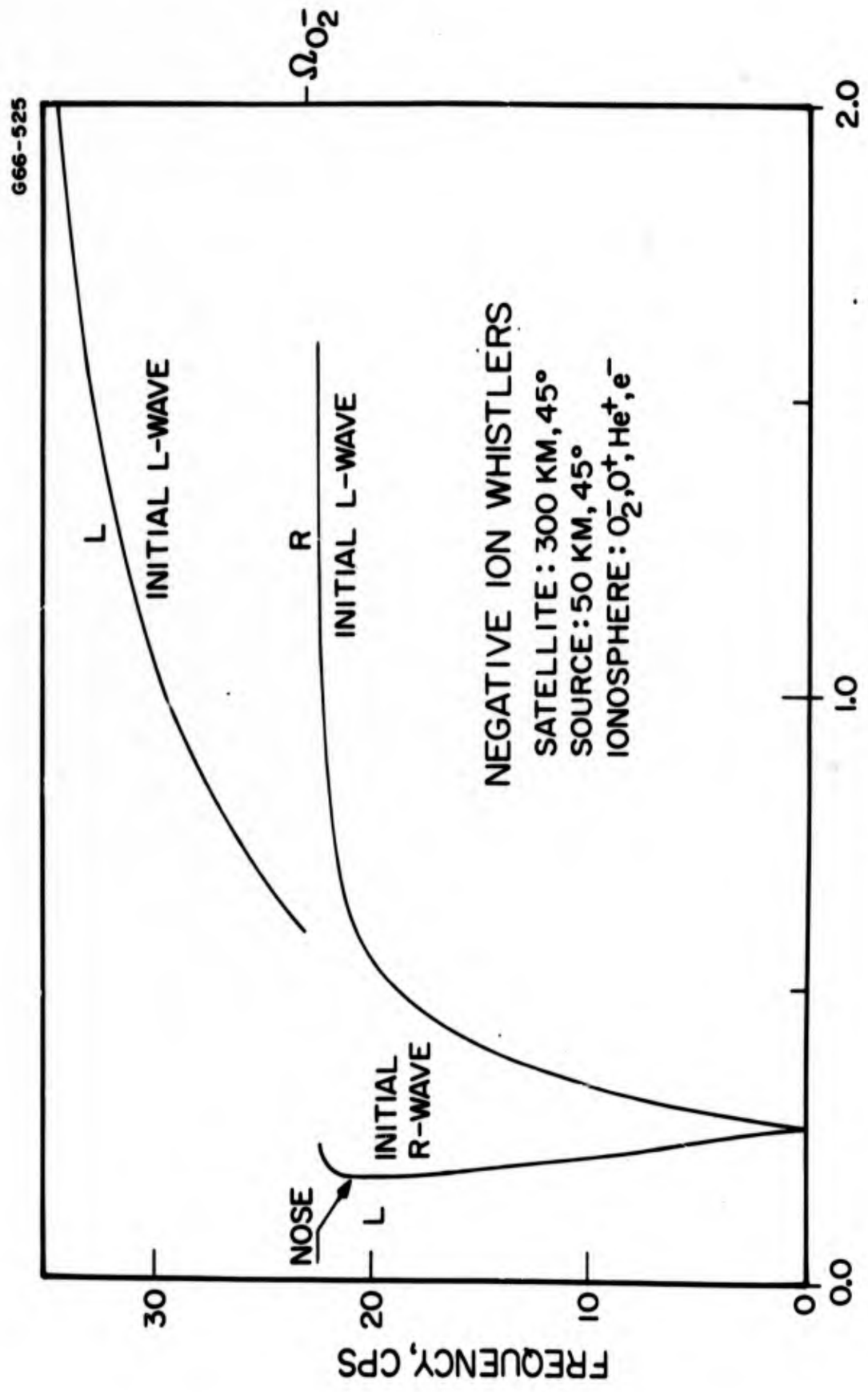
G66-525
$\Omega_{O_2^-}$
2.0
1.0
0.0
TIME, SEC
30
20
10
0
FREQUENCY, CPS
L
INITIAL L-WAVE
R
INITIAL L-WAVE
NEGATIVE ION WHISTLERS
SATELLITE: 300 KM, 45°
SOURCE: 50 KM, 45°
IONOSPHERE: O_2^-, O^+, He^+, e^-
NOSE
L
INITIAL R-WAVE

Figure 21

G 66-478

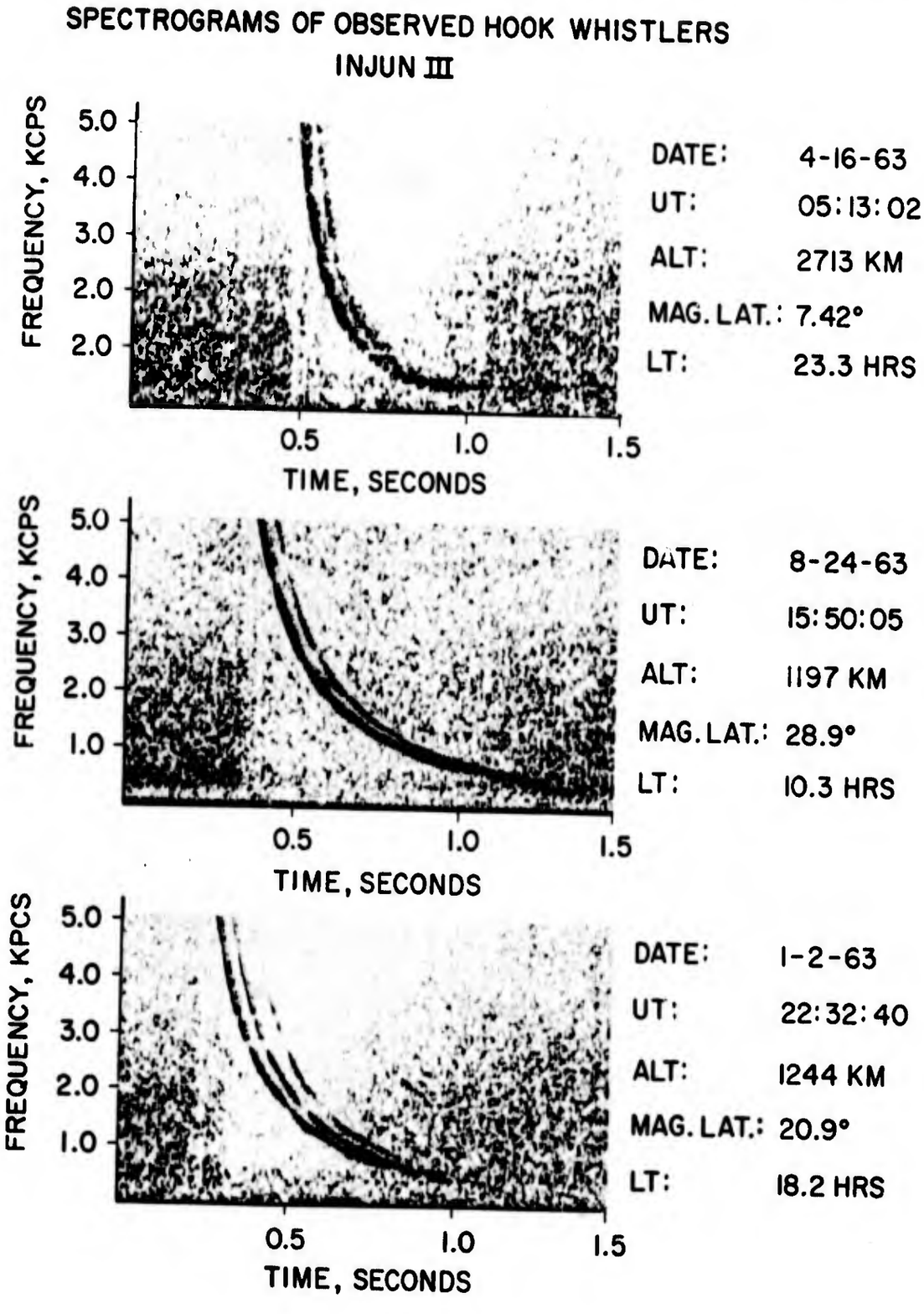

Figure 22

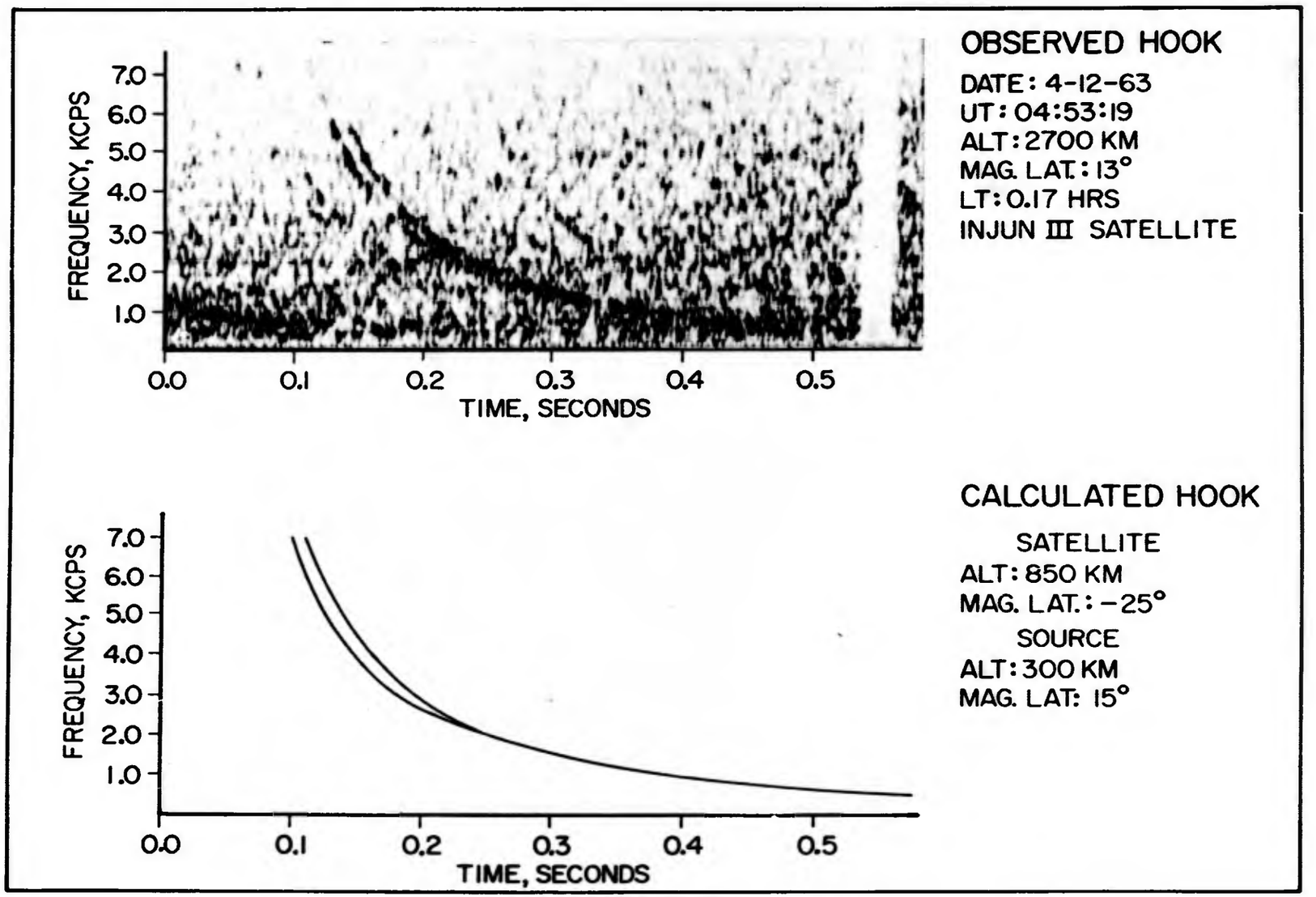
OBSERVED HOOK
DATE: 4-12-63
UT: 04:53:19
ALT: 2700 KM
MAG. LAT.: 13°
LT: 0.17 HRS
INJUN III SATELLITE
FREQUENCY, KCPS
7.0
6.0
5.0
4.0
3.0
2.0
1.0
0.0
0.1
0.2
0.3
0.4
0.5
TIME, SECONDS
CALCULATED HOOK
SATELLITE
ALT: 850 KM
MAG. LAT.: −25°
SOURCE
ALT: 300 KM
MAG. LAT: 15°
FREQUENCY, KCPS
7.0
6.0
5.0
4.0
3.0
2.0
1.0
0.0
0.1
0.2
0.3
0.4
0.5
TIME, SECONDS

Figure 23

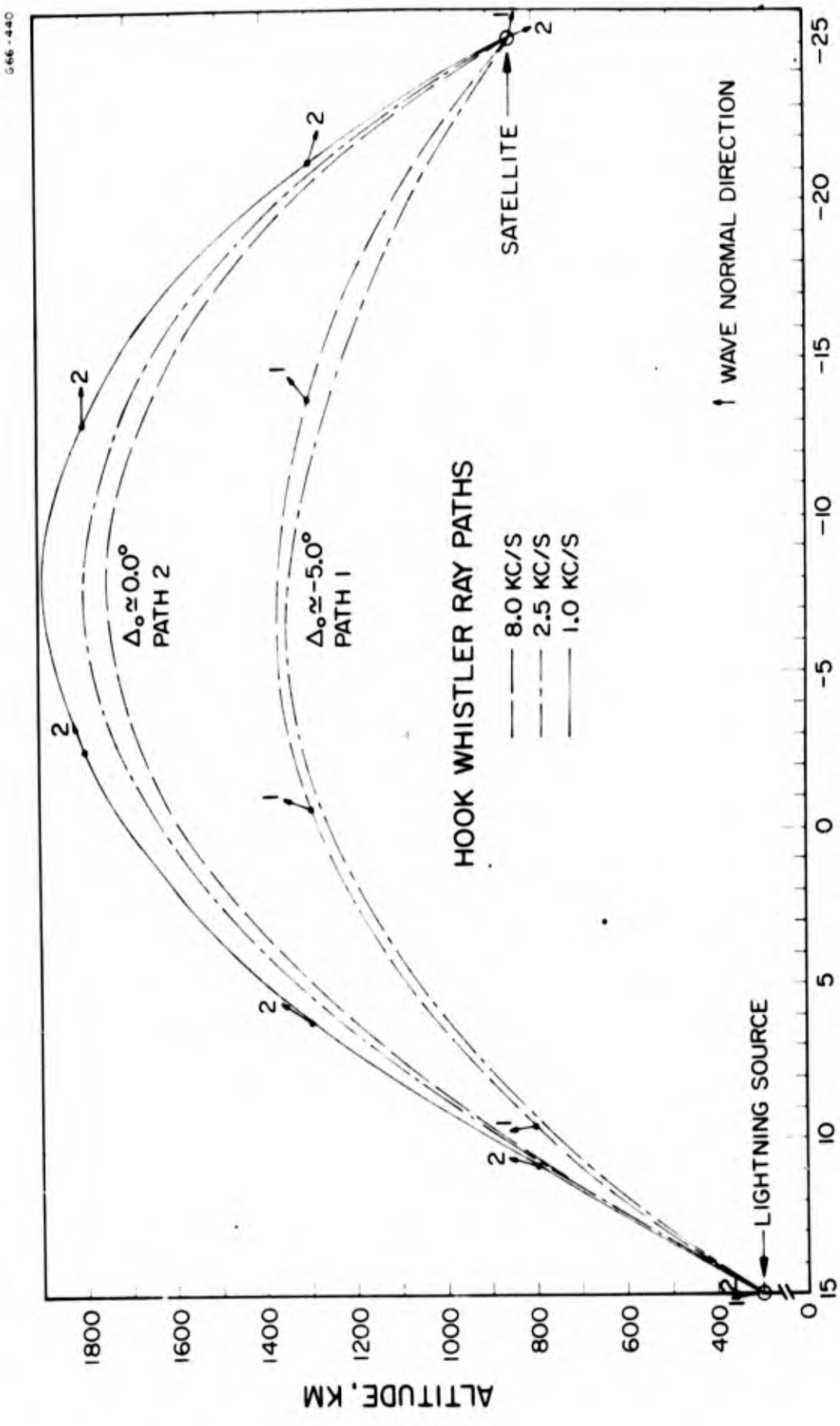
HOOK WHISTLER RAY PATHS
8.0 KC/S
2.5 KC/S
1.0 KC/S
$\Delta_o \simeq 0.0°$
PATH 2
$\Delta_o \simeq -5.0°$
PATH 1
SATELLITE
LIGHTNING SOURCE
WAVE NORMAL DIRECTION
ALTITUDE, KM
MAGNETIC LATITUDE, DEGREES

Figure 24

G66-473

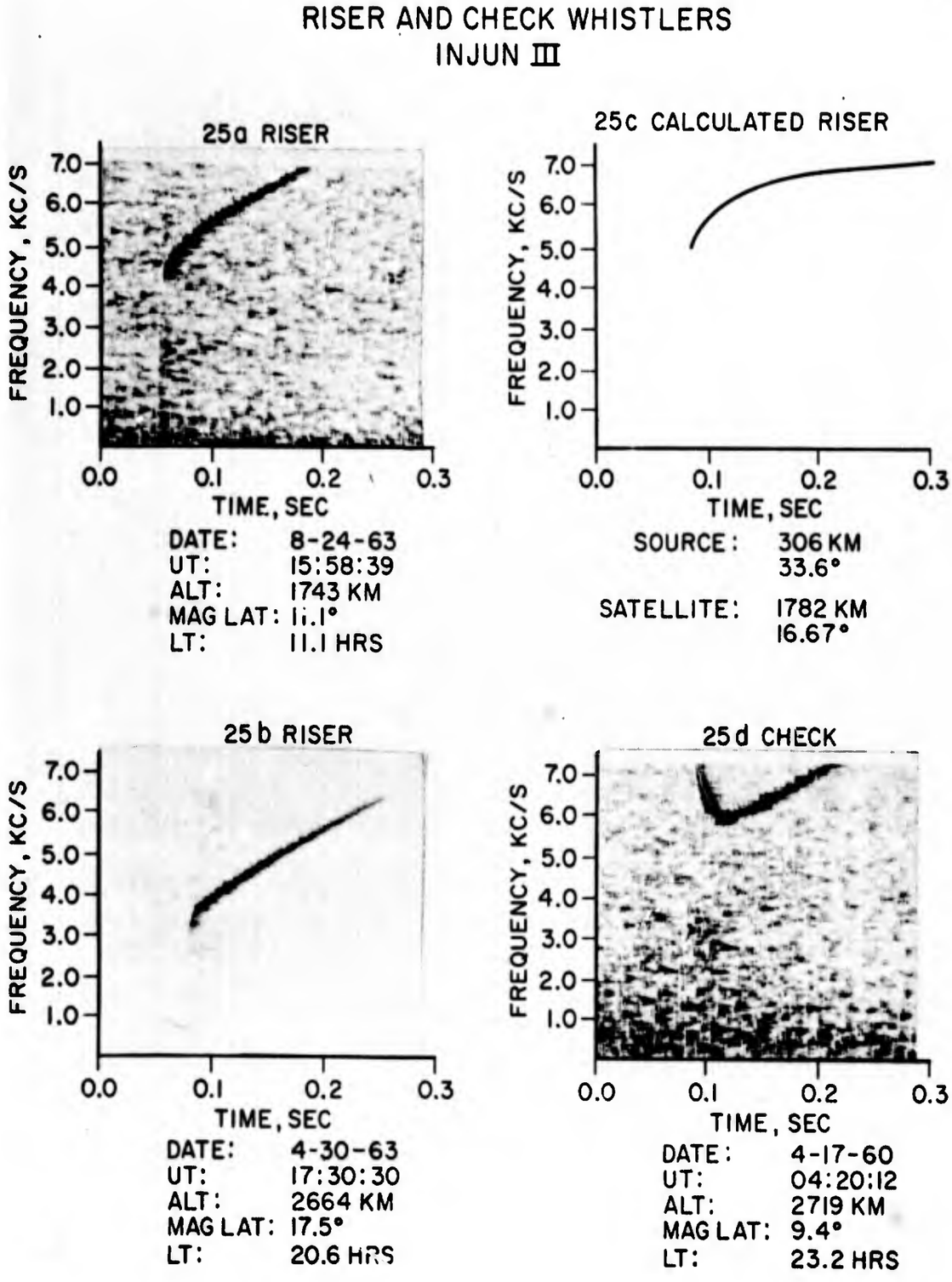

Figure 25

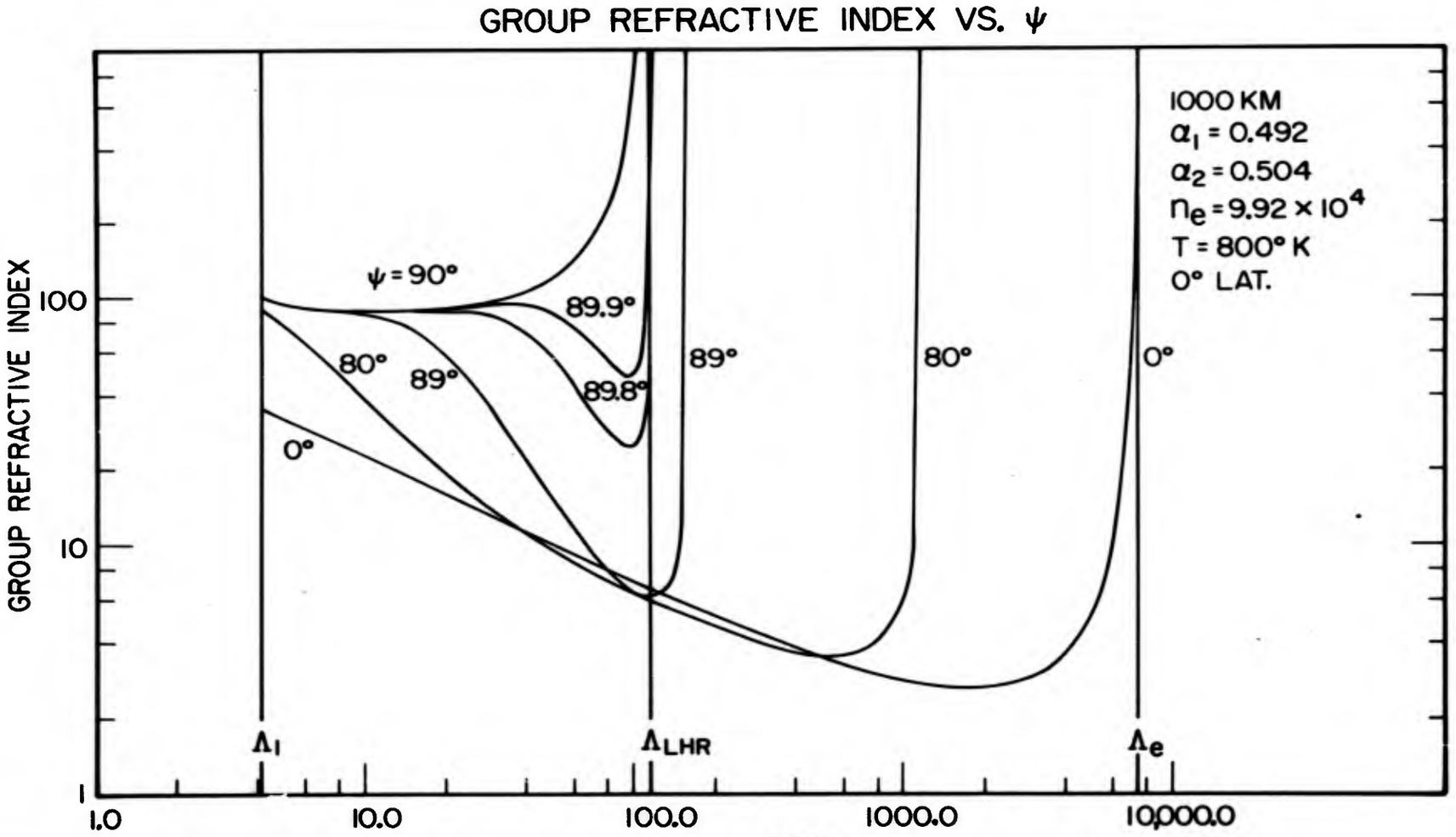
GROUP REFRACTIVE INDEX VS. ψ
GROUP REFRACTIVE INDEX
100
10
1
1000 KM
α1 = 0.492
α2 = 0.504
ne = 9.92 x 10^4
T = 800° K
0° LAT.
ψ = 90°
89.9°
89.8°
89°
80°
89°
80°
0°
0°
Λ1
ΛLHR
Λe
1.0
10.0
100.0
1000.0
10,000.0
Λ = ω/Ω2

Figure 26

G66-526

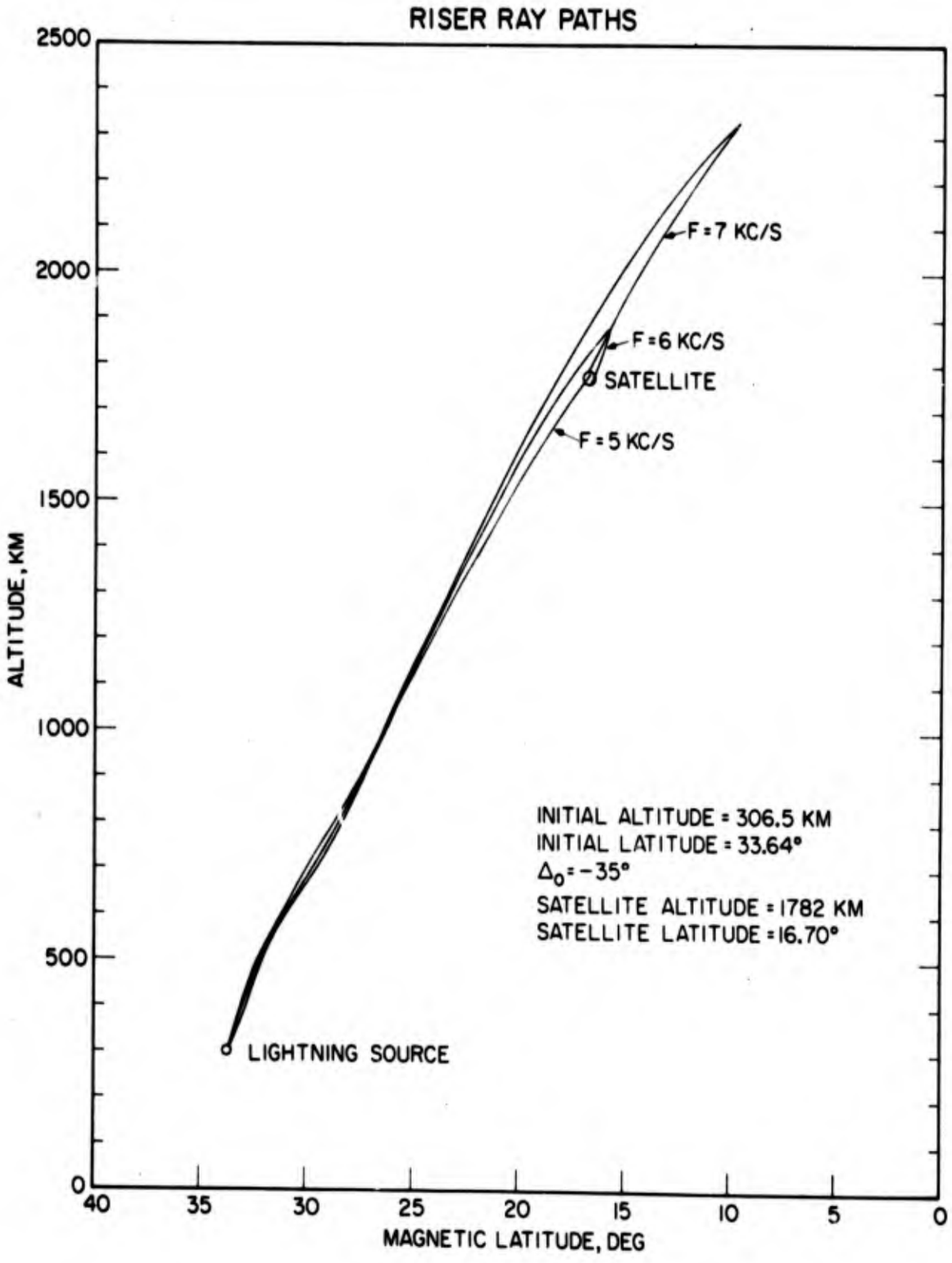

Figure 27

JAN. 14, 1963 10:46:10 UT, 05:20LT, ALTITUDE = 640 Km
L = 7.2 Ω_1 = 675 c/s.

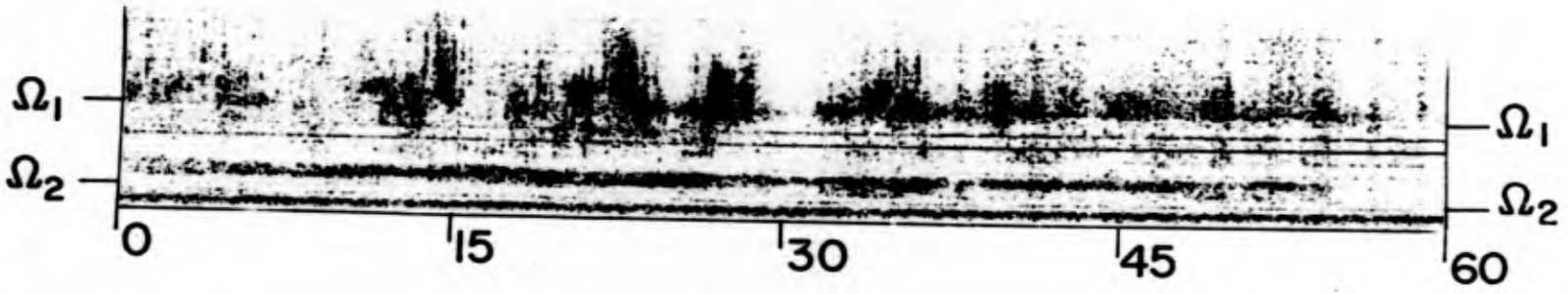

JAN. 17, 1963, 10:24:00 UT, 05:11LT ALTITUDE = 527 Km
L = 9.9 Ω_1 = 725 c/s.

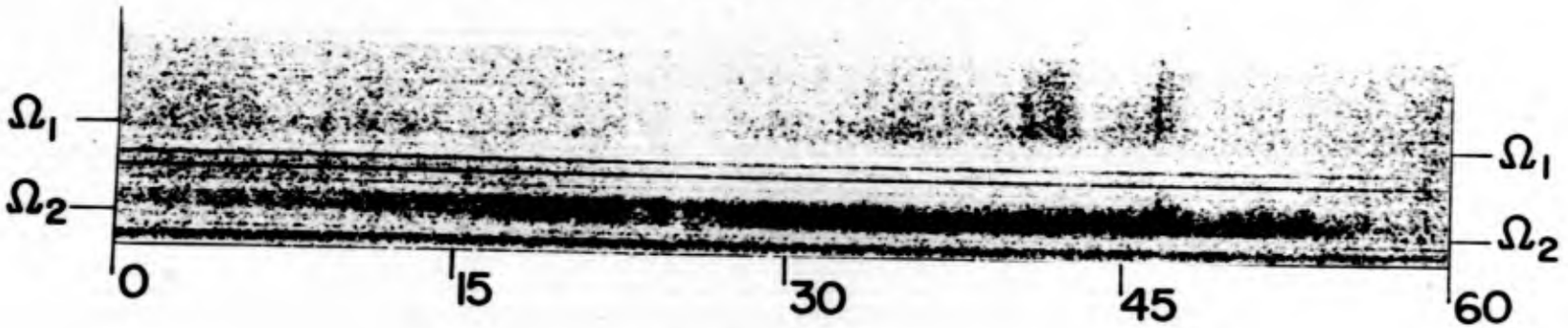

TIME (sec.)

Figure 28

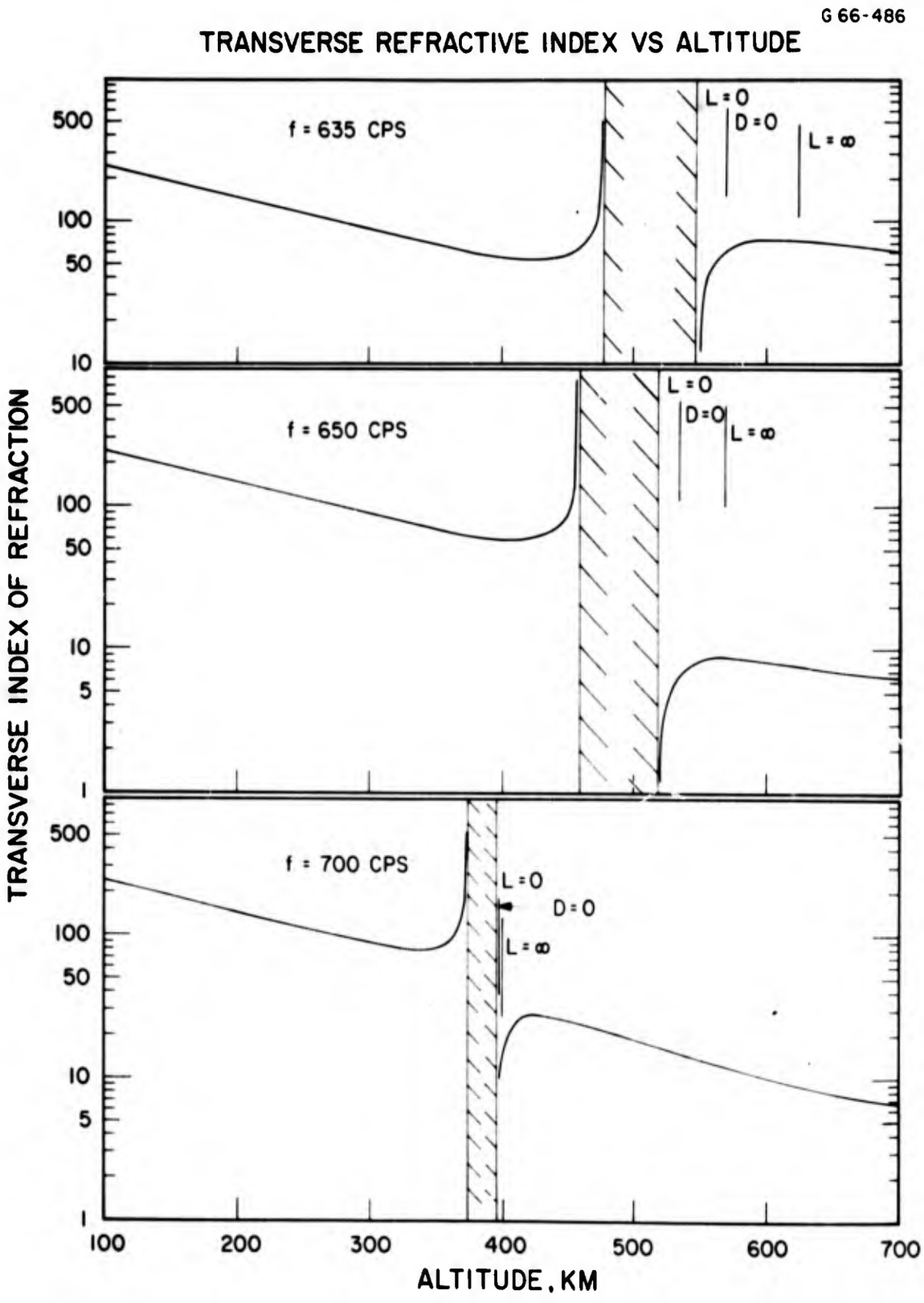
G 66-486
TRANSVERSE REFRACTIVE INDEX VS ALTITUDE
f = 635 CPS
L = 0
D = 0
L = ∞
f = 650 CPS
L = 0
D = 0
L = ∞
f = 700 CPS
L = 0
D = 0
L = ∞
TRANSVERSE INDEX OF REFRACTION
500
100
50
10
5
1
100
200
300
400
500
600
700
ALTITUDE, KM

Figure 29

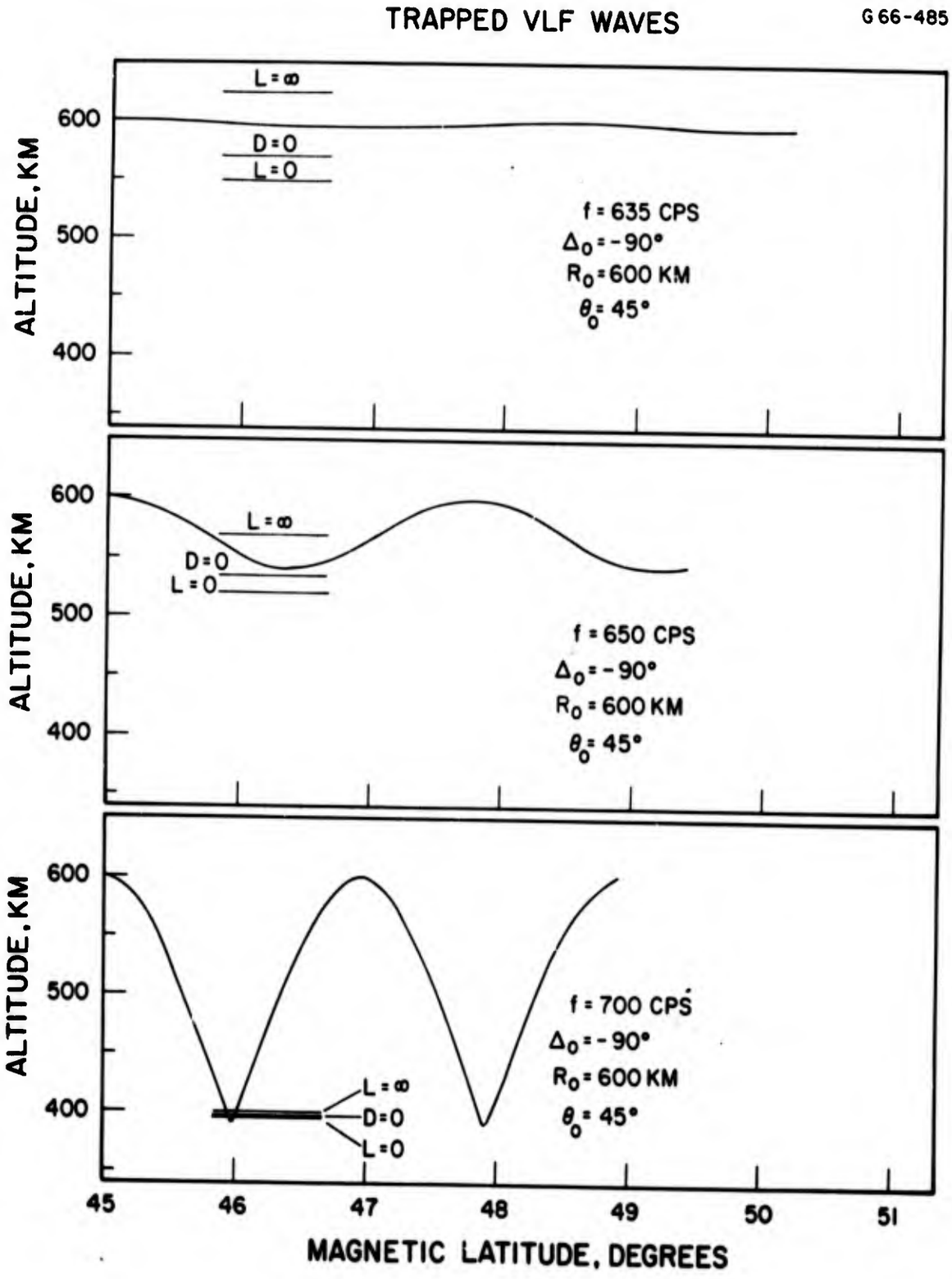
TRAPPED VLF WAVES
G 66-485
ALTITUDE, KM
600
500
400
L = ∞
D = 0
L = 0
f = 635 CPS
Δ0 = -90°
R0 = 600 KM
θ0 = 45°
f = 650 CPS
f = 700 CPS
45
46
47
48
49
50
51
MAGNETIC LATITUDE, DEGREES

Figure 30

Figure 31

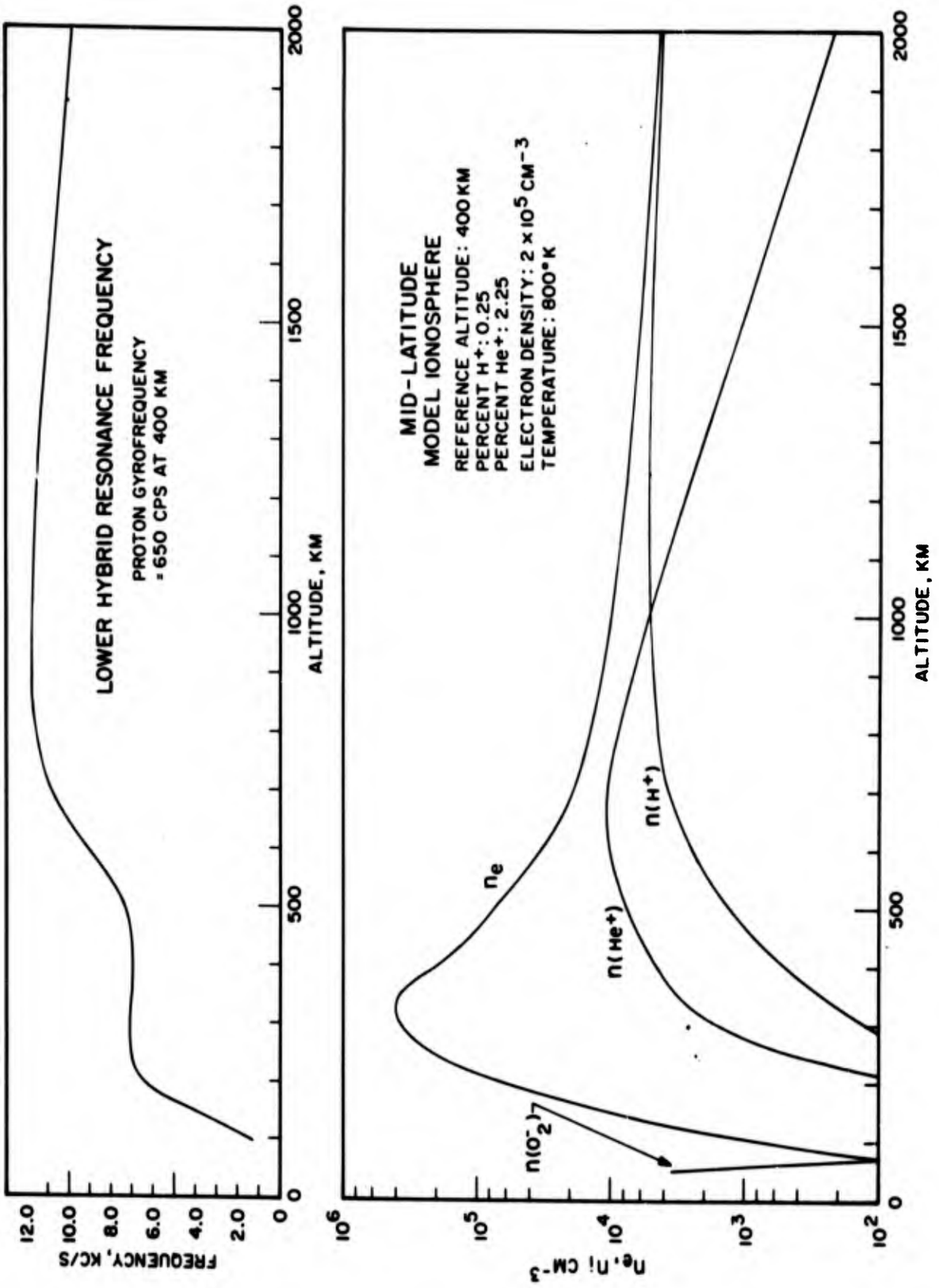
G66-393
LOWER HYBRID RESONANCE FREQUENCY
PROTON GYROFREQUENCY
= 650 CPS AT 400 KM
FREQUENCY, KC/S
12.0
10.0
8.0
6.0
4.0
2.0
0
0
500
1000
1500
2000
ALTITUDE, KM
MID-LATITUDE
MODEL IONOSPHERE
REFERENCE ALTITUDE: 400 KM
PERCENT H+: 0.25
PERCENT He+: 2.25
ELECTRON DENSITY: 2 × 10^5 CM^-3
TEMPERATURE: 800° K
ne
n(He+)
n(H+)
n(O2-)
ne, ni CM-3
10^6
10^5
10^4
10^3
10^2
0
500
1000
1500
2000
ALTITUDE, KM

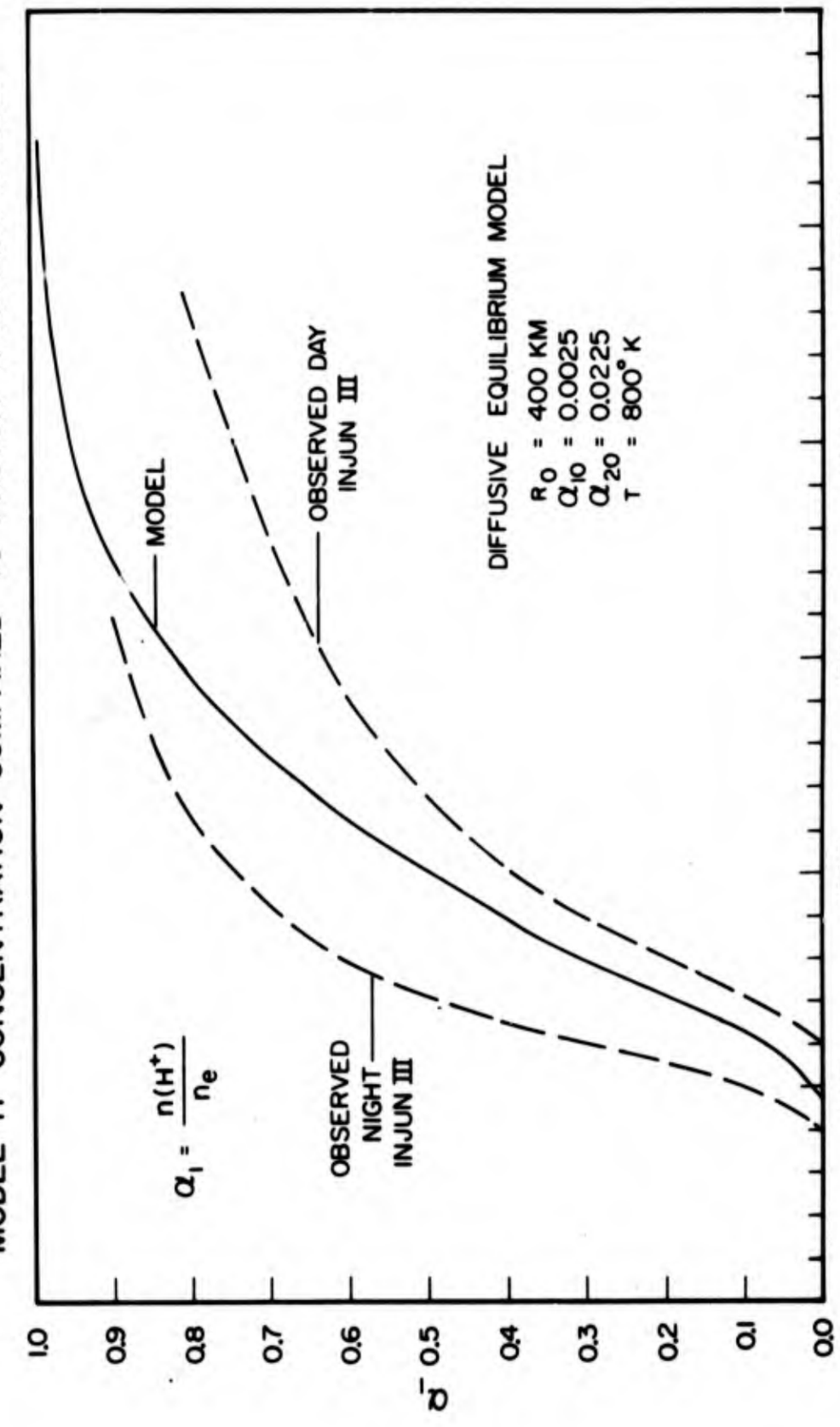
G66-387
MODEL H+ CONCENTRATION COMPARED TO PROTON WHISTLER VALUES
$\alpha_i = \frac{n(H^+)}{n_e}$
MODEL
OBSERVED DAY
INJUN III
OBSERVED
NIGHT
INJUN III
DIFFUSIVE EQUILIBRIUM MODEL
R_0 = 400 KM
α_{10} = 0.0025
α_{20} = 0.0225
T = 800° K
α^-
1.0
0.9
0.8
0.7
0.6
0.5
0.4
0.3
0.2
0.1
0.0
500
1000
1500
2000
2500
ALTITUDE, KM

Figure 32

Figure 33

G 66-408

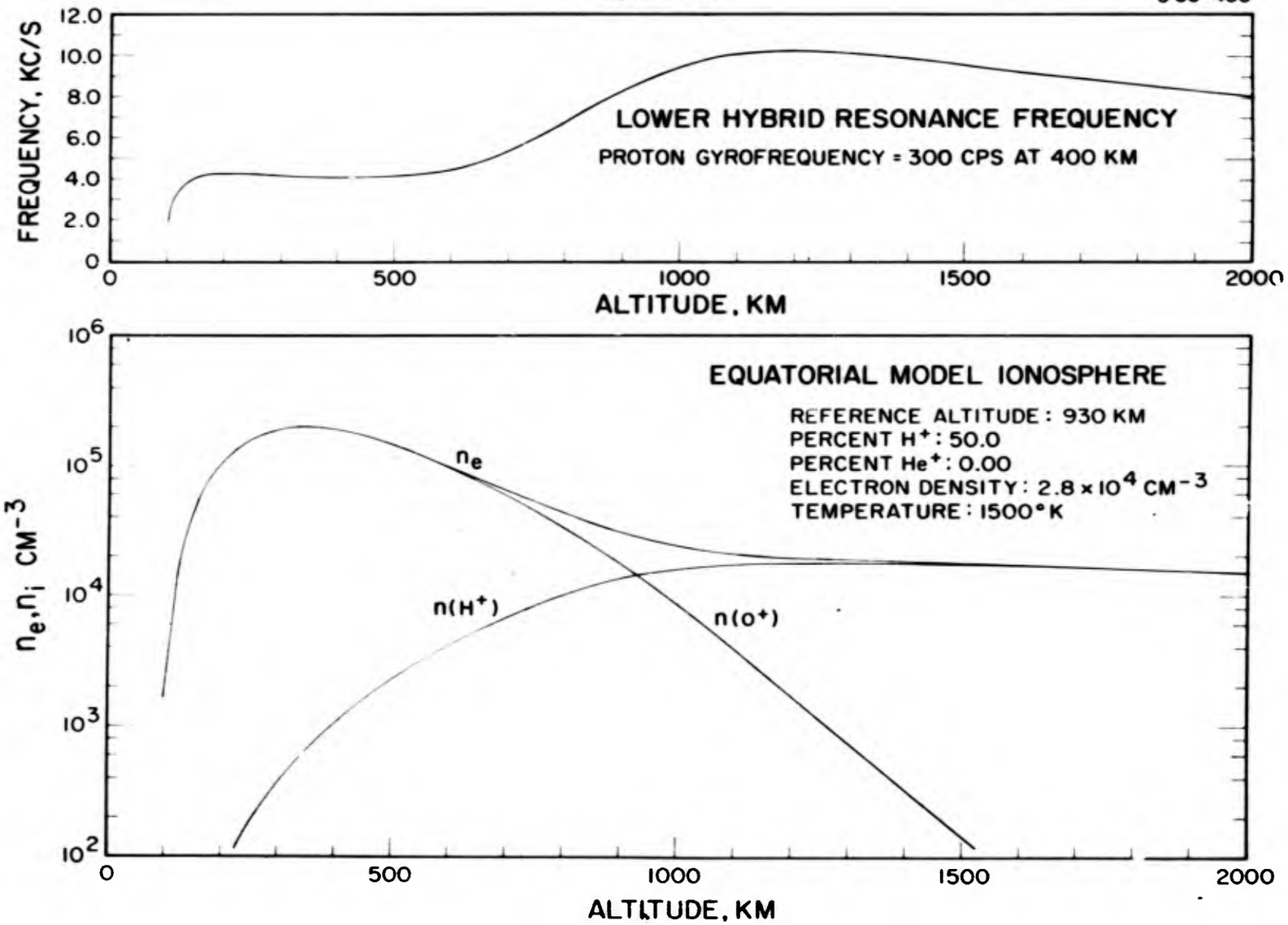

(Security classification of title, body of abstract and indexing annotation must be entered when the overall report is classified)

1. ORIGINATING ACTIVITY (Corporate author)	2a. REPORT SECURITY CLASSIFICATION
University of Iowa, Department of Physics and Astronomy	UNCLASSIFIED
	2b. GROUP

3. REPORT TITLE

VLF Ray Tracing in a Model Ionosphere

4. DESCRIPTIVE NOTES (Type of report and inclusive dates)

Progress

5. AUTHOR(S) (Last name, first name, initial)

SHAWHAN, Stanley D.

6. REPORT DATE	7a. TOTAL NO. OF PAGES	7b. NO. OF REFS
August 1966	186	62

8a. CONTRACT OR GRANT NO.	9a. ORIGINATOR'S REPORT NUMBER(S)
Nonr-1509(06)	U. of Iowa 66-33
b. PROJECT NO.	
c.	9b. OTHER REPORT NO(S) (Any other numbers that may be assigned this report)
d.	

10. AVAILABILITY/LIMITATION NOTICES

Qualified requesters may obtain copies of this report from DDC.

11. SUPPLEMENTARY NOTES	12. SPONSORING MILITARY ACTIVITY
	Office of Naval Research

13. ABSTRACT

A VLF ray tracing study in a model ionosphere including ions is presented. A review of previous VLF ray tracing methods is given. The physical meaning of rays and ray paths is discussed and it is concluded that for ray tracing in the ionosphere the wave packet and Poynting vector approaches give the same results. Two-dimensional ray tracing equations are derived for the case of a horizontally stratified ionosphere and the derivation of three dimensional equations for the curved ionosphere is sketched. These ray tracing equations are integrated for the special cases of exactly transverse and exactly longitudinal propagation but it is concluded that neither case can persist for very-low-frequency radio waves in the ionosphere. Also the conditions for reversibility of a ray path are derived. It is found that the computer program for numerical integration of the ray tracing equations can retrace a path to 0.3% in latitude and 0.02% in wave normal angle and can reproduce known results for the horizontally stratified model.

Using this ray tracing program the behavior of ray paths for variations of frequency, initial latitude, initial wave normal angle, initial altitude and ionospheric model are shown. The most important results were with

DD FORM 1 JAN 64 1473

UNCLASSIFIED
Security Classification

variation of the initial wave normal angle; two ray paths for the same frequency can cross and rays can turn around at low altitudes for frequencies less than the local lower hybrid resonance frequency. Spectrograms of proton, helium, and oxygen whistlers as well as negative ion whistlers are presented. It is predicted that oxygen whistlers can be observed at all altitudes below the oxygen gyrofrequency and that negative ion whistlers can be observed below 30 cps at altitudes near 300 km. Experimental data on the hook whistler, riser and check whistlers, 'transverse' whistlers, and satellite observed VLF noise bands are presented and summarized. The hook whistler is explained as a multiple path whistler at equatorial latitudes for which the earlier trace has increased dispersion at low frequencies due to large wave normal angles along the path. This increased dispersion gives the characteristic joining of the two traces at low frequencies. A calculated hook whistler spectrogram is presented. The riser and check whistlers are explained as whistlers for which the ray has propagated transverse and nearly transverse to the magnetic field line along its path. The point of transverse propagation produces the characteristic riser dispersion of increasing time delay with increasing frequency. For the check whistler apparently both the upgoing and downgoing rays are observed at the satellite giving a normal whistler dispersion followed by a riser-like tail. It is demonstrated that previous experimental data on the 'transverse' whistler may have been misinterpreted and that the dispersion increases with decreasing frequency rather than decreases as previously reported. The transverse whistler is explained as a whistler which has acquired added dispersion at low frequencies because of propagation nearly transverse to the magnetic field along the path. Finally it is shown that waves can be trapped in the ionosphere between altitudes of decreasing transverse refractive index. It is proposed that these trapped waves can explain the satellite and ground observed ion gyrofrequency noise bands.

	ROLE	WT	ROLE	WT	ROLE	WT
Ray Tracing						
Very-Low-Frequency						
Whistlers						
VLF Emissions						
Injun 3 VLF Data						

INSTRUCTIONS

1. ORIGINATING ACTIVITY: Enter the name and address of the contractor, subcontractor, grantee, Department of Defense activity or other organization *(corporate author)* issuing the report.

2a. REPORT SECURITY CLASSIFICATION: Enter the overall security classification of the report. Indicate whether "Restricted Data" is included. Marking is to be in accordance with appropriate security regulations.

2b. GROUP: Automatic downgrading is specified in DoD Directive 5200.10 and Armed Forces Industrial Manual. Enter the group number. Also, when applicable, show that optional markings have been used for Group 3 and Group 4 as authorized.

3. REPORT TITLE: Enter the complete report title in all capital letters. Titles in all cases should be unclassified. If a meaningful title cannot be selected without classification, show title classification in all capitals in parenthesis immediately following the title.

4. DESCRIPTIVE NOTES: If appropriate, enter the type of report, e.g., interim, progress, summary, annual, or final. Give the inclusive dates when a specific reporting period is covered.

5. AUTHOR(S): Enter the name(s) of author(s) as shown on or in the report. Enter last name, first name, middle initial. If military, show rank and branch of service. The name of the principal author is an absolute minimum requirement.

6. REPORT DATE: Enter the date of the report as day, month, year; or month, year. If more than one date appears on the report, use date of publication.

7a. TOTAL NUMBER OF PAGES: The total page count should follow normal pagination procedures, i.e., enter the number of pages containing information.

7b. NUMBER OF REFERENCES: Enter the total number of references cited in the report.

8a. CONTRACT OR GRANT NUMBER: If appropriate, enter the applicable number of the contract or grant under which the report was written.

8b, 8c, & 8d. PROJECT NUMBER: Enter the appropriate military department identification, such as project number, subproject number, system numbers, task number, etc.

9a. ORIGINATOR'S REPORT NUMBER(S): Enter the official report number by which the document will be identified and controlled by the originating activity. This number must be unique to this report.

9b. OTHER REPORT NUMBER(S): If the report has been assigned any other report numbers *(either by the originator or by the sponsor)*, also enter this number(s).

10. AVAILABILITY/LIMITATION NOTICES: Enter any limitations on further dissemination of the report, other than those imposed by security classification, using standard statements such as:

(1) "Qualified requesters may obtain copies of this report from DDC."

(2) "Foreign announcement and dissemination of this report by DDC is not authorized."

(3) "U. S. Government agencies may obtain copies of this report directly from DDC. Other qualified DDC users shall request through _____."

(4) "U. S. military agencies may obtain copies of this report directly from DDC. Other qualified users shall request through _____."

(5) "All distribution of this report is controlled. Qualified DDC users shall request through _____."

If the report has been furnished to the Office of Technical Services, Department of Commerce, for sale to the public, indicate this fact and enter the price, if known.

11. SUPPLEMENTARY NOTES: Use for additional explanatory notes.

12. SPONSORING MILITARY ACTIVITY: Enter the name of the departmental project office or laboratory sponsoring *(paying for)* the research and development. Include address.

13. ABSTRACT: Enter an abstract giving a brief and factual summary of the document indicative of the report, even though it may also appear elsewhere in the body of the technical report. If additional space is required, a continuation sheet shall be attached.

It is highly desirable that the abstract of classified reports be unclassified. Each paragraph of the abstract shall end with an indication of the military security classification of the information in the paragraph, represented as *(TS)*, *(S)*, *(C)*, or *(U)*.

There is no limitation on the length of the abstract. However, the suggested length is from 150 to 225 words.

14. KEY WORDS: Key words are technically meaningful terms or short phrases that characterize a report and may be used as index entries for cataloging the report. Key words must be selected so that no security classification is required. Identifiers, such as equipment model designation, trade name, military project code name, geographic location, may be used as key words but will be followed by an indication of technical context. The assignment of links, roles, and weights is optional.